Mapping and monitoring heterogeneous landscapes: spatial, spectral and temporal unmixing of MERIS data

Promotor:
Prof. dr. sc. nat. M. E. Schaepman
Hoogleraar Geo-informatiekunde mbav Remote Sensing,
Wageningen Universiteit (Nederland)

Co-promotor:
Dr. ir. J. G. P. W. Clevers
Universitair hoofddocent bij het Laboratorium voor Geo-informatiekunde en Remote Sensing,
Wageningen Universiteit (Nederland)

Promotiecommissie:
Prof. dr. A. A. M. Holtslag
Wageningen Universiteit (Nederland)
Prof. dr. A. J. Plaza
Universiteit van Extremadura (Spanje)
Prof. dr. ir. R. L. Lagendijk
Technische Universiteit Delft (Nederland)
Dr. Mathias Kneubühler
Universiteit van Zürich (Zwitserland)

Dit onderzoek is uitgevoerd binnen de C. T. de Wit onderzoekschool
Production Ecology and Resource Conservation (PE&RC)

Mapping and monitoring heterogeneous landscapes: spatial, spectral and temporal unmixing of MERIS data

Raúl Zurita-Milla

Proefschrift

ter verkrijging van de graad van doctor
op gezag van de rector magnificus
van Wageningen Universiteit
Prof. dr. M. J. Kropff
in het openbaar te verdedigen
op woensdag 17 september 2008
des namiddags te half twee in de Aula

Raúl Zurita-Milla, 2008

Mapping and monitoring heterogeneous landscapes:
spatial, spectral and temporal unmixing of MERIS data

PhD Thesis, Wageningen University, Wageningen, The Netherlands
With summaries in English, Dutch and Spanish

ISBN: 978-90-8504-988-3

For every complex problem there is an answer that is clear, simple, and wrong

(attributed to H. L. Mencken)

Table of Contents

CHAPTER 1

Introduction

1.1 Background

During the last few centuries anthropogenic activities have intensified in order to fulfil the demands of an ever increasing global population (United Nations 2007). Although these activities have substantially contributed to an increasing human well-being and supported the economic development of many regions all around the world, they are responsible for the current ecological degradation of our planet (Christensen et al. 1996; Gardner 2005; Steffen et al. 2005). Reduction of global biodiversity, overexploitation of fresh water resources and erosion, salinization and contamination of agricultural soils are some of the consequences of intensifying anthropogenic activities (Millennium Ecosystem Assessment 2005). Furthermore, anthropogenic activities are actively modifying atmospheric composition and, as a consequence, changing our climate (Foley et al. 2005; Pielke Sr. 2005). In this context, having accurate and up-to-date information about our environment is essential for quantifying the nature and extent of the activities that are reshaping the Earth surface and to study their potential impact on our future welfare.

Earth observation satellites deliver synoptic, timely and cost effective data that, if properly processed, can be transformed into an invaluable source of information about the ecological condition of our planet (DeFries and Townshend 1994; Running et al. 1995; Townshend et al. 1991). A number of applications such as forecasting weather conditions, forecasting crop yield, mapping urban areas, monitoring natural resources or addressing emergencies would not be possible without Earth observation satellites.

This thesis focuses on the use of Earth observation satellites for land applications. The "land remote sensing" era was initiated in 1972 when the first Landsat satellite, at that time known as Earth Resources Technology Satellite, was launched at Vandenberg Air Force Base in California (Hall 1992). Since then, Earth observation satellites have revolutionized the way that scientists, politicians and the general public view the Earth (Lauer et al. 1997). Land remote sensing data is used for deriving information like land cover maps or continuous maps on, for instance, vegetation properties.

Because of the evident advantages offered by land remote sensing, land cover maps are nowadays operationally produced by several national and international agencies using remotely sensed data (Gutman et al. 2004). These maps are used for a wide range of applications like estimation of the area covered by agricultural crops (Gallego 2004) or to report greenhouse gas fluxes for the United Nations framework convention on climate change (UNFCC) and the Kyoto protocol (Wigjey 1998). Land cover and land use maps are also a pre-requisite for environmental monitoring activities like the one proposed for the European Union (EU) Habitat Directive, the EU Common Agricultural Policy or, more recently, the ones that will be used in the framework of the Global Monitoring for Environment and Security, GMES (European Commission 2003; Schreier and Dech 2005). In this respect, GMES has defined a priority theme on "Land cover change in Europe" that should contribute to the requirements of the United Nations Convention on Biodiversity (United Nations 1992). In addition, land cover maps are consistently used as input in several climate and agro-ecosystem models (Champeaux et al. 2000; Dickinson et al. 1998). Last but not least, land cover maps are of great help to constrain the retrieval of biophysical and biochemical parameters of vegetated canopies (Myneni et al. 1997b). Continuous parameters like leaf area index (LAI), fraction of absorbed photosynthetically active radiation (fAPAR) or leaf

chlorophyll content (C_{ab}) can be mapped at different spatial scales with far better accuracy when land cover type is known. Knowledge on these parameters is very important because they are a pre-requisite for various applications such as crop yield forecasts (Boegh et al. 2004) or monitoring ecosystem productivity (Running et al. 2004).

Despite the large variety of Earth observation sensors and derived products, our current understanding of the Earth system and land cover change dynamics is still far from complete (Foody 2002). One of the reasons for this is the difficulty of mapping and monitoring complex landscapes where processes take place at very different spatial and temporal scales (Hall et al. 1988).

1.2 Remote sensing of heterogeneous landscapes

Remote sensing images are acquired using the so-called "raster data model" (Atkinson 2007). This model is comprised of non-overlapping areal units called pixels that are arranged in a regular grid (Burrough and McDonnell 1998). This means that remote sensing images are acquired using a defined pixel and grid size that are fixed prior to data acquisition (Atkinson 2007). Traditional remote sensing processing techniques work according to this fixed pixel size. The recorded signal for a pixel is processed to create products where a unique land cover class label or a unique biophysical parameter value is assigned to each pixel. In principle, this approach is useful when the pixel size and the spatial scale of the feature or process, that we want to study, closely match. However, even in this case, mixed pixels will occur in the image. Mixed pixels are pixels that contain information from more than one land cover type or, when fully covered by one land cover type, a pixel that is not homogeneous in all its properties (Chikara 1984; Fisher 1997; Napelka and Hyde 1972). This kind of pixels can be described by the inherit heterogeneity of vegetation and soils, which is often augmented by anthropogenic activities that create heterogeneous and fragmented landscapes with a mixture of urban areas, water, natural, semi-natural and agricultural areas.

The mixed pixel problem is minimized when using very high or high spatial resolution data like Quickbird, IKONOS, Landsat Thematic Mapper (TM) or SPOT High Resolution Visible and Infra-Red (HRVIR) data which provide pixel sizes ranging from sub-meter to about 30 m. In these images, object oriented image processing techniques or the use of contextual information can assist in dealing with mixed pixels (Burnett and Blaschke 2003; Hay et al. 2003). However, the use of very high and high spatial resolution sensors has some associated difficulties. First of all, sensor design constraints prohibit recording at a very wide swath at a high spatial resolution. Secondly, the amount of data collected by high spatial resolution sensors is limited by the current downlink capabilities as well as by the current possibilities for archiving, distributing and processing the data. In practical terms, this means that there is a trade-off between the spatial, spectral and temporal resolutions provided by Earth observation sensors. As a result, sensors working at high spatial resolution typically offer less spectral bands and less spatial coverage than sensors working at coarser resolutions.

With respect to the spectral resolution, very high and high spatial resolution sensors typically offer data in less than 6 or 7 spectral bands. Nevertheless, for ecological or mineralogical applications, hyper-spectral sensors measuring the reflected radiation in hundreds of narrow bands are preferred (Turner et al. 2003). Airbone sensors can supply hyper-spectral data at very high spatial resolutions. However, they do not provide continuous

and regular acquisitions and their data are more expensive than the ones provided by spaceborne sensors (Aplin 2004).

The reduced spatial coverage offered by very high and high spatial resolution sensors results in relatively poor revisit times. For instance, the Landsat TM sensor has a revisit time of 16 days as compared to typical coarse resolution sensors (>1 km pixel size) like the Advanced Very High Resolution Radiometer (AVHRR) onboard National Oceanic and Atmospheric Administration (NOAA) satellites, which deliver daily images over the same area. This is a significant limitation to the use of high spatial resolution sensors for monitoring vegetated areas. Furthermore, northern countries have a short growing season and regular acquisitions are hampered by extensive cloud coverage. For instance, in the United Kingdom only 1 every 6 passes of Landsat TM data is usable (Legg 1991; Marshall et al. 1994). Similar cloud coverage problems are found in other northern regions (Jorgensen 2000) and, as discussed by Asner (2001), clouds are also a major obstacle to monitor tropical regions using high spatial resolution data. Moreover, the use of very high spatial resolution can result in an oversampling problem for certain landscapes where land cover classification accuracy might even decrease because of spectral confusion caused by within-class variability (Aplin 2006). Finally, very high and high spatial resolution imagery is usually not freely available. Therefore, using this kind of data to monitor large regions can be prohibitively expensive (Fraser et al. 2005).

Because of their high revisit time, coarse spatial resolution sensors are potentially more successful in acquiring cloud free images but at the expense of providing images with (potentially) many mixed pixels. However, recent developments of imaging devices have resulted into a new kind of sensor that works at a medium spatial resolution while providing a spectrally enhanced configuration. Two sensors belong to this category, the MODerate-Resolution Imaging Spectroradiometer (MODIS) and the MEdium Resolution Imaging Spectrometer (MERIS):

- MODIS is a payload instrument onboard two NASA platforms: Terra and Aqua, which were respectively launched in 1999 and in 2002 (Salomonson et al. 1992). MODIS captures information at 3 spatial resolutions (2 bands at 250 m, 5 bands at 500 m and 29 bands at 1000 m) and it covers the entire Earth every 1-2 days.

- MERIS was launched in 2002 onboard the ESA/ENVISAT-1 platform which is the largest ever built Earth observation satellite (Rast and Bézy 1990). MERIS is a programmable device that measures the radiation reflected by the Earth surface in the solar spectral range (390 to 1040 nm) and delivers data in 15 bands. Two spatial resolutions are provided: 300 m in the so-called “Full Resolution” (FR) mode and 1200 m at “Reduced Resolution” (RR) mode. MERIS also has a global coverage at a revisit time of 2-3 days.

In this thesis, we concentrate on exploring the use of MERIS images because of the following reasons: (i) MERIS has a better spectral resolution in the visible and near-infrared region than MODIS: 15 narrow bands vs. 7 bands. More spectral bands might offer a better class separability and potentially better classification results. In addition, MERIS delivers data in the spectral region known as the "red-edge" (Clevers et al. 2002). This region is particularly interesting for studying canopies because it is linked to the amount of chlorophyll in the vegetation (Horler et al. 1983). (ii) MERIS is a pushbroom sensor that offers high quality data at unprecedented spectral and spatial resolutions. MODIS has some operationally limiting characteristics. For instance, because of the whiskbroom design, consecutive scans overlap at large viewing angles, which causes discontinuities of the latitude/longitude fields (Khlopenkov and Trishchenko 2008). In addition, MODIS has a pronounced triangular point spread function (PSF). This means that only 75 % of the information assigned to a MODIS pixel is coming from the corresponding nominal observation area (Tan et al. 2006). Besides, the geometric processing and gridding artifacts of MODIS products result in an average overlap between the observations and their grid cells of less than 30 % (Tan et al. 2006). Finally, there is a band-to-band registration error in the MODIS sensor onboard Aqua (Xiong et al. 2006). Because of these effects, MODIS is, in principle, less suitable for sub-pixel analysis than its European counterpart (Kristof et al. 2007). (iii) MERIS is a European satellite so its application at the European scale is promoted and supported both by ESA and the EU.

Despite its enhanced spatial, spectral and temporal resolutions, MERIS is still not able to fully capture the variability present in typical European landscapes (Addink et al. 2006). Medium spatial resolution images of heterogeneous and highly fragmented landscapes contain a significant number of mixed pixels. Dealing with this kind of pixels is important for both thematic and quantitative applications. For instance, land cover area estimation by simply counting pixels belonging to each class can only be accepted if the classification accuracy is very good and if the impact of mixed pixels is negligible (Gallego 2004).

Moreover, dealing with mixed pixels is also required for an accurate retrieval of biophysical and biochemical parameters (Garrigues et al. 2006). For instance, it has been shown that when there is a lot of mixing, the retrieval uncertainty of MODIS products can be quite high (Tan et al. 2005). Sub-pixel snow cover reduces the accuracy of MODIS LAI and fAPAR estimates (Tian et al. 2004). This is also true for sub-pixel water bodies and sub-pixel cloud coverage. This is why the validation of products derived from medium and coarse spatial resolution data is done over relatively homogeneous sites and using high spatial resolution data (SPOT or Landsat) as a reference (Baret et al. 2006; Garrigues et al. 2006).

An operational solution to the mixed pixel problem is, therefore, required. One approach could be to only use coarse and medium spatial resolution sensors to pinpoint major regions of change that can later be studied with high spatial resolution sensors. In this case, the size of the minimum patch size that can be identified depends on many factors like fragmentation of the landscape, magnitude of change or the resolution of the sensor (Fraser et al. 2005). For instance, Fraser et al. (2000) found that patches of at least 10 km^2 were needed to accurately map burned areas using AVHRR data. This patch size is too large for most of the European landscapes. Another approach to deal with mixed pixels could be to combine or merge images acquired at different spatial resolutions. This is an example of data fusion.

1.3 Data fusion

Given the complexity of the Earth surface and the diversity of processes that take place on it, innovative approaches able to make use of the wide variety of Earth observation sensors and of the already existing ancillary data are required to further improve our mapping and monitoring capabilities (Woodcock and Ozdogan 2004). In this respect, the use of data fusion methods and techniques seems to be one of the most logical approaches to continue the exploration of our planet. Wald (1998) proposed the following definition for data fusion among the remote sensing community: "Data fusion is a formal framework in which are expressed means and tools for the alliance of data originating from different sources. It aims at obtaining information of greater quality; the exact definition of "greater quality" will depend upon the application".

The same year, this definition was adopted by the European Association of Remote Sensing Laboratories, EARSeL. According to it, combining data from different spectral bands to create vegetation indices, or combining images acquired by the same sensor at different points in time should be considered as a data fusion exercise (Wald 1999). Moreover, *strictu sensu*, data assimilation can also be considered as data fusion because it deals with the inclusion of measured data into a model so that the quality of the output is increased (Wald 1999). However, in practice data fusion is associated with the process of combining two or more datasets using diverse algorithms (Ehlers 1991; Pohl and Van Genderen 1998).

In the last decades, a large number of data fusion methods have been described in the remote sensing literature (see Yu el al. (2006) for a review). This is a consequence of the increasing need to integrate the enormous amount of data that is operationally collected by remote sensors. Besides this, Earth observation data is inherently complementary because of the current sensor design (cf. section 1.2). This is why fused images generally offer increased interpretation capabilities and more reliable results (Hall and Llinas 1997; Pohl and Van Genderen 1998) than using a single sensor. Data fusion should, however, be understood as a framework to study complex problems and not merely as a collection of tools and means to combine remote sensing images (Wald 1999). This framework should support the interpretation of multi-sensor and multi-resolution images (Quattrochi and Goodchild 1997; Tate and Atkinson 2001) because there is not a (unique) solution to the problem of finding the "right" spatial resolution to map and monitor the Earth surface (Aplin 2006; Ju et al. 2005). Thus understood, data fusion can assist dealing with mixed pixels. The next section presents the main model to deal with mixed pixels and sketches its use to combine data acquired over the same area but at different spatial resolutions.

1.4 The linear mixing model

Physical models are commonly used by the remote sensing community to extract quantitative information about leaves (Jacquemoud and Baret 1990), vegetated canopies (Verhoef 1984; Widlowski et al. 2007) and soil properties (Hapke 1981; Liang and Townshend 1996). These models are simplified versions of reality that describe the photon-matter interactions and that allow us to derive quantitative information. Although of a different nature, a physical model is also commonly used to deal with mixed pixels. This model is known as the linear mixing model (LMM) and it describes how the solar radiation

mixes when interacting with the different land cover types present in the pixel footprint (Adams and Gillespie 2006). The LMM is formulated as follows:

$$\mathrm{DN}_i = \sum_{c=1}^{nc} \left(f_c \cdot \mathrm{DN}_{c,i} \right) + e_i \qquad i = 1,2,...,nb \tag{1.1}$$

where DN_i is the measured value of a mixed pixel in the spectral band i, $\mathrm{DN}_{c,i}$ is the measured value of the pure class c in the spectral band i, f_c is the fraction of class c present in the mixed pixel, e_i is the residual that accounts for the difference between the modelled and the measured spectra (again, in band i) and nc and nb are respectively the number of classes in the mixed pixel and the number of spectral bands of the sensor.

Laboratory experiments have shown that the mixing can also be nonlinear (Adams and Gillespie 2006). Nonlinear mixing occurs when radiance is modified by one material before interacting with another one (multiple scattering occurs). Neural networks, decision trees or vegetation indices are often used to tackle nonlinear unmixing (Borel and Gerstl 1994). These methods typically require a large dataset of training pixels, for which both the fractional coverage and the spectra are known (Plaza et al. 2005). Other methods have been proposed to deal with mixed pixels like the use of fuzzy classifiers or use of a posteriori probabilites from a maximum likelihood classification (Bastin 1997; Foody 2004). However, several studies have shown that in complex and non-random landscapes, the linear mixing model offers a reasonable approximation (Adams et al. 1995; DeFries et al. 2000; Du and Chang 2004; Hall et al. 1995; Ramsey and Christensen 1998; Roberts et al. 1993; Shimabukuro and Smith 1991). Furthermore, the implementation of linear unmixing is, in general, less complex and more stable than nonlinear methods (Chen and Vierling 2006).

The main application of the linear mixing model is the retrieval of the proportions of the land cover types present in a pixel (Settle and Drake 1993). This application is known as spectral unmixing or, more generally, as spectral mixture analysis (SMA). The proportions retrieved using SMA are useful for a wide range of applications (Adams and Gillespie 2006). For instance, they can be used to get more accurate estimations of the area cover by the main components of a landscape than by counting classified pixels (Cross et al. 1991). Furthermore, SMA can also be used to mitigate background effects and improve the retrieval of continuous parameters like LAI. In this case, the percentage covered by the relevant class is first estimated and, subsequently, it is used to retrieve the values of the biophysical variable of interest (Peddle et al. 2001; Peddle et al. 1999). SMA has been used to separate forest from understory so that "pure" forest NDVI time series could be obtained for running a forest productivity model (Maselli and Chiesi 2005, 2006). A similar approach was used by Yang et al. (2007) to estimate crop abundance and relate it to crop yield. The results were better than when using vegetation indices. Finally, North (2002) has shown that the use of SMA with coarse spatial resolution data to estimate fractional cover also outperforms the use of vegetation indices. It is also worth noting that several authors have tried to spatially allocate the proportions within the pixel. This technique is known as sub-pixel mapping (Atkinson 2004). Artificial neural networks and other optimization and geo-statistical techniques are used to produce a map with the fractions derived from the SMA (Atkinson et al. 2008; Tatem et al. 2003). However, sub-pixel mapping is an under-determined inverse problem and,

therefore, it is very difficult to design a generally applicable method valid for all kinds of images, spatial resolutions and landscapes (Atkinson 2004; Boucher and Kyriakidis 2006).

The results of the SMA are strongly influenced by the selection of the main constituents of the image (the endmembers). In spite of the progress made to develop (semi-)automatic endmember extraction methods (Martinez et al. 2006; Plaza et al. 2004), this remains a challenging task (especially when most pixels in the image are mixed because then hardly any pure signal can be found in the scene). Furthermore, the number of components that can be unmixed is limited by the number of spectral bands of the image (Boardman 1990). This implies, for instance, that panchromatic images cannot be used for spectral unmixing and that hyperspectral images are preferred over multispectral ones. However, if a high and a low spatial resolution image are simultaneously available over a certain study area, the LMM can also be used to combine the information provided by these images. This application is known as unmixing-based data fusion and it aims at downscaling the spectral information of the low spatial resolution image to the spatial resolution provided by the high spatial resolution image (Zhukov et al. 1999). This kind of unmixing does not require a priori knowledge of the main components present in the low spatial resolution image because there is no need to identify their pure signals. In fact, these signals are the output. Therefore, the unmixing-based data fusion approach can be applied even if the low resolution image only has mixed pixels or a small number of spectral bands.

1.5 Objectives

The main objective of this thesis is to develop a multi-sensor and multi-resolution data fusion approach that allows mapping and monitoring heterogeneous and highly fragmented landscapes using medium spatial resolution data. More precisely, we explore the possibilities of using the linear mixing model (LMM) to downscale MERIS full resolution (300 m) data to a Landsat-like spatial resolution (25 m). To fulfil this aim, the synergic use of high spatial resolution datasets and MERIS data is required. The Netherlands is selected as test site because of its typical mixed landscapes: small patches of arable land, urban areas, water, natural vegetation and forests are easily found next to each other. Besides this, cloud coverage is also an important problem in The Netherlands.

In order to achieve the main objective of this thesis, the following research questions are formulated:

A. What is the radiometric quality of MERIS data and what are the potential impacts of miscalibration on MERIS land products?

B. Can we use the linear mixing model to downscale MERIS FR data to a Landsat-like spatial resolution? What is the quality of the resulting fused images?

C. Can we use MERIS fused images to derive spatially improved MERIS products like land cover and vegetation status maps?

D. Can we use downscaled time series of MERIS data to monitor heterogeneous and fragmented landscapes with a high spatial, spectral and temporal resolution?

1.6 Outline

The core of this thesis, chapters 2 to 5, is devoted to answering the research questions mentioned in the previous section. Each chapter has been prepared as a peer reviewed publication and contains a specific introduction linked to the research question that will be tackled in it, a detailed description of the case study and the datasets used, a wide discussion of the obtained results and a summary of the main findings (conclusions) followed by some recommendations for further research.

Chapter 2 explores the implications of deriving MERIS land products using MERIS FR data at different radiometric levels. More precisely, the effects of the smile and the vicarious calibration corrections on regional land cover mapping and vegetation status assessment are studied. Three vegetation indices are used to assess vegetation status: the MGVI (linked to fAPAR), the MTCI (related to the canopy chlorophyll content) and the NDVI (an indicator of vegetation "greenness").

Chapter 3 presents a data fusion approach to downscale MERIS FR data using the linear mixing model and a high spatial resolution dataset (used to characterize the spatial patterns of the area under study). The selected approach requires the optimization of two parameters: the number of classes used to classify the high spatial resolution dataset (*nc*) and the size of the MERIS neighbourhood used to solve the unmixing equations (*k*). A quantitative data fusion quality assessment is used to assist with the identification of the best fused image. The resulting fused images have a Landsat-like spatial resolution (25 m) and the MERIS spectral resolution (15 spectral bands).

Chapter 4 builds on chapter 3 and assesses the potential of MERIS fused images to produce land cover maps and to assess vegetation status. First, all the fused images are classified in order to identify the best combination of *nc* and *k*. Then, the best fused image is used to compute the same three vegetation indices used in chapter 2: the MGVI, the MTCI and the NDVI. For comparison purposes, these threee indices are computed from the MERIS FR (300 m) images and the NDVI is also computed from the TM (25 m) image.

Chapter 5 focuses on exploiting the high temporal resolution provided by MERIS. An improved version of the unmixing-based data fusion approach described in chapter 2 is used to downscale a time series of seven MERIS FR images. In this case, the Dutch land use database is used to derive the high spatial resolution information. The MTCI and the MGVI are used to assess vegetation status at the original (300 m) and downscaled (25 m) resolutions.

Chapter 6 concludes this thesis with a summary and discussion of the main findings of this thesis and offers some suggestions for further work.

Finally, this thesis closes with the references, summaries in English, Dutch and Spanish and the curriculum vitae of the author.

CHAPTER 2

Effects of MERIS L1b radiometric calibration on regional land cover mapping and land products*

* Based on: Zurita-Milla, R., Clevers, J.G.P.W., Schaepman, M.E. and Kneubuehler, M. (2007). Effects of MERIS L1b radiometric calibration on regional land cover mapping and land products. *International Journal of Remote Sensing*, 28, 653-673.

Effects of MERIS L1b radiometric calibration on regional land cover mapping and land products

Abstract

The information derived from remotely sensed data must be carefully used because there are many sources of error that can potentially affect its quality. In this respect, an accurate radiometric calibration is essential for any Earth observation sensor because it maximises the quality of the final products.

This paper presents several calibration efforts performed on MERIS data and subsequently focuses on the smile effect and on the vicarious calibration corrections. The implications of these corrections are evaluated using a MERIS full resolution level 1b image acquired over The Netherlands. A thematic approach, based on regional land cover mapping using linear spectral unmixing, and a continuous approach, based on land products (fAPAR, MTCI and NDVI), are used to quantify these implications.

Even though MERIS has a very high radiometric quality, results point out that radiometric effects are consistently present in the final MERIS products. Our results also show that MERIS, after including all potential corrections investigated here, does not exhibit significant radiometric deficiencies. However, from a strict point of view, all the radiometric corrections should be applied to the data so that the retrieval of quantitative information can be done with the highest possible quality. The use of fully radiometrically corrected data will also facilitate multitemporal comparisons. Therefore, we conclude that a systematic application of all relevant calibration parameters will increase the long term comparability of MERIS measurements in such a way that more emphasis can be put on the retrieval of MERIS products.

2.1 Introduction

2.1.1 Calibration of the MERIS instrument

In March 2002, the Medium Resolution Imaging Spectrometer (MERIS (Bézy et al. 1998)), was launched on board of the ESA's ENVISAT platform (Laur et al. 2002; Louet 2001). MERIS is a fully programmable pushbroom imaging spectrometer that delivers data at 300 m in the full resolution mode (FR) and at 1200 m in the reduced resolution mode (RR). The instrument consists of 5 identical cameras arranged in a fan shape configuration that together provide a 68.5° field-of-view (equivalent to 1150 km of swath width at nadir). MERIS allows global coverage of the Earth in three days, and since its launch it has been operated with a fixed configuration of 15 spectral bands covering the visible and near infra-red region of the electromagnetic spectrum. These 15 spectral bands are in reality the sum of one or more CCD detectors pixel elements with a Full-Width Half-Maximum (FWHM) equal to 1.25 nm and a Gaussian response function for each element (Dubuisson et al. 2003).

MERIS was originally designed for oceanographic applications. However, Verstraete et al. (1999) found that MERIS could be very useful over land areas too. Indeed, its fine spectral resolution, its medium spatial resolution, and its high revisit time make MERIS an appropriate sensor to study most of the land surface processes occurring at regional to global scales.

The information derived from MERIS, or in general from any Earth observation sensor, must be carefully used because there are many sources of errors that can seriously affect the quality of the end product. In this respect, an accurate radiometric calibration is essential for any sensor because it maximizes the quality of the final products and makes the data more suited for quantitative and multitemporal applications. Consequently, a full radiometric calibration is a prerequisite for a correct use of the remotely sensed data.

As described by Goryl and Huot (2003), the MERIS radiometric quality is based on a calibration scheme consisting of a pre-flight, an on-board and a vicarious calibration.

The pre-flight characterisation of the MERIS instrument discovered a gradual spectral shift in the order of 1.0 nm within individual cameras. This spectral shift has been reported as the smile effect and it results in the CCD lines appearing tilted with respect to their isowavelength. The smile effect can hardly be noticed in the MERIS images because it is very small. However, this effect can introduce artefacts in algorithms that require high quality spectral measurements. MERIS Level 1b products are, however, distributed without the smile correction.

The on-board radiometric calibration is designed to validate the instrument radiometric performance while MERIS is in operation. It is executed every two months when Envisat is flying over the South Pole and it consists of observing a well characterised Spectralon panel illuminated by the sun. These observations are then used to update the absolute calibration coefficients (Rast et al. 1999). A second Spectralon panel is available on-board and occasionally deployed to check for the possible degradation of the first panel (Courrèges-Lacoste et al. 2003; Delwart and Bourg 2003).

Finally, MERIS in-flight performance is also checked by means of a number of vicarious calibration efforts (Govaerts and Clerici 2004; Kneubuehler et al. 2004; Nieke et al. 2003). Vicarious calibration is an independent method to monitor the radiometric performance of an

instrument. It assesses the radiometric error of that instrument by using reflectance standards, field instruments, and atmospheric radiation measurements simultaneous to the satellite overpass (Abdou et al. 2002). In other words, vicarious calibration includes all the relevant steps required to convert raw sensor data into accurate and useful radiometric quantities without making use of the on-board calibration.

2.1.2 Aim of this study

In this contribution we focus on the smile and the vicarious calibration corrections because these two correction methods are external to the standard MERIS level 1b processing approaches. The implications of applying these radiometric corrections will be evaluated using a MERIS full resolution level 1b image acquired over The Netherlands.

Two approaches will be used to illustrate the impact of these corrections: (i) regional land cover mapping using linear spectral unmixing and (ii) calculation of a selection of MERIS land products.

2.1.2.1 Regional land cover mapping

Land cover information is essential for planning and management activities as well as for modelling and understanding the Earth system (DeFries and Townshend 1999; Foody 2002; Vogelmann et al. 2001). However, our current understanding of land cover and its dynamics is in general deficient. Therefore, many current and future Earth observation missions, projects, and initiatives such as the Global Monitoring for Environment and Security (GMES) are focussing on land use and land cover mapping. In this framework, MERIS offers the possibility of providing information at a spatial scale in-between the current low and high spatial resolution sensors (Clevers et al. 2005).

Linear spectral unmixing will be applied to classify the main land cover types over The Netherlands, since it is likely that more than one land cover type will be present within the area covered by one MERIS pixel. This classification method, which has been previously used at regional to global scales (DeFries and Townshend 1999), provides abundance maps related to land cover classes and an indication of the quality of the unmixing: root mean square error (RMSE) per pixel. In this paper, the RMSE is used to analyse the quality of the unmixing of MERIS images at different radiometric levels.

2.1.2.2 MERIS land products

To date, a number of land products have successfully been derived from MERIS data. One of these land products is the fraction of absorbed photosynthetically active radiation (fAPAR), which is an integrated indicator of the status of the plant canopy. The fAPAR is computed through the MERIS global vegetation index (MGVI) (Gobron et al. 1999). Another relevant product for monitoring vegetation status is the MERIS terrestrial chlorophyll index (MTCI) as described in Dash and Curran (2004). Finally, the MERIS NDVI, computed as described by Teillet et al. (1997) and Steven et al. (2003), is also used in this study, because NDVI temporal series can be used, for instance, to monitor vegetation phenology (Teillet et al. 1997).

2.2 Materials and methods

2.2.1 MERIS radiometric calibration

In this study we used a cloud free MERIS FR level 1b image acquired the 14th of July 2003 and processed on the 16th of December 2003 by the MERIS processor v.4.07. The image, covering the whole of The Netherlands, was first reprojected into the Dutch National reference coordinate system (RD) and then overlaid with a vector map of coast boundaries to assess the co-registration accuracy. Visual interpretation indicated that the number and quality of the ground control points provided with the image were sufficient to achieve a good image-to-map registration (sub-pixel accuracy). This finding is supported by Clevers et al. (2007).

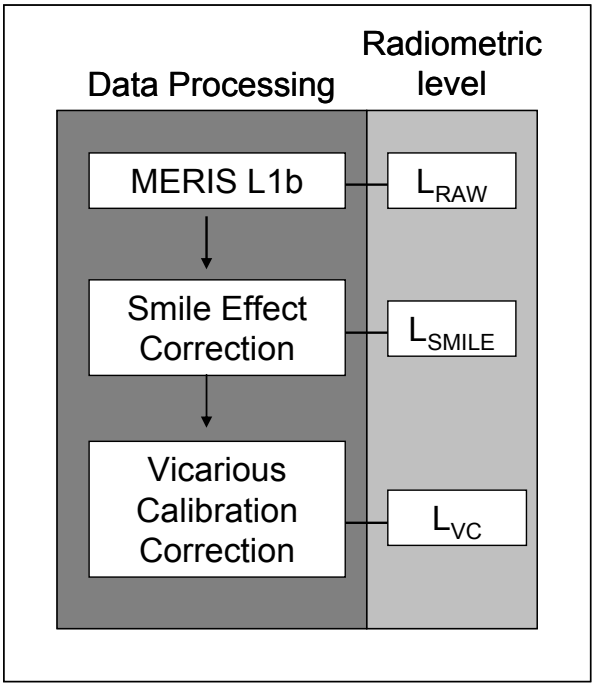

Figure 2.1. Conceptual flow-chart of MERIS radiometric corrections performed.

The reprojected image was first corrected for the smile effect and then corrected using vicarious calibration data. This resulted in three calibration levels: raw (L_{RAW}), smile corrected (L_{SMILE}) and smile + vicariously corrected (L_{VC}) radiances (Figure 2.1). A more detailed description of these corrections can be found in the following subsections.

2.2.1.1 Smile effect correction

The smile effect correction consists of two additive terms: the irradiance and the reflectance correction (see Goodenough et al. (2003) and Mouroulis et al. (2000) for a more exhaustive description of this effect). For MERIS land pixels, the reflectance correction is difficult to determine. As a result, the irradiance correction is usually the only one applied to the MERIS land pixels (only bands 1, 2 and 3 are subject to both corrections).

The irradiance correction compensates for the difference in the solar irradiance caused by the shift in the pixel wavelength with respect to the reference wavelength. This is, if L^{λ}_{RAW} represents the measured radiance in a given pixel and for a given wavelength (λ), and S^{λ}_{ref} and S^{λ}_{pixel} are the solar irradiances for the reference and the pixel wavelengths, respectively, then the corrected radiance can be computed as follows:

$$L^{\lambda}_{SMILE} = L^{\lambda}_{RAW} \cdot \frac{S^{\lambda}_{ref}}{S^{\lambda}_{pixel}} \tag{2.1}$$

This correction is therefore a linear transformation for each pixel or more precisely for each CCD detector. Figure 2.2 depicts the irradiance correction coefficients per wavelength and for all 5 MERIS cameras. These irradiance correction coefficients were taken from the metadata available in the Basic ERS & Envisat (A)ATSR and MERIS toolbox (BEAM[1] version 3.1); notice that the shape of the irradiance correction factors function was used to name this effect because it somehow resembles a (half) smile.

In this study, the smile correction was done using the BEAM smile correction processor (version 1.1) because it is an exact implementation of the algorithm that is routinely applied to all MERIS Level 2 products.

2.2.1.2 Vicarious calibration

The vicarious calibration presented here is based on Kneubühler et al. (2003) and follows a so-called reflectance-based approach with ground measurements of the atmospheric optical depth and surface reflectance over a bright natural target.

The Railroad Valley Playa (RRVP, Nevada, USA; 38.504° N, 115.692° W) was used as a bright natural target. RRVP is a desert playa commonly used for vicarious calibration of moderate spatial resolution sensors due to its optical properties, frequent sunny conditions and low atmospheric aerosol loading (Thome 2002).

The experiment consisted of taking in-situ sun photometer data for a number of dates for which MERIS acquisitions were available. Next, the MODTRAN-4 radiative transfer code (Berk et al. 1998; Kneisys et al. 1995) was used to predict the top-of-atmosphere (TOA) radiance. The MODTRAN-4 runs were constrained by field data, such as ground measurements of the surface reflectance, sun-target-sensor geometry and atmospheric properties (aerosol model, horizontal visibility). After that, calibration errors at the TOA level were computed for all the MERIS acquisition dates (Eq. 2.2) by comparing these predicted radiances with the MERIS measured radiances for the RRVP site:

$$RME^{i}[\%] = 100 \cdot \left(\frac{L^{i}_{RAW} - L^{i}_{VC\_TOA}}{L^{i}_{RAW}} \right) \tag{2.2}$$

[1] The BEAM toolbox is available at the following URL: http://envisat.esa.int/beam

Where: RME^i is the relative mean error for each MERIS spectral band, L^i_{RAW} is the MERIS FR level 1b TOA radiance [W sr^{-1} m^{-2} μm^{-1}] for band-*i* and $L^i_{VC\_TOA}$ is the simulated TOA radiance for the same band based on the ground measurements.

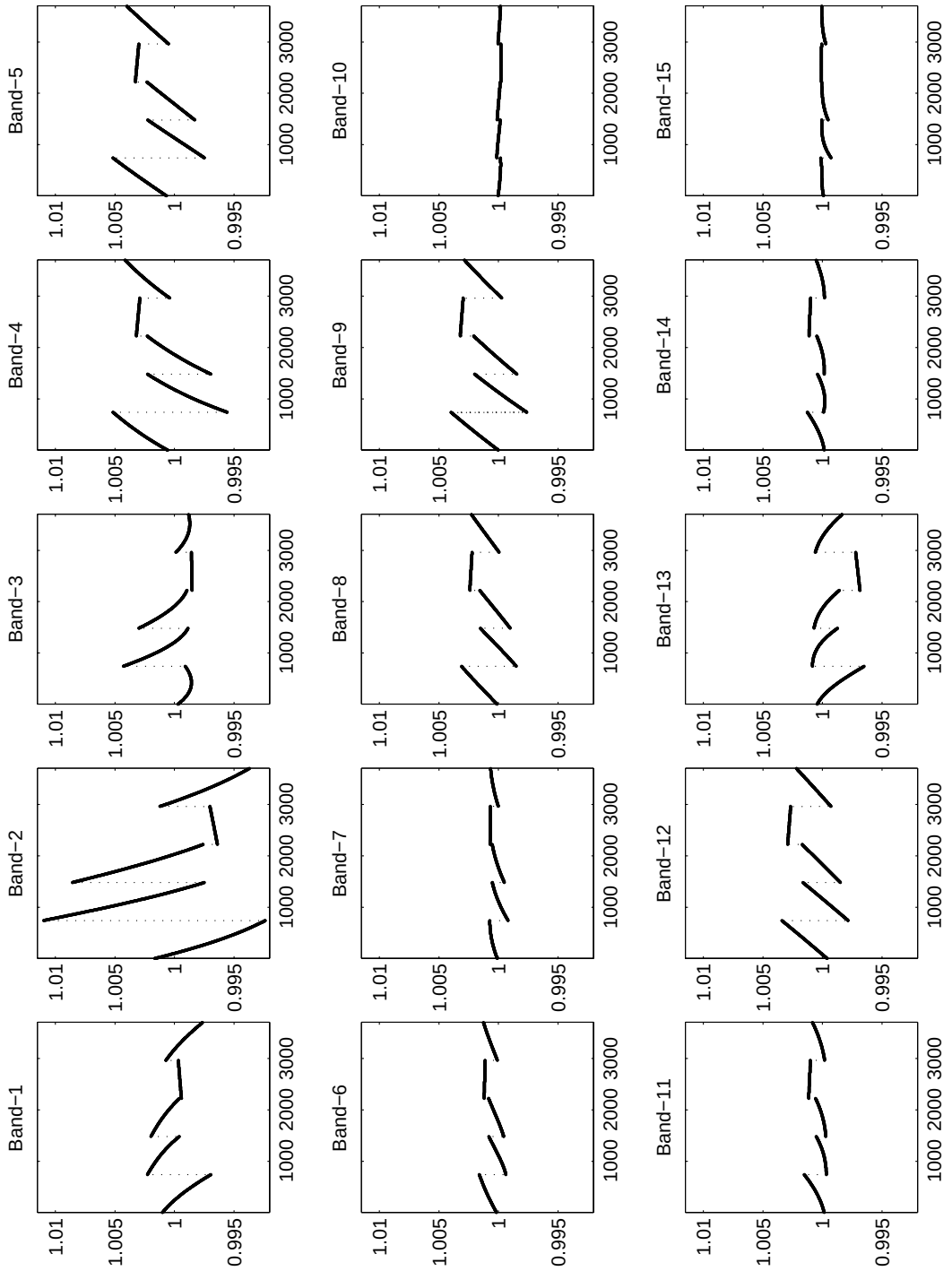

Figure 2.2. Irradiance correction factors for each CCD detector (x axis) and MERIS spectral band.

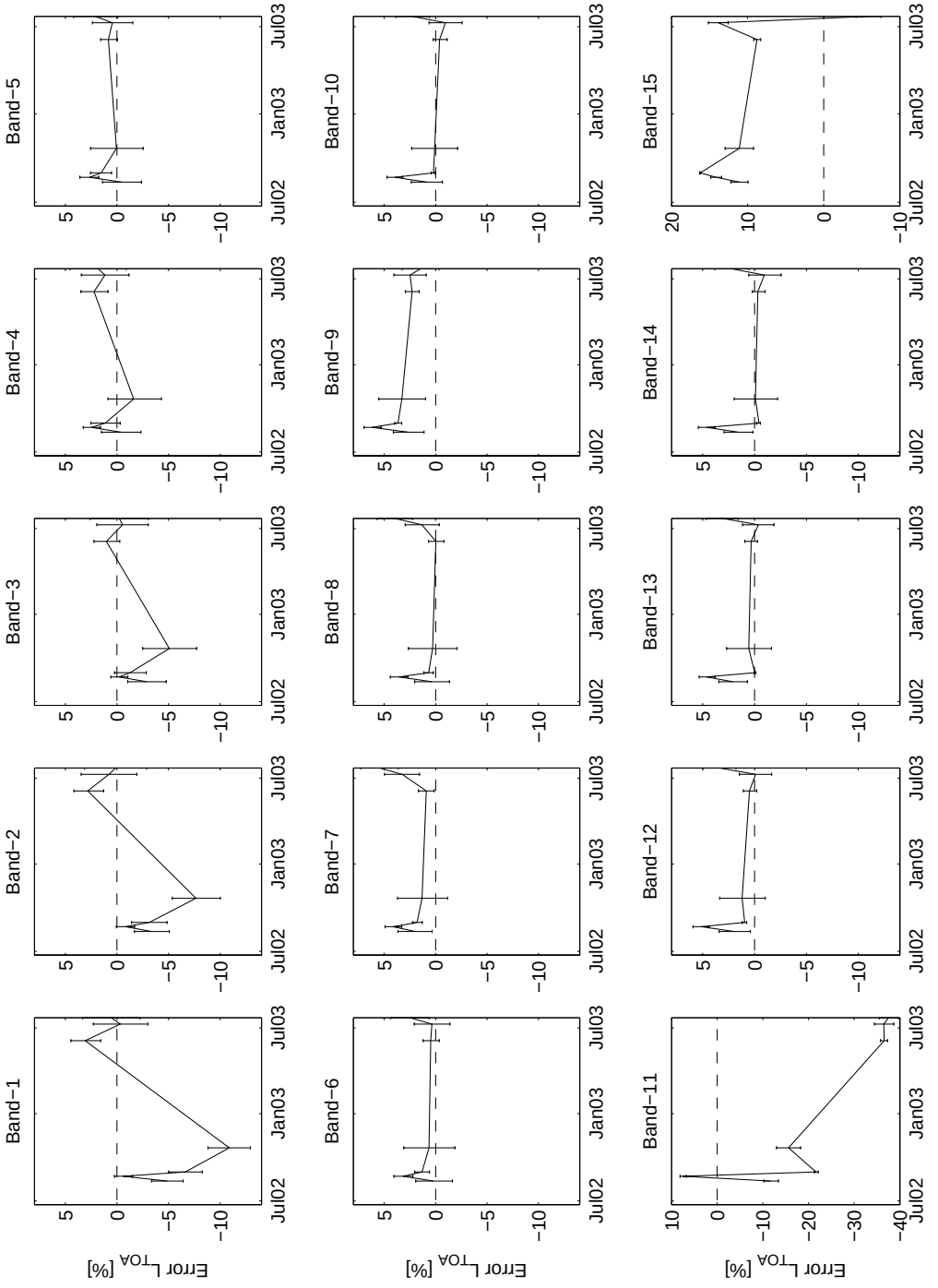

Figure 2.3. Temporal evolution of the calibration uncertainties for each MERIS band. Relative mean errors, in terms of L_{TOA}, are plotted on the y-axis. Figure based on the following MERIS FR acquisition dates (values between brackets correspond to the ground measuring dates): 12/08/2002 (15/08/2002), 22/08/2002 (22/08/2002), 31/08/2002 (22/08/2002), 21/10/2002 (21/09/2002), 09/07/2003 (22/07/2003) and 22/07/2003 (22/07/2003).

Figure 2.3 illustrates the vicarious calibration errors obtained for each MERIS band and acquisition date of the vicarious calibration experiment. The y-axis of the bands most affected by the atmosphere (bands 11 and 15) has been rescaled due to the large errors present in these bands. The error bars used in Figure 2.3 represent the uncertainty of the vicarious calibration errors. These uncertainties can be mostly attributed to variations of aerosol optical properties originating from a short delay between ground measurements and MERIS data acquisition, as well as the approach used to invert the sun-photometer data to retrieve horizontal visibility using a radiative transfer based approach. The calibration approach for the ground spectrometer is discussed in detail in Schaepman and Dangel (2000), whereas the vicarious calibration procedure and resulting uncertainties can be found in Kneubühler et al. (2004; 2002).

Two assumptions are made here: (i) the uncertainty of the radiometric error can be disregarded, therefore, the vicarious correction will be based on the mean error; and (ii) a linear interpolation technique can be used to estimate the mean radiometric error of any acquisition located in-between of two given vicarious calibration efforts.

Table 2-1 presents the linearly interpolated vicarious calibration correction factors for the 14th of July. Equation 2.3 (derived from Eq. 2.2) shows how to compute the MERIS vicarious corrected radiances (L^i_{VC}) based on the measured radiances (L^i_{RAW}) and the relative mean error (*RME*).

$$L^i_{VC} = L^i_{RAW} \cdot \left(1 - \frac{RME^i}{100}\right) \tag{2.3}$$

Table 2-1. MERIS FR Level 1b vicarious correction factors (VC) interpolated from the RRVP vicarious calibration experiments to the 14th of July 2003 acquisitions over The Netherlands.

Band	3	4	5	6	7	8	9	10	12	13	14
VC	1.004	0.985	0.989	0.988	0.959	0.976	0.979	0.997	0.987	0.990	0.997

2.2.2 Land use database

In this study, the latest version of the Dutch land use database (LGN4) was used as reference (Hazeu 2004). This geographical database describes 39 main land uses in The Netherlands based on multi-temporal classification of high resolution satellite data and integration of ancillary data. The LGN4 has a grid structure (cell size of 25 meters) and is based on data from the years 1999 and 2000. The overall classification accuracy is between 85 and 90 % (de Wit and Clevers 2004).

The initial 39 land use classes of the LGN4 were aggregated into 9 main land cover classes: grassland, arable land, greenhouses, deciduous forest, coniferous forest, water, built-up areas, bare soil (incl. sand dunes), and natural vegetation. These 9 classes were chosen in correspondence with the International Geosphere-Biosphere Programme (IGBP) land use class definition.

A spatial aggregation of the LGN4 database was also performed in order to match the MERIS FR pixel size (Figure 2.4, left). This aggregation was based on a majority filter with a

kernel size of 12 original LGN pixels (25 m × 12 = 300 m). The land cover class having the highest abundance in each 12 by 12 kernel was selected to label the new 300 m pixel.

The spatial aggregation of the LGN was also used to support the selection of the endmembers to be used for the spectral unmixing (see section 2.2.3 for more details). The proportion of every class within the kernel was recorded during the aggregation process, such that a so-called standard purity index (SPI) could be calculated from each kernel window, as noted in Eq. 2.4:

$$SPI = \sqrt{\frac{\sum_{i=1}^{nc}\left(f_i - f_{\text{maxclass}}\right)^2}{nc-1}} \tag{2.4}$$

where f represents the fraction of each land use in the kernel, f_{maxclass} is the maximum fraction (the class driving the labelling process), and nc is the total number of classes. Consequently, the SPI equals one when there is only one class in the kernel window (or pixel at 300 m spatial resolution) and the SPI equals zero when all the classes are present in the same proportion.

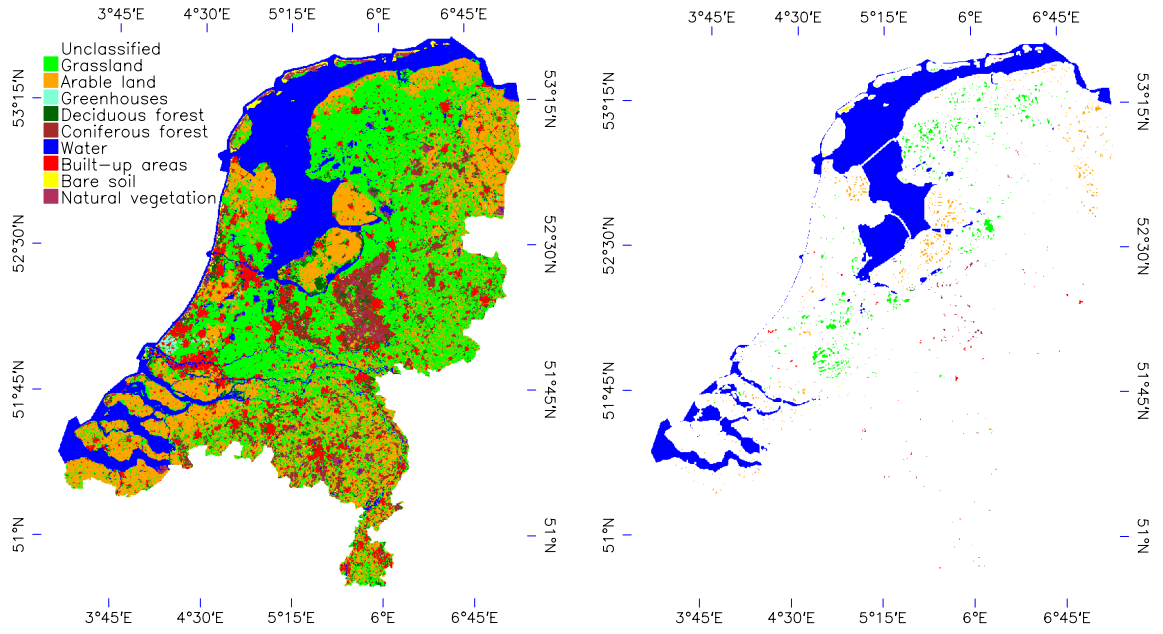

Figure 2.4. Left: The Dutch land use database LGN4 aggregated into 9 land use classes and resampled to 300 m pixel size. Right: 'Pure' pixel selection in The Netherlands using the Standard Purity Index (SPI) combined with the moving window filter.

A threshold SPI of 0.9 was defined as minimum criterion to define "pure" areas for all the classes except for the class greenhouses where the SPI threshold was set to 0.6 in order to

obtain at least a few pixels of this sparse and relatively small class. After selecting the most homogeneous pixels present in the LGN, a moving window filter of 3 by 3 pixels was applied in order to minimize possible adjacency effects. Thus, only "the most pure" pixels surrounded by the same land cover class were finally selected. Figure 2.4 (right) displays all the pixels that cover the homogeneity criteria as developed above. Table 2-2 lists the number of homogeneous pixels per class that will subsequently be used to generate pure land cover signals or endmembers. At this point, it is interesting to notice that the class arable land might present a wide range of situations. For instance, some of the homogeneous areas might belong to developed crops whereas some other areas could be just planted or even bare soils. For the 14th of July, we expect to find developed crops in most of the country. Therefore, arable land will be mapped using a unique spectral signature (endmember).

Table 2-2. Number of identified homogeneous pixels per aggregated land cover class in LGN4.

Land cover	Number of pixels
Greenhouses	25
Grassland	4927
Arable land	2629
Deciduous forest	33
Coniferous forest	201
Water	58285
Built up areas	390
Bare soil	132
Natural vegetation	169

In this paper, the Jeffries-Matusita (JM) distance will be used to quantify the spectral separability of the endmembers. The comparison of the JM distance computed at different radiometric levers will be used to assess the impact of such radiometric corrections on the spectral separability of the different land cover classes. The JM distance ranges between 0 and 2, where 2 means perfect class separability (Richards 1986).

2.2.3 Spectral unmixing

A fully constrained linear spectral unmixing (Hu et al. 1999; Nielsen 2001) was applied to classify the MERIS FR scene because at that scale it is likely that more that one land cover type will be present within one pixel. Linear spectral unmixing provides two main outputs: the sub-pixel fractional land cover composition and the spectral root mean square error (RMSE) per pixel. This RMSE will be used to analyse the effects of classifying MERIS images at different radiometric levels (Schaepman et al. 2004).

All linear unmixing techniques assume that there is no multiple scattering occurring within the different land cover types present in each pixel (Settle and Drake 1993). In that case, the signal received per pixel is a linear combination of the signals corresponding to "pure" areas of each land cover type weighted by their area within the pixel. This can be formalised in a set of mixing equations. Let *nb* and *nc* represent the number of bands and classes respectively, then:

$$p_i = \sum_{c=1}^{nc} (f_c \cdot \mu_{ci}) + e_i \qquad i = 1,2,...,nb \tag{2.5}$$

Where p_i is the pixel value for the band-*i*, f_c is the fraction of the land cover-*c* present in that pixel and μ_{ci} is the pure signal of the land cover-*c* in the band-*i*. The term *e* represents the errors due to (sensor) noise.

In this case, two conditions were added to make the unmixing fully constrained (Eq. 2.6). This guaranteed a physical interpretation of the results since the fractions will sum up to 100 % and we ensure that all the fractions are positive. Poor performances have been reported when using uncontrained linear unmixing (Chang and Heinz 2000).

$$0 \le f_c \le 1 \text{ and } \sum_{c=1}^{nc} f_c = 1.0 \tag{2.6}$$

The fully constrained linear spectral unmixing was rewritten in a matrix-vector notation (Eq. 2.7) and implemented in MATLAB.

$$\mathbf{A}_{(nbxnb)} \cdot \mathbf{P}_{(nbx1)} = \mathbf{B}_{(nbxnb)} \cdot \mathbf{M}_{(nbxnc)} \cdot \mathbf{F}_{(ncx1)} + \mathbf{E}_{(nbx1)} \tag{2.7}$$

where **P** is the vector storing the MERIS radiance values per pixel, **M** is the matrix containing the spectra of the endmembers, **F** is the vector of the fractions or abundances that we seek and finally, **E** is the vector of errors. In this paper, **M** was determined by averaging the homogeneous areas that were identified during the LGN aggregation (Table 2-2; Figure 2.4). Notice that two extra matrices, namely **A** and **B**, have been added to the standard matrix-vector notation of the linear spectral unmixing to account for the different radiometric calibration levels. **A** and **B** are therefore $nb \times nb$ matrices that contain the smile or the smile + vicarious correction factors for a given pixel and for the endmembers, respectively. In general these two matrices are not equal since the correction factors have a spatial dependence. For instance, the smile correction factors are specific for each CCD detector.

Because of the set of inequalities present in Eq. 2.6, the Lagrange multipliers method cannot be used to solve Eq. 2.5 subject to Eq. 2.6. As a result, the problem is transformed into a constrained linear least squares problem. The solution for the vector **F** should result in the smallest possible residual error (where the operator MIN{} represents a minimising function for the expression):

$$\text{MIN}\{(\mathbf{A} \cdot \mathbf{P} - \mathbf{B} \cdot \mathbf{M} \cdot \mathbf{F})^T (\mathbf{A} \cdot \mathbf{P} - \mathbf{B} \cdot \mathbf{M} \cdot \mathbf{F})\} \tag{2.8}$$

The vicarious correction represents a particular case because the correction factors are unique for each band (i.e. not spatially dependent) and therefore **A** is equal to **B** and equal to

the diagonal matrix containing the vicarious correction factors presented in Table 2-1. For this specific case Eq. 2.8 can be re-written as follows:

$$\mathrm{MIN}\{(\mathbf{P} - \mathbf{M}\cdot\mathbf{F})^{\mathrm{T}}(\mathbf{A}^{\mathrm{T}}\cdot\mathbf{A})(\mathbf{P} - \mathbf{M}\cdot\mathbf{F})\} \quad (2.9)$$

Contrarily to other classifiers (e.g. maximum likelihood), a linear transformation of the data will result in a different solution (classification) since the factor $\mathbf{A}^{\mathrm{T}}\cdot\mathbf{A}$, which summarises the vicarious correction factors, will modify the weights of the unmixing equations.

The land cover mapping approach described in this paper involves the classification (unmixing) of the MERIS image at the L_{RAW}, L_{SMILE} and L_{VC} radiometric levels. To do this, a unique set of endmembers was generated for each of these radiometric levels and subsequently used to unmix the images at the different radiometric levels.

As noted in literature, endmembers can be obtained from spectral libraries or from the images themselves (Ichoku and Karnieli 1996). In this study, we selected all the endmembers from the images and we simulated the effect of working with endmembers coming from another source (spectral library) by classifying the L_{RAW} and the L_{SMILE} image with radiometrically enhanced endmembers. Table 2-3 shows the six unmixing study cases selected in this paper.

Table 2-3. Spectral unmixing study cases.

Case #	Image	Endmembers
1	L_{RAW}	L_{RAW}
2	L_{RAW}	L_{SMILE}
3	L_{RAW}	L_{VC}
4	L_{SMILE}	L_{SMILE}
5	L_{SMILE}	L_{VC}
6	L_{VC}	L_{VC}

The usage of a unique set of endmembers to unmix large regions has previously been reported in literature (Fernandes et al. 2004). However, in our case this approach is limited by two major assumptions: (i) the test site is atmospherically constant and, thus it can be approximated by one singular atmosphere and (ii) the potential directional effects present in the endmembers can be disregarded. We base our approach on these assumptions, recognizing that the major contributor to the final uncertainty is inherently the heterogeneity of the land cover classes present at the MERIS pixel level.

Similar to other authors, MERIS bands 1 and 2 were omitted from this study, as they are very susceptible to atmospheric influences; bands 11 and 15 were also excluded because these bands coincide with the absorption features of oxygen and water vapour; thus not adding relevant information to land cover classification approaches (Clevers et al. 2007).

2.2.4 MERIS land products and vegetation indices

The effects of the radiometric corrections on the fAPAR, the MTCI and the NDVI were evaluated by comparing these products at the three radiometric levels under study: L_{RAW}, L_{SMILE} and L_{VC}.

The fAPAR products were computed using the BEAM FaparProcessor (version 1.0) developed by Aussedat and Gobron (2004). This processor was designed to work with Level 1b data and reproduces the algorithms used for the MERIS level 2 product.

The MTCI and NDVI products were computed using equations 2.10 and 2.11 respectively. In these equations, Bx represents the x^{th} band of MERIS transformed to TOA reflectances (planetary reflectances).

$$MTCI = \frac{B10 - B9}{B9 - B8} \tag{2.10}$$

$$NDVI = \frac{B13 - B7}{B13 + B7} \tag{2.11}$$

This transformation was required because the MTCI was designed to operate on reflectance data. To convert from TOA radiance to TOA reflectance, the average solar irradiance per band, S^i ($Wm^{-2}\mu m^{-1}$), and the solar angle, ϑ_s, should be known. Both parameters were obtained from the MERIS metadata provided in the data header. After that, the planetary reflectances were computed using Eq. 2.12.

$$R^i_{TOA} = \frac{\pi \cdot L^i_{TOA}}{S^i \cdot \cos\vartheta_s} \tag{2.12}$$

2.3 Results and discussion

2.3.1 Land cover classification

The matrix **M** of endmembers (or **B**×**M** when working with the smile or vicariously corrected images) was computed by averaging the most homogeneous areas identified via the SPI thresholds and the moving window (Table 2-2; Figure 2.4, right). As an example, Figure 2.5 shows the spectral signatures of the 9 endmembers obtained from the raw image.

The JM distance was computed for the different pairs of endmembers and for the different radiometric levels. Table 2-4 shows the JM distances for the L_{RAW} and the L_{SMILE} calibration levels. L_{VC} distances are equal to the L_{SMILE} distances since the transformation from one level to the other is linear. All distances were ranging between 1.93 and 2 (Table 2-4), therefore, no clear conclusion could be drawn from these results. Nonetheless, the high values obtained for this distance prove that the selection of the homogeneous areas to identify image endmembers was correct.

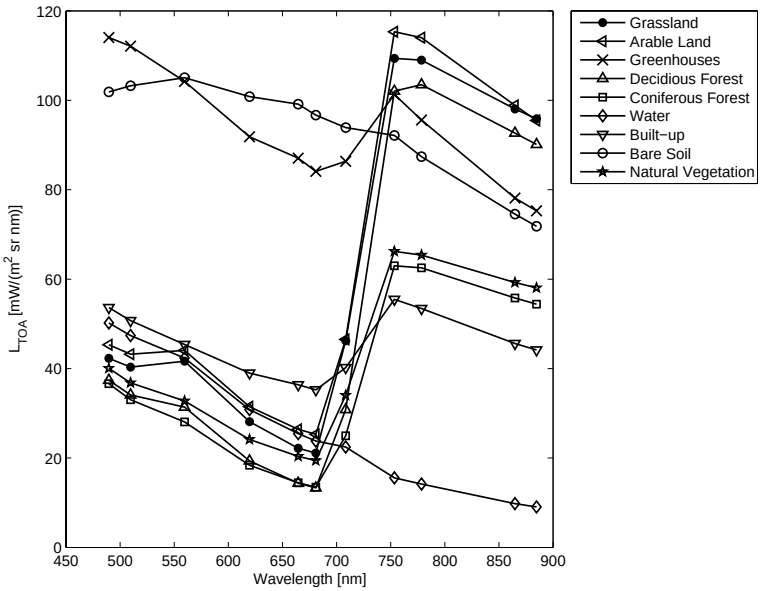

Figure 2.5. Endmembers derived from the L_{RAW} image.

The unmixing results were turned into a hard classification by using the class having the highest abundance to label the pixel. This transformation facilitates the classification accuracy analysis. Figure 2.6 illustrates, as an example, the hard classified and the RMSE image at the best radiometric level (case 6). The overall classification accuracies for the different cases described in Table 2-3 are given in Table 2-5.

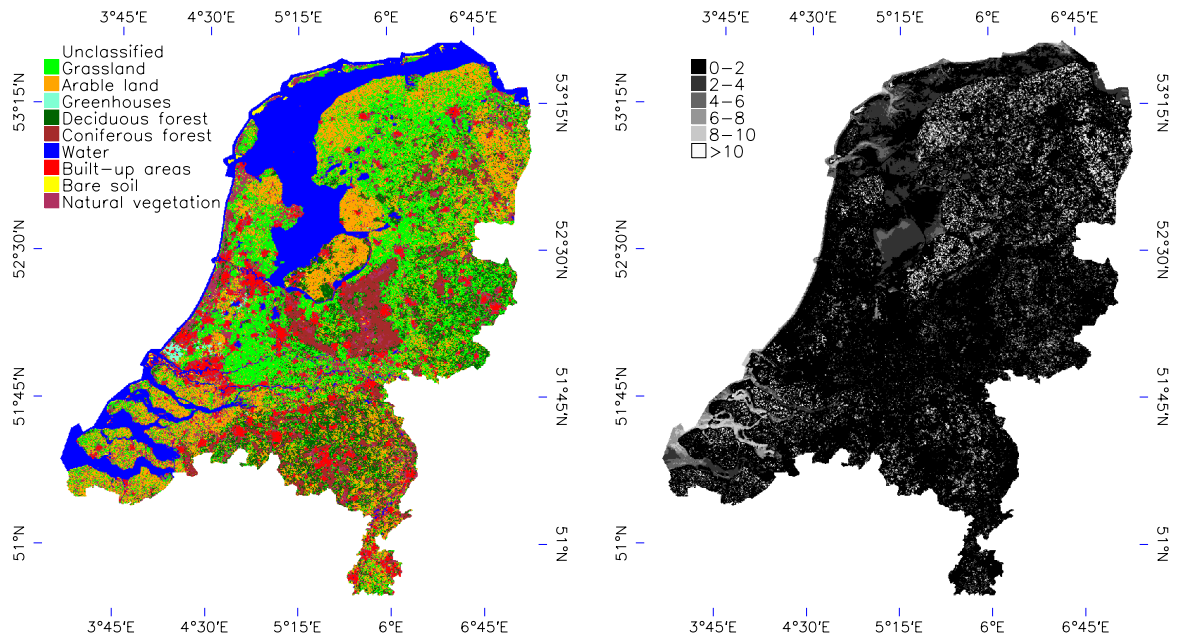

Figure 2.6. Left: classified image according to case 6 (Table 2-3); Right: corresponding RMSE image.

Table 2-4. JM distance for the L_{RAW} and the L_{SMILE} endmembers.

Classes	Greenhouses	Grassland	Arable Land	Dec. Forest	Con. Forest	Water	Built-up	Bare soil	Natural veg.
Greenhouses	--								
Grassland	1.99999717 1.99999706	--							
Arable Land	1.99995346 1.99996802	1.93644338 1.92882990	--						
Dec. Forest	1.99999996 1.99999999	1.99666961 1.99696890	1.99539317 1.99513582	--					
Con. Forest	1.99999832 1.99999928	1.99999876 1.99999890	1.99997188 1.99997193	1.99994947 1.99995120	--				
Water	1.99999997 1.99999998	2 2	2 2	2 2	2 2	--			
Built up	1.99995717 1.99997119	1.99995610 1.99995130	1.99800714 1.99785055	1.99999849 1.99999830	1.99621152 1.99624770	1.99992187 1.99990880	--		
Bare soil	2 2	2 2	1.99999984 1.99999986	2 2	2 2	1.99978554 1.99980370	1.99999999 2	--	
Natural Veg.	1.99989368 1.99992909	1.91033970 1.91363220	1.98445527 1.98291530	1.98912581 1.98781610	1.95284747 1.95033170	1.99999937 1.99999930	1.99196590 1.99158020	2 2	--

Upper and lower JM distance values were computed using the L_{RAW} and the L_{SMILE} images respectively.

Table 2-5. Classification accuracy and RMSE statistics for the different study cases.

Case #	Class Acc.	Mean RMSE	SD RMSE	CV RMSE
1	53.5279	1.9528	3.1101	159.2636
2	53.5329	1.9523	3.1100	159.2993
3	53.7096	2.0999	3.1127	148.2309
4	53.5400	1.9503	3.1100	159.4626
5	53.7068	2.0993	3.1122	148.2494
6	53.5355	1.9269	3.0753	159.5983

SD = Standard deviation; CV = Coefficient of variation

From these classification results, we can conclude that when the endmembers are selected from the image itself (cases 1, 4 and 6), the level of calibration is not very critical because the overall classification accuracy is almost the same. These results were expected since the smile and the vicarious correction factors were close to one (Figure 2.2; Table 2-1). The overall classification accuracy achieved for these cases was around 53.5 %.

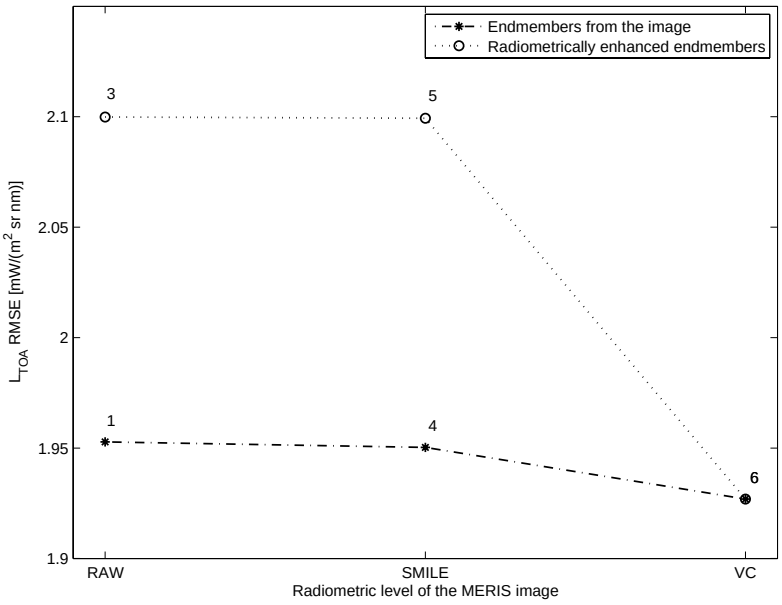

Figure 2.7. Mean RMSE for the different classification cases (numbers refer to the cases in Table 2-3).

With respect to the mean RMSE, we observed a decreasing trend (Figure 2.7; cases 1, 4 and 6) that shows that working with radiometrically enhanced images improves the fit of the data to the endmembers. Recall that although the smile effect is very small, it is spatially dependent and, therefore, its correction makes the pixels on different CCDs more comparable.

For the cases 2, 3 and 5, where a more radiometrically sound endmember is applied to an image with a lower radiometric level, we found that the classification accuracy was slightly better that for the cases 1, 4 and 6. However, the mean RMSE for the cases 3 and 5 was larger

than before (Figure 2.7). This is because the images still contain the "radiometric noise" that was removed from the endmembers.

Considering that the spectral unmixing was performed over the whole of The Netherlands, and the degree of heterogeneity present at sub-pixel level, we believe that the classifier performed reasonably well. Most of the misclassifications occurred in the eastern and southern parts of the country, which correspond to the most fragmented landscapes of The Netherlands (according to the SPI values). The application of a majority filter to remove the "salt and pepper" effect found in the classified images might result in an improvement of the final classification accuracy (Lillesand and Kiefer 2000).

In general, we can conclude that spectral unmixing of MERIS images is a promising option. The results presented here have demonstrated that it is possible to identify endmembers for the main land cover types. Nevertheless, further research needs to be devoted to improve and refine the methods so that better classification accuracies can be obtained.

2.3.2 MERIS land products and vegetation indices

The fAPAR, MTCI and NDVI products were computed from the L_{RAW}, L_{SMILE} and L_{VC} data. The mean, standard deviation and coefficient of variation of these products over the study area are given in Table 2-6.

Table 2-6. Mean, standard deviation and coefficient of variation for the MERIS products computed at different radiometric calibration levels.

		fAPAR	MTCI	NDVI
Raw	Mean	0.58481	3.4402	0.67586
	SD	0.19572	0.73591	0.13361
	CV	33.468	21.392	19.77
Smile	Mean	0.58415	3.4409	0.67583
	SD	0.19581	0.73686	0.13367
	CV	33.52	21.414	19.778
Smile +VC	Mean	0.58407	3.5373	0.68399
	SD	0.19538	0.74695	0.13167
	CV	33.452	21.116	19.25

These results show that both the smile effect present in the MERIS instrument and the radiometric shifts observed during the vicarious calibration experiment did not have a big effect on the fAPAR, MTCI and NDVI products. The RMSE and correlation coefficient using the L_{RAW} data as a reference were computed to better quantify the effects of the radiometric correction over these products (Table 2-7). The MTCI appears to be the product most sensitive to the radiometric corrections.

Table 2-7. RMSE and coefficient of correlation with respect to the L_{RAW} data.

		fAPAR	MTCI	NDVI
Smile	RMSE	0.0021	0.0111	0.0002
	Coef Corr	0.9999	0.9999	1
Smile+VC	RMSE	0.0033	0.1007	0.0086
	Coef Corr	0.9999	0.9995	1

A mean-difference plot (Cleveland 1985) was used to show the difference between the MERIS products computed at different radiometric calibration levels (Figure 2.8). In this type of plot, the difference between the two series is plotted against the mean value of these series. In our case, the L_{RAW} data was considered as a reference. Therefore, the y-axis in Figure 2.8 presents L_{RAW} minus L_{SMILE} data (upper row) and L_{RAW} minus L_{VC} (bottom row).

The fAPAR subplots of Figure 2.8 indicate that this product is computed on the basis of isolines: the correction factors need to pass a certain threshold value to be attributed to a change of isoline (this explains the zero difference values and the horizontal striping of these subplots). When there is an fAPAR change it is always a multiple of 0.004 because the fAPAR values given by the fAPAR processor are scaled as integers in the range from 1 to 250. Therefore, 1 unit change is translated in 1/250 fAPAR change which is equal to 0.004.

For the MTCI, the smile correction resulted in an asymmetrical mirrored image around the zero line (Figure 2.8, top row, middle plot). This asymmetrical shape might be introduced by land use specific behaviour or a non-perfect smile corrections in the 5 MERIS cameras. The result of the vicarious calibration effort on the MTCI (Figure 2.8, bottom row, middle plot) shows that the MTCI values computed at the L_{VC} level are always greater than when using the L_{RAW} data. These differences are driven by the magnitude of the vicarious calibration correction factors as well as by the land cover types (mainly urban versus vegetated areas).

Similar to the fAPAR, the smile correction resulted in hardly any change for the NDVI values (notice the 10^{-4} factor on the y-axis, top row, right plot). However, in this case the changes are symmetric with respect to the zero line and this explains why the mean values for the L_{RAW} and L_{SMILE} based products were so similar (Table 2-7). After the vicarious correction, the NDVI plot follows a parabolic function. This is because (in this case) the correction factor for band 7 is smaller than for band 13 (Table 2-1) and, as a result, the L_{VC}-based NDVI values are higher (the difference is always negative). Additionally, from the NDVI expression (Eq. 2.11) we see that the relative changes in NDVI are higher for low NDVI values. In summary, the NDVI based on L_{RAW} data underestimates the "real" NDVI values and this underestimation is larger for low NDVI values.

The spatial component of these radiometric corrections was also explored in this study. As an example, Figure 2.9 illustrates the ratio between the L_{SMILE}-based and the L_{RAW}-based products (the figure was similar for the fAPAR, MTCI and NDVI products). This figure shows that for some areas the ratio is under one (red), for some areas it is equal to one (black), and for some it is greater than one (blue). We can observe that the smile correction is camera dependent because the ratio values on the Western part of the image (covered by the MERIS camera 3) are generally smaller than one, whereas in the Eastern part of the country (MERIS camera 2) the values tend to be higher after the radiometric correction (ratio above 1).

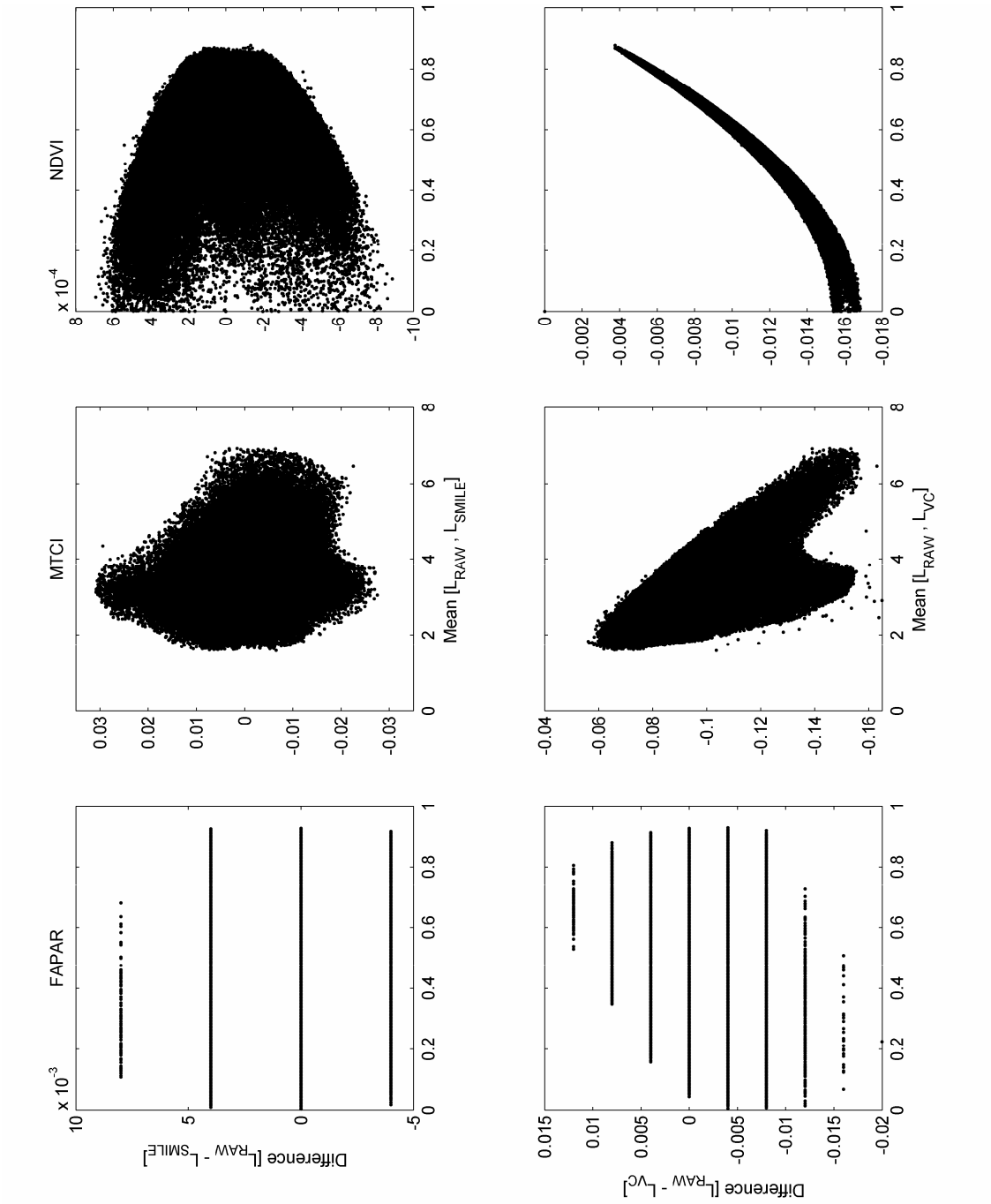

Figure 2.8. Mean-difference plot for all the MERIS products.

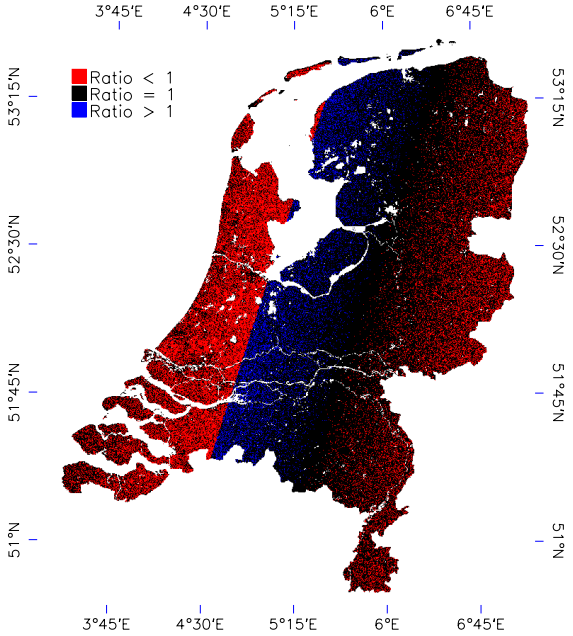

Figure 2.9. Ratio L_{SMILE}-based/L_{RAW}-based product (the colours red, black and blue indicate the areas where the ratio was smaller than one, equal to one or greater than one, respectively).

2.4 Conclusions

In this paper we have studied the smile effect and the vicarious calibration corrections for the MERIS instrument and their impact on radiometry and product accuracy. The implications of applying these radiometric corrections to compensate for these shifts have been evaluated using two approaches: regional land cover mapping using linear spectral unmixing and the calculation of MERIS land products: fAPAR, MTCI and NDVI.

The regional land cover mapping case has shown that if the classifier is trained with data coming from the same image (image based endmembers), then the level of calibration is not that critical because the impact of both the smile and the vicarious corrections is very small (the correction factors are close to 1). If the image is to be classified with endmembers that are coming from a not well corrected image or if we plan to build our own spectral library, then classification differences become significant. In this respect, for multitemporal MERIS analysis, all recommended correction factors must be applied in order to preserve highest possible classification accuracy.

With respect to the MERIS land products, a relevant difference was observed between the L_{VC} and the L_{RAW} based products. In addition, we have shown that the magnitude of the smile correction factors can be locally very important (Figure 2.9).

In order to generate long term, stable observations, it is of utmost importance to generate stable and reproducible HDRF (Hemispherical-Directional Reflectance Factor) measurements. Current calibration approaches as the one applied for MERIS have uncertainties that are much smaller than the estimated atmospheric or product uncertainties.

Acknowledgements

We would like to thank Carsten Brockmann, from Brockmann Consult, for timely MERIS data processing and delivery. Kurt Thome from the University of Arizona is thanked for providing ground data of the RRVP. The two anonymous reviewers are also thanked for helping in improving the quality of the manuscript. The contribution of R. Zurita-Milla is granted through the Dutch SRON GO programme (EO-061).

CHAPTER 3

Unmixing-based Landsat TM and MERIS FR data fusion*

* Based on: Zurita-Milla, R., Clevers, J.G.P.W. and Schaepman, M.E. (2008). Unmixing-based Landsat TM and MERIS FR data fusion. *IEEE Geoscience and Remote Sensing Letters*, 5, 453-457.

Unmixing-based Landsat TM and MERIS FR data fusion

Abstract

An unmixing-based data fusion technique is used to generate images that have the spatial resolution of Landsat TM and the spectral resolution provided by the MERIS sensor. The method requires the optimization of two parameters: the number of classes used to classify the TM image and the size of the MERIS 'window' (neighborhood) that is used to solve the unmixing equations. The ERGAS index is used to assess the quality of the fused images at the TM and at the MERIS spatial resolutions and to assist with the identification of the best combination of the two parameters that need to be optimized. Results indicate that it is possible to successfully downscale MERIS full resolution data to a Landsat-like spatial resolution while preserving the MERIS spectral resolution.

3.1 Introduction

During the last few years, data fusion methods have received more and more attention from the remote sensing community because of the increasing need to integrate the vast amount of data that is being collected by Earth observation satellites. As a result, a large number of data fusion methods have been developed (see, for example, (Ehlers 1991; Hall and Llinas 1997; Pohl and Van Genderen 1998; Wald 2002) for a review). In this letter, we focus on the implementation and evaluation of the so-called unmixing-based data fusion approach (Zhukov et al. 1999). The aim of this data fusion approach is to combine two images acquired over the same area but at different spatial resolutions to produce an image with the spatial resolution of the high spatial resolution image and the spectral resolution of the low spatial resolution image. Often, the selected low spatial resolution image has a better spectral resolution than the high spatial resolution image. As a result, the fused image has (potentially) more information than each of the original images. A simplified version of this data fusion approach has been used by Minghelli-Roman et al. (2001; 2006) to combine MERIS full resolution (FR) and Landsat ETM data for coastal water monitoring. In their approach only one parameter, namely the number of classes used to classify the high resolution image, needs to be optimized because they solve the unmixing equations for the whole image at once. A large number of classes (typically >100) is needed to achieve good results with this method (Minghelli-Roman et al. 2001; Minghelli-Roman et al. 2006). However, such a large number of classes is not always feasible or realistic. For instance, if an existing land cover classification is used to get the high spatial resolution information, then the number of classes is limited and in most cases well below 100. Furthermore, solving the unmixing equations for the whole image at once might severely hamper the quality and usability of the fused images because all pixels belonging to one class will get the same spectral signature. In other words, if we apply the method as described by Minghelli-Roman et al. (2001; 2006), we implicitly reject all the within class variability. Therefore, we believe that using a neighborhood should be preferred over simultaneously solving the unmixing for all the pixels present in the scene. For that reason, here we implement a detailed version of the unmixing-based fusion algorithm where two parameters, the number of classes used to classify the TM image and the size of the MERIS FR neighborhood used to solve the unmixing equations, need to be optimized. The ERGAS index (Wald 2002) is used to support the optimization of these two parameters and to quantitatively assess the quality of the fused images.

Finally, this letter presents a case study that uses MERIS FR and Landsat TM data over land because several studies have proven the potential of MERIS for this kind of applications (Clevers et al. 2002; Clevers et al. 2007; Verstraete et al. 1999). If the proposed data fusion approach proves to be successful, the resulting fused images could be used to improve land cover maps and/or to monitor ecosystems at high spatial and spectral resolutions.

3.2 Methodology

The study area covers approximately 40 km × 60 km of the central part of The Netherlands (52.19° N, 5.91° E). A Landsat-5 TM image from 10 July 2003 and a MERIS full resolution (FR) level 1b image acquired on 14 July 2003 were available over this area. The TM image was geo-referenced to the Dutch national coordinate system (RD) using a cubic convolution resampling method and a pixel size of 25 m. The digital numbers of the TM image were

converted into radiances (W m^{-2} sr^{-1} μm^{-1}) using the latest calibration coefficients (Chander and Markham 2003) to ensure that both the TM and the MERIS image are in the same radiometric units. The MERIS FR level 1b image (300 m pixel size with radiances in W m^{-2} sr^{-1} μm^{-1}) was first corrected for the smile effect (Zurita-Milla et al. 2007a). Then, an image-to-image co-registration was performed in order to ensure the best possible match between the two images. In this process, the TM image was used as a reference and a nearest neighbor resampling was used not to modify the original MERIS pixel values. The pixel sizes of the TM and MERIS FR sensors were preserved, which implies that 144 TM pixels are inside each MERIS FR pixel. Subsequently, the TM and the MERIS FR images were fused using an unmixing-based data fusion approach. The method consists of four main steps (Zhukov et al. 1999):

First, the high spatial resolution image is used to identify the main components (i.e. spectral groups) of the study area. For this purpose, the TM image was classified into *nc* unsupervised classes using the ISODATA classification rule. In this work five *nc* values were used: 10, 20, 40, 60 and 80.

Secondly, a sliding window of $k \times k$ MERIS FR pixels is applied to each of the TM classified images to generate class proportion matrices. These matrices contain the proportions of each of the *nc* classes that fall within each of the MERIS FR pixels that are inside the $k \times k$ window. In this study, 14 window sizes (from now on referred to as neighborhoods) were tested: from $k = 5$ to $k = 53$ in steps of 4.

Thirdly, the spectral information of all the classes present in the $k \times k$ neighborhood is unmixed using the proportion matrices and their corresponding MERIS FR radiance values. Here it is important to notice that the unmixing is solved for each low resolution band independently. Therefore, care must be taken to select a neighborhood size (k^2) larger than or equal to the number of classes present in the neighborhood because each MERIS FR pixel provides only one (mixing) equation. Although the unmixing is solved for all the classes present in the neighborhood, only the spectral information of the classes present in the central pixel of the neighborhood is kept because that is the pixel that is being effectively unmixed.

Finally, each of the TM unsupervised classes present in the central pixel of the neighborhood is replaced by its corresponding unmixed MERIS signal. By repeating this operation for all the MERIS FR pixels, for all MERIS bands and for all the possible combinations of *nc* and *k*, a series of fused images is generated.

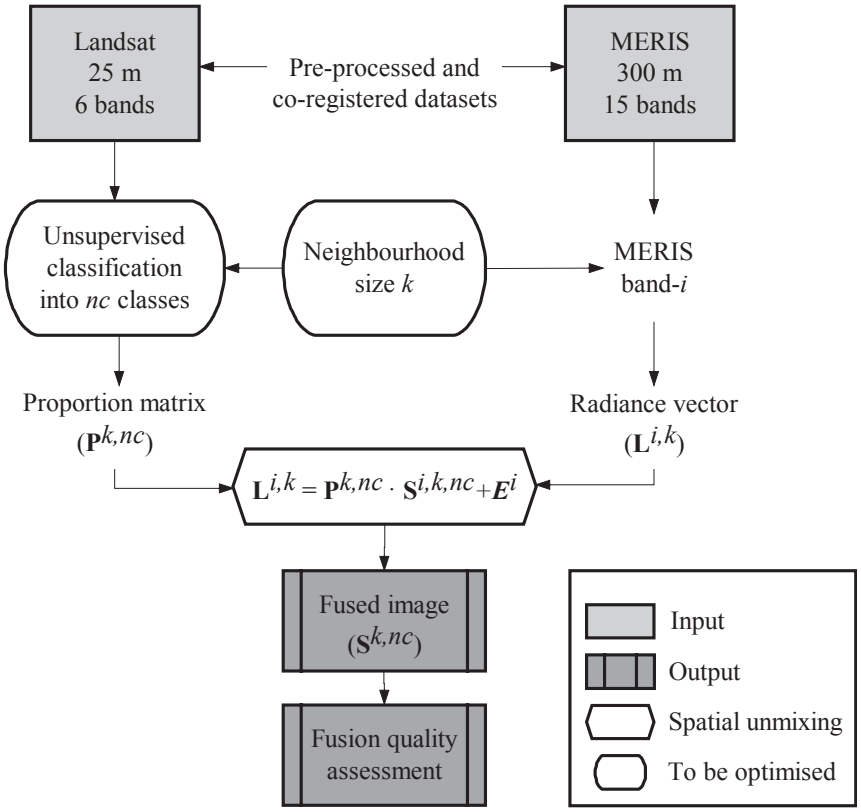

Figure 3.1. Scheme of the general methodology.

Figure 3.1 summarizes the four steps of the unmixing-based data fusion approach and presents a matrix-vector notation for the third step (i.e. the unmixing). This notation should be interpreted as follows:

$$\mathbf{L}^{i,k} = \mathbf{P}^{k,nc} \cdot \mathbf{S}^{i,k,nc} + \mathbf{E}^{i} \quad i = 1,2,\ldots,\mathrm{N} \tag{3.1}$$

where: $\mathbf{L}^{i,k}$ is a ($k^2 \times 1$) vector that contains the values of band-i for all the MERIS FR pixels present in the neighborhood k. $\mathbf{P}^{k,nc}$ is a ($k^2 \times nc$) matrix containing the proportions of the TM unsupervised classes that fall inside each of the MERIS FR pixels present in the neighborhood k. $\mathbf{S}^{i,k,nc}$ is the ($nc \times 1$) unknown vector of unmixed spectral information (band-i radiances) for each of the classes present in k. After iterating over all MERIS pixels and all MERIS bands, $\boldsymbol{S}^{k,nc}$ is the fused image. $\mathbf{E}^{i}$ is a ($k^2 \times 1$) vector of residual errors and N is the total number of bands of the low resolution image.

This formulation of the unmixing-based data fusion indirectly implies that the number of classes used to classify the TM image (nc) and the size of the MERIS FR neighborhood (k) need to be optimized. nc needs to be optimized because it depends on the spectral variability of the scene (heterogeneous scenes will most likely require a larger nc value than homogeneous ones). k also needs to be optimized because it has a great impact on the spectral quality of the fused image. On the one hand k should be kept as small as possible so that the fused image is spectrally dynamic and consistent with the variability recorded by the low spatial resolution sensor. On the other hand k should be sufficiently large to provide enough

equations to solve the unmixing. In other words, Eq. 3.1 is a system of k^2 equations (one equation per low resolution pixel in the neighborhood) with up to *nc* unknowns (depending on the number of classes present in such a neighborhood). This means that k^2 must be greater than or equal to the number of classes inside the MERIS neighborhood. However, if we use very large *k* values, the output image will have low spectral variability because each system of equations results in a unique solution. For instance, if the size of the neighborhood matches the size of the scene (*k* = image size), then all the pixels of one class identified with Landsat TM will have the same spectral response independently of their position within the scene. Using *k* = image size, therefore, results in a fused image with a low spectral dynamic range where each of the classes is represented by an approximation of its mean spectral response. The latter approach was the one used by Minghelli-Roman et al. (2001; 2006). Although it is computationally fast (only one system of equations needs to be solved), here we prefer to also optimize the size of the neighborhood *k* such that we can account for the natural variability of the components present in the scene.

Finally, a constrained least-squares method was used to retrieve $\mathbf{S}^{i,k,nc}$ from Eq. (3.1). The use of a constrained method is justified because the solution should fulfill the following two conditions: a) the radiance values must be positive and b) the radiance values cannot be larger than the MERIS radiance saturation values (ESA EOHelpdesk (personal communication) 2006).

3.2.1 Data fusion quality and optimization of *nc* and *k*

A quantitative assessment of the quality of the fused images was done at the level of the TM and of the MERIS spatial resolution. This assessment was used to support the selection of the best combination of *nc* and *k*.

Bearing in mind that any fused image should be as identical as possible to the original low resolution image once degraded back to its original resolution (coherence property (Wald et al. 1997)), we degraded the fused images, $\boldsymbol{S}^{k,nc}$, to 300 m using a mean filter. After this, we assessed the quality of the degraded fused images by comparing them with the original MERIS FR image. The ERGAS index (Wald 2002) was used for this comparison:

$$ERGAS = 100 \frac{h}{l} \sqrt{\frac{1}{N} \sum_{i=1}^{N} \left(RMSE_i^2 / M_i^2 \right)} \tag{3.2}$$

where: *h* is the resolution of the high spatial resolution image (TM). *l* is the resolution of the low spatial resolution image (MERIS FR). N is the number of spectral bands involved in the fusion. $RMSE_i$ is the root mean square error computed between the degraded fused image and the original MERIS image (for the band-*i*) and M_i is the mean value of the band-*i* of the reference image (MERIS).

The ERGAS index equals zero when the degraded fused image (300 m) is equal to the original MERIS FR image. Therefore, low ERGAS values indicate high image fusion quality.

If we assume that spectrally corresponding bands are highly correlated for images that have been acquired nearly at the same date, then the ERGAS index can also be used to evaluate the quality of the fused images at 25 m. This ERGAS will be named $ERGAS_{TM}$ (because the

Landsat TM image will be used as a reference) whereas the ERGAS computed at 300 m will be referred to as $ERGAS_M$ (MERIS used as a reference). Other terms, like spatial and spectral ERGAS, have been identified in literature to indicate that the ERGAS index is computed at different spatial resolutions (González-Audícana et al. 2006; Lillo-Saavedra and Gonzalo 2006, 2007; Lillo-Saavedra et al. 2005).

The expression used to compute the $ERGAS_{TM}$ is basically the same as Eq. 3.2 except that: a) the $RMSE_i$ is computed between Landsat TM bands 1 till 4 and their spectrally corresponding fused bands (3, 5, 7 and 13, respectively) and b) M_i corresponds to the mean of the band-*i* of the TM image. The $ERGAS_{TM}$ index never reaches a zero value because the bands that were used for the calculation of this index have slightly different characteristics (band centers and bandwidths). Despite this, its values can be used to assess the quality of the fused images because - similar to the $ERGAS_M$ - the lower the $ERGAS_{TM}$, the better the quality of the fused image.

In order to better understand, evaluate and benchmark the values obtained for the $ERGAS_{TM}$, the average coefficient of correlation ($\bar{r}$) was also computed at 25 m. First, the coefficient of correlation was computed for the 4 pairs of bands used to compute the $ERGAS_{TM}$. Then, these values were averaged to produce a single $\bar{r}$ value for each of the fused images.

3.3 Results and discussion

Figure 3.2 illustrates the ERGAS indices and the $\bar{r}$ values for all fused images that were generated for the different combinations of *nc* and *k*.

Most fused images yielded low ERGAS values (Figure 3.2a and Figure 3.2b), which means that the unmixing-based data fusion succeeded in synthesizing the spectral information of the MERIS FR image at a high spatial resolution. However, relatively high $ERGAS_{TM}$ values (>3) were found for the images unmixed using small *k* values. This might indicate that the solution of the unmixing equations is not stable when few equations are used and that regularization methods might be needed in these cases. Poor $\bar{r}$ values (< 0.45) were found when unmixing with small *k* values (Figure 3.2c), whereas high $\bar{r}$ values (>0.75) were always associated with low $ERGAS_{TM}$ values (<2). Because of this opposite behavior, we conclude that the information given by the $ERGAS_{TM}$ and $\bar{r}$ is equivalent. For this reason, we mainly discuss the results obtained using the ERGAS indices.

Two additional observations can be made from Figure 3.2. First, the ERGAS indices are inversely correlated: the $ERGAS_M$ decreases when increasing the number of classes and it increases with larger neighborhood sizes, whereas the $ERGAS_{TM}$ presents the opposite behavior. This means that there is a trade-off between the quality of the fused images at 25 m and at 300 m and that we cannot find an optimum combination of *nc* and *k* that minimizes both ERGAS values. Secondly, both ERGAS indices and the average coefficient of correlation show a saturation behavior. This means that increasing *nc* or *k* beyond the values that were tested in this study will not improve the quality of the fused images.

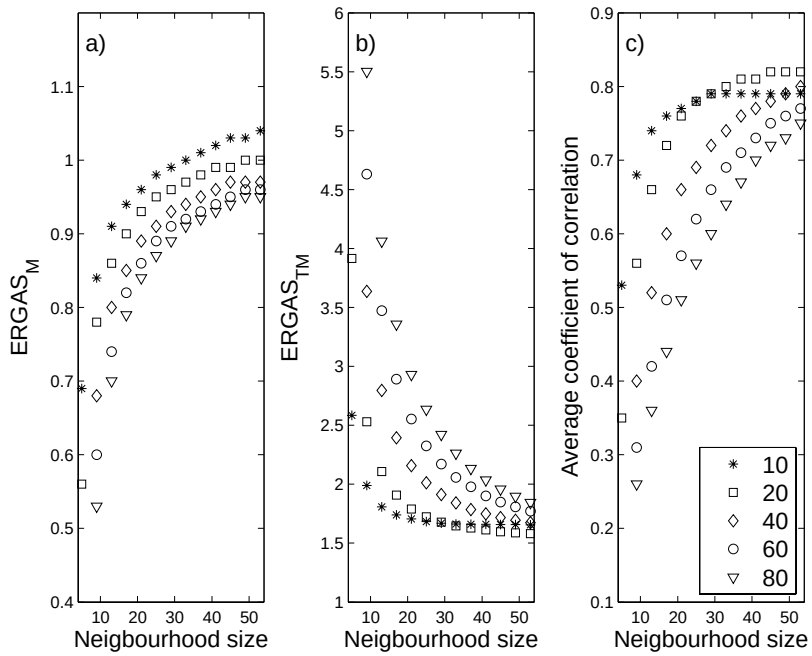

Figure 3.2. Results for the $ERGAS_M$ (a), $ERGAS_{TM}$ (b) and the average coefficient of correlation (c). Each symbol represents the number of classes used to classify the TM image. Notice that the neighbourhood size of 5 does not provide sufficient equations to solve the unmixing when the TM image is classified into 40, 60 and 80 classes.

The selection of the best fused image is not straightforward because there is no combination of *nc* and *k* that simultaneously minimizes the two ERGAS indices. However, from Figure 3.2a we recognize that the range of variation of the $ERGAS_M$ is rather small (the smoothing effect caused by increasing the window size is apparently not very important). Therefore, we could select as the best fused image the one that first minimizes the $ERGAS_{TM}$ and then the $ERGAS_M$. Nevertheless, a large number of fused images potentially meet this criterion. Furthermore, a visual check of these fused images showed that, indeed, they are very similar. As an illustration, Figure 3.3 shows an RGB color composite of the fused image obtained with $nc = 60$ and $k = 45$ (upper row: whole study area; lower row: a 25 × 25 pixel subset). For comparison purposes, an RGB color composite of the original TM and MERIS FR images is also provided in Figure 3.3.

In general, the fused image preserves well the spatial patterns found in the TM image while remaining spectrally similar to the MERIS FR image. However, some deviating pixels can be seen at the boundary between objects (e.g., river shorelines). These pixels correspond to mixed pixels and they are difficult to unmix because the TM unsupervised classification is rather noisy in those areas and because they cover a very small fraction of the neighborhood under study.

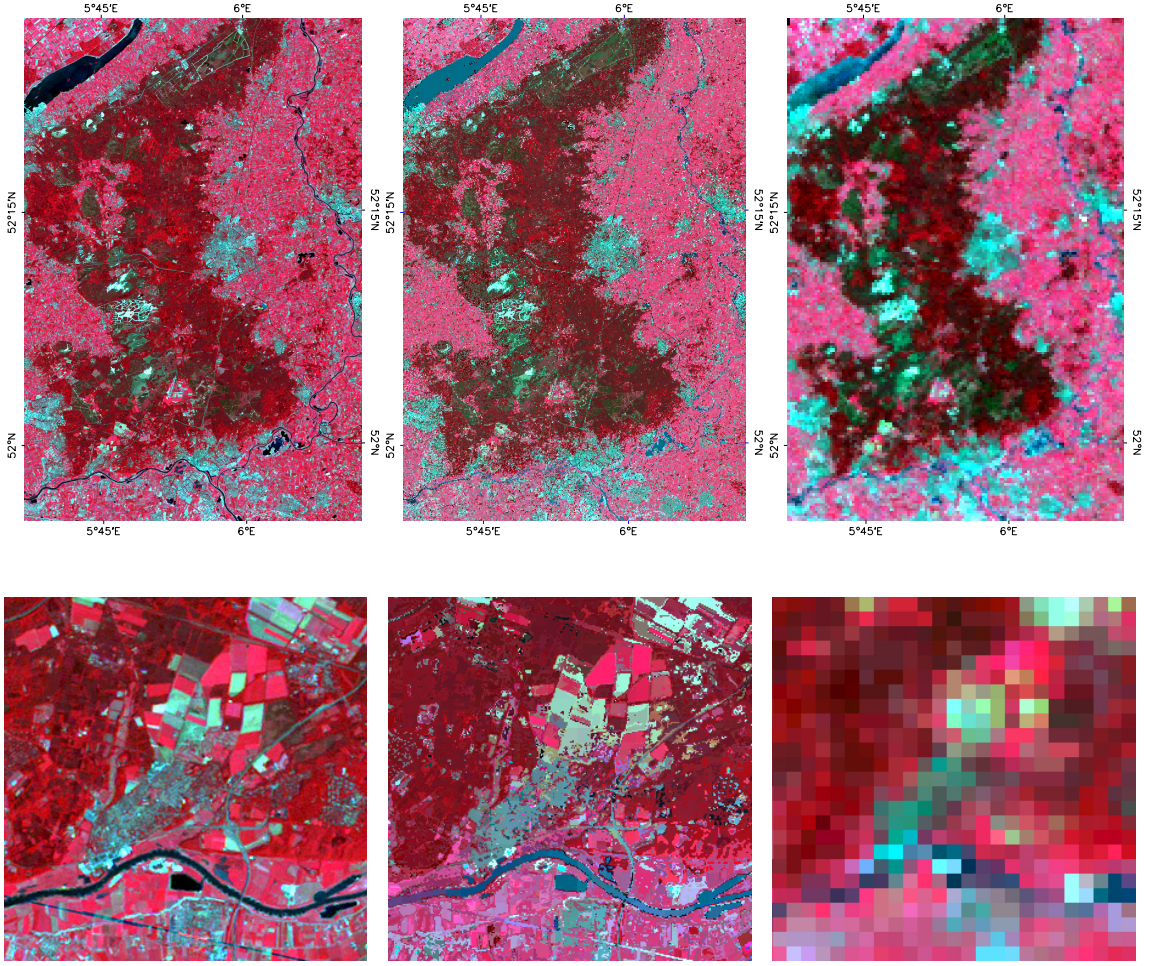

Figure 3.3. RGB color composite of bands 4, 3 and 2 of the TM image (a), bands 13, 7 and 5 of the fused image obtained for *nc* = 60 and *k* = 45 (b) and bands 13, 7 and 5 of the original MERIS FR image (c). Upper row shows the whole study area, whereas the lower row shows a subset of 25 by 25 MERIS FR pixels.

3.4 Conclusions

In this letter we have studied the applicability of the linear mixing model to fuse a Landsat TM and a MERIS full resolution level 1b image. The method, known as unmixing-based data fusion, requires the optimization of two parameters: the number of classes used to classify the TM image, *nc*, and the size of the MERIS neighborhood, *k*, used to solve the unmixing equations. Several combinations of *nc* and *k* have been tested.

The ERGAS index computed at 25 m and at 300 m, together with the average coefficient of correlation ($\bar{r}$) computed at 25 m, were used to assess the quality of the fused images and to assist in the identification of the best fused image. The results of the fusion quality assessment indicate that a) the unmixing-based data fusion approach presented here succeeded in preserving the spectral information of MERIS: low values were found for the $ERGAS_M$ since all the spectral information present in the fused image comes from MERIS; in addition, high $\bar{r}$ values were found between the first 4 TM bands and its spectrally corresponding fused bands, and b) there is always a trade-off between the quality of the fused images at 25 m and

at 300 m because the ERGAS indices are inversely correlated. Therefore, we suggest using a specific application (e.g. land cover mapping) to better identify the best fused image. For illustration purposes, we selected as the best fused image the one obtained for nc = 60 and k = 45 because it is one of the images that minimizes the $ERGAS_{TM}$ while keeping one of the lowest possible $ERGAS_M$ values. Nevertheless, further work is required in order to estimate the real possibilities and limitations of this data fusion method. Special attention should be paid to the co-registration of the high and low spatial resolution images and to the criteria used to select the best fused image.

The unmixing-based data fusion approach may also be used to fuse MERIS FR time series with one or more TM images. This multitemporal data fusion exercise will be of great interest for land cover mapping and for monitoring vegetation dynamics (e.g. in terms of fAPAR, LAI or chlorophyll content) at high spatial, spectral and temporal resolutions. Nevertheless, it is important to realize that these fused images will only be an approximation of what the MERIS sensor would be measuring if it had a spatial resolution of 25 m. In addition, possible landscape changes between the dates of the Landsat TM acquisition and the MERIS images might further affect the quality of the fused images (Minghelli-Roman et al. 2006) since the number and location of land cover classes may change if the time span becomes too wide.

Acknowledgements

The contribution of R. Zurita-Milla is granted through the Dutch SRON GO programme (EO-061). The authors would also like to thank the three anonymous reviewers for their valuable comments and recommendations.

CHAPTER 4

Using MERIS fused images for land cover mapping and vegetation status assessment in heterogeneous landscapes*

* Based on: Zurita-Milla, R., Clevers, J.G.P.W., van Gijsel, J.A.E. and Schaepman, M.E. (2008). Using MERIS fused images for land cover mapping and vegetation status assessment in heterogeneous landscapes. *International Journal of Remote Sensing* (In review).

Using MERIS fused images for land cover mapping and vegetation status assessment in heterogeneous landscapes

Abstract

In this paper we evaluate the potential of Envisat-MERIS fused images for land cover mapping and vegetation status assessment in heterogeneous landscapes. A series of MERIS fused images (15 spectral bands; 25 m pixel size) is created using the linear mixing model and a Landsat TM image acquired over The Netherlands. First, the fused images are classified to produce a map of the 8 main land cover types of The Netherlands. Subsequently, the maps are validated using the Dutch land cover/land use database as a reference. Then, the fused image with the highest overall classification accuracy is selected as the best fused image. Finally, the best fused image is used to compute three vegetation indices: the NDVI and two indices specifically designed to monitor vegetation status using MERIS data: the MERIS terrestrial chlorophyll index (MTCI) and the MERIS global vegetation index (MGVI).

Results indicate that the selected data fusion approach is able to downscale MERIS data to a Landsat-like spatial resolution. The spectral information in the fused images is fully originating from MERIS and not confounded by TM data. Classification results for the TM and for the best fused image are similar and when comparing spectrally similar images (i.e. TM with no SWIR bands), the results of the fused image outperform those of TM. With respect to the vegetation indices, a good correlation was found between the NDVI computed from TM and from the best fused image (in spite of the spectral differences between these two sensors). In addition, results show the potential of using MERIS vegetation indices computed from fused images to monitor individual fields. This is not possible using the original MERIS FR image. Therefore, we conclude that MERIS-TM fused images are very useful to map heterogeneous landscapes.

4.1 Introduction

The MEdium Resolution Imaging Spectrometer (MERIS) is one of the core instruments aboard the ENVISAT/ESA platform, the world largest environmental satellite (Bézy et al. 1999). MERIS provides hyperspectral data in 15 narrow bands and at 2 spatial resolutions: 300 m in the so-called full resolution (FR) mode and 1200 m in the reduced resolution (RR) mode. This imaging spectrometer was originally intended for monitoring coastal zones (FR mode) and for ocean applications (RR mode). For that reason, it was designed with a fine spectral and radiometric resolution and a high revisit time (2-3 days) (Curran and Steele 2005). Nevertheless, long before its launch a few modifications were introduced in its final design (e.g. the position of some bands) so that MERIS could also be used for atmospheric and land applications (Curran and Steele 2005; Verstraete et al. 1999).

The final MERIS spectral configuration, together with its high temporal resolution, has indeed proven to be very useful for land applications. For instance, MERIS data have been used to produce regional and global land cover maps (Arino et al. 2005; Clevers et al. 2007). Furthermore, its unique spectral configuration allows the retrieval of canopy chlorophyll content through the red-edge position (Clevers et al. 2001). Other MERIS land products include: leaf area index (LAI), fraction of absorbed photosynthetically active radiation (fAPAR) and fraction of vegetation cover (fCover) (Bacour et al. 2006). More recently, MERIS has been used to study solar-induced vegetation fluorescence (Guanter et al. 2007). In addition, two vegetation indices have been specifically designed for this sensor: the MERIS Terrestrial Chlorophyll index, MTCI (Dash and Curran 2004), which is linked to canopy chlorophyll content, and the MERIS Global Vegetation index, MGVI (Gobron et al. 1999), which is directly related to fAPAR. Both vegetation indices have been integrated in the processing chain of MERIS data and they are provided as MERIS level 2 datasets.

Although the above mentioned products/applications show the potential of MERIS for monitoring at regional or global scales, the spatial resolution provided by this instrument might be too coarse to capture relevant details of fragmented landscapes. In such heterogeneous areas, at the MERIS spatial scale, pixels very often contain more than one land cover type.

In general, mixed pixels are difficult to handle and they limit the operational utility of medium and coarse spatial resolution imagery. For instance, mixed pixels are responsible for the so-called low resolution bias when estimating land cover areas using medium and coarse spatial resolution data (Boschetti et al. 2004). High spatial resolution sensors like SPOT XS or Landsat TM/ETM+ can be used to study heterogeneous or fragmented landscapes. However, their revisit time (26 days in the case of SPOT XS and 16 days for Landsat TM or ETM+) is not very appropriate for monitoring purposes. This is especially true for areas that have extensive cloud coverage throughout the year (Asner 2001; Jorgensen 2000; Kontoes and Stakenborg 1990).

Data fusion methods (Wald 1999) can be used to overcome both the mixed pixel and the cloud coverage problems. Fused images, i.e. images created by combining two or more types of data, can offer increased interpretation capabilities and more reliable results because the data collected by different Earth observation (EO) sensors are complementary (Pohl and Van Genderen 1998). Besides this, if successful data fusion methods are implemented, continuous time series of vegetation status can be produced by combining all the EO data currently

collected. Therefore, downscaling medium and coarse spatial resolution imagery will improve the optical remote sensing (global) monitoring capabilities and help with the quantification of land cover changes over heterogeneous areas where a Landsat-like resolution is required (Janetos and Justice 2000).

Several data fusion methods have been described in literature (c.f. Ehlers (1991); Pohl and van Genderen (1998)). However, most of them are operator or data type dependent (Zhang 2002, 2004). For instance, most of the recent data fusion methods based on wavelet transformation require that the ratio of the spatial resolution of the images to be fused is a power of 2 (Shi et al. 2005), or they require that the images to be fused are in the same spectral domain (Otazu et al. 2005). Furthermore, spectral normalization of the original data is required by several data fusion methods (Acerbi-Junior et al. 2006). Nevertheless, the main difficulty is that most of the current data fusion methods do not properly preserve the spectral information of the input images because they are mainly concerned with the visual enhancement of the images (Pellemans et al. 1993). The preservation of the spectral information is, for instance, a prerequisite to derive reliable land cover maps because the classes that were spectrally separable in the original image should still be separable in the fused image. Additionally, it ensures a physical interpretation of the fused image and facilitates the retrieval of landscape properties using radiative transfer models.

In this respect, Zurita-Milla et al. (2008a) have recently introduced a detailed implementation of the unmixing-based data fusion approach as initially described by Zhukov et al. (1999). This implementation succeeded in synthesizing fused images with the spectral resolution of MERIS but with the spatial resolution provided by Landsat TM.

In this paper, we further evaluate the performance of the unmixing-based data fusion approach by assessing the potential of MERIS FR fused images to derive spatially improved land products: land cover maps and vegetation status assessment using the MTCI and the MGVI vegetation indices.

The remainder of this paper is organized as follows: section 4.2 summarises the unmixing-based data fusion approach used to produce the MERIS fused images. Section 4.3 presents the study area, the images used in this study and the two case studies: land cover mapping and assessment of vegetation status. Section 4.4 presents the results of both case studies and, finally, section 4.5 summarises the main conclusions and offers some recommendations for further research.

4.2 Unmixing-based data fusion

If a high and a low spatial resolution image are simultaneously available over a given study area, the linear mixing model (Adams and Gillespie 2006) can be used to combine the information provided by these images. This application is known as spatial unmixing or unmixing-based data fusion (Minghelli-Roman et al. 2001; Minghelli-Roman et al. 2006; Zhukov et al. 1999). The aim of this kind of unmixing is to downscale the spectral information of the low spatial resolution image to the spatial resolution provided by the high spatial resolution image.

Once the high and low spatial resolution images are co-registered, the selected unmixing-based data fusion approach can be summarised in four main steps (Zurita-Milla et al. 2008a):

- The high spatial resolution image is classified into *nc* unsupervised classes.

- The fractional coverage of the high spatial resolution unsupervised classes is computed for each low spatial resolution pixel.
- The spectral response of each of the *nc* unsupervised classes is unmixed using the fractional coverages obtained in the second step and the spectral information provided by the low spatial resolution image. This unmixing is done per band and using a neighbourhood of $k \times k$ low spatial resolution pixels.
- Finally, a fused image is constructed by assigning the corresponding unmixed signals to the unsupervised classes present in the central pixel of each $k \times k$ neighbourhood.

The third step of the unmixing-based data fusion approach can be written as follows:

$$\mathbf{L}^{i,k} = \mathbf{F}^{k,nc} \cdot \mathbf{S}^{i,k,nc} + \mathbf{E}^{i} \quad i = 1,2,\ldots,\mathrm{N} \tag{4.1}$$

where: $\mathbf{L}^{i,k}$ is a ($k^2 \times 1$) vector that contains the low spatial resolution values (for band *i*) of all the low spatial resolution pixels present in the neighbourhood *k*. $\mathbf{F}^{k,nc}$ is a ($k^2 \times nc$) matrix containing their corresponding fractional coverages in terms of the *nc* unsupervised classes. $\mathbf{S}^{i,k,nc}$ is the ($nc \times 1$) unknown vector of spectrally downscaled values (band *i*) for each of the classes present in the neighbourhood. $\mathbf{E}^{i}$ is a ($k^2 \times 1$) vector of residual errors. Finally, N is the number of low spatial resolution bands.

It is worth noting that Eq. 4.1 is typically solved using a constrained least-squares method because the downscaled spectral information (DN, radiance or reflectance values) should fulfil the following two conditions: (i) all the spectral values must be positive and (ii) none of the spectral values can be larger than the saturation value of the low spatial resolution sensor.

4.3 Materials and methods

4.3.1 Study area and input datasets

The study area covers approximately 40 km by 60 km of the central part of The Netherlands (52.19° N, 5.91° E; Figure 4.1). The selected study area includes the largest lowland natural area of north-western Europe as well as grasslands, croplands and some relatively important urban nuclei. The landscape of the natural area is characterized by a mixture of heather, woodlands and sand drifts. One of the largest and oldest national parks of The Netherlands, "*De Hoge Veluwe*", lies in the southern part of the natural area. Part of the rivers Rhine and IJssel are located in the southern and eastern part of the study area. Finally, the north-western corner of the selected area corresponds to the province of Flevoland, a polder mainly used for agricultural purposes. The shallow lake known in Dutch as "*Veluwemeer*" separates Flevoland from the mainland.

The study area was selected considering both the heterogeneity of the landscape and the availability of cloud free high and medium spatial resolution satellite data acquired nearly simultaneously: a Landsat-5 TM image from 10 July 2003 and a MERIS full resolution level 1b image acquired 14 July 2003 were available over this area. Both images were in top of atmosphere (TOA) radiance and they were co-registered with a root mean square error of 0.47 MERIS pixels. The main characteristics of the TM and the MERIS sensors are given in Table 4-1.

Figure 4.1. Location of the study area within The Netherlands.

Table 4-1. Comparison of the TM and the MERIS FR sensors.

	TM		MERIS FR	
Band	centre (nm)	bandwidth (nm)	centre (nm)	bandwidth (nm)
1	485	70	412.5	9.9
2	560	80	442.4	10
3	660	60	489.7	10
4	830	140	509.7	10
5	1650	200	559.6	10
6	(α)	(α)	619.6	10
7	2215	270	664.6	10
8			680.9	7.5
9			708.4	10
10			753.5	7.5
11			761.6	3.7
12			778.5	15
13			864.8	20
14			884.8	10
15			899.8	10
Spatial resolution	25 m		300 m	
Revisit time	16 days		2-3 days	

(α): the 6th band of the TM sensor was not used in this study because it is located in the thermal domain and has a different spatial resolution (60 m).

4.3.2 Fused images

The unmixing-based data fusion approach formulated in Eq. 4.1 inherently requires the optimization of two parameters: the number of classes used to classify the high spatial resolution image (*nc*) and the size of the neighbourhood used to solve the unmixing equations (*k*). Like in our previous study (Zurita-Milla et al. 2008a), 5 *nc* values (10, 20, 40, 60 and 80) and 14 *k* values (from $k = 5$ to $k = 53$ in steps of 4) were used to generate a series of fused images. In that study, the quality of the fused images was quantitatively assessed at the TM and at the MERIS FR spatial resolutions by using the so-called ERGAS index (Lillo-Saavedra et al. 2005; Ranchin et al. 2003; Wald 2002) and by computing the average correlation coefficient between spectrally similar TM and MERIS bands. The results of this quality assessment indicated that a trade-off exists between the reconstruction of fused images at 25 and at 300 m and suggested that a specific application should be used to select the best combination of *nc* and *k*. In order to try to clarify this issue, here land cover mapping was chosen as such an application.

4.3.3 Land cover classification

All fused images, as well as the original TM image, were classified using a supervised maximum likelihood classification rule. Similar to other studies (Clevers et al. 2007; Zurita-Milla et al. 2007a), the MERIS bands 1, 2, 11 and 15 were excluded from all the fused images before their classification. These bands are either very susceptible to atmospheric influences (bands 1 and 2) or they coincide with atmospheric absorption features (bands 11 and 15) and, hence, they do not provide relevant information for land cover mapping.

The latest version of the Dutch land use database, LGN5, was used to support the selection of the training samples and to validate the classification results (Figure 4.2). This dataset is based on a multi-temporal classification of high resolution satellite data and the integration of ancillary data (Hazeu 2005). The LGN5, which is based on operator supported interpretation of Landsat imagery from the year 2003 for the study site, has a spatial resolution of 25 m and a detailed legend consisting of 39 classes. In order to simplify the classification process and reduce spectral confusion, the LGN5 was thematically aggregated into the 8 main land cover classes of The Netherlands: grassland, arable land, deciduous forest, coniferous forest, water, built-up, natural vegetation and bare soil (including sand dunes).

Two additional experiments were designed to further assess the potential of the fused images for land cover classification. First, the MERIS image was resampled from 300 m to 25 m using cubic convolution and then it was classified to evaluate the added value of the fusion process. In the second experiment, bands 5 and 7 of the TM image were omitted from the TM classification because MERIS does not collect information in the SWIR region. This allows us to compare classification results of spectrally similar images. Finally, the overall classification accuracies, the user's and producer's accuracies as well as the kappa coefficient were used to compare the classification results.

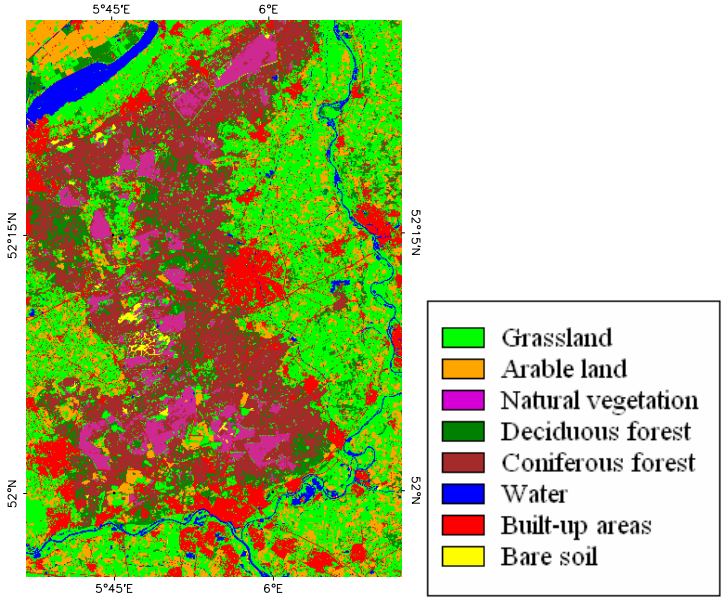

Figure 4.2. Thematically aggregated land cover map (LGN5) over the study area.

4.3.4 Assessing vegetation status

As mentioned in section 4.1, two vegetation indices are operationally produced to monitor vegetation status using MERIS data: the MTCI, which is related to canopy chlorophyll content, and the MGVI, which is directly linked to fAPAR. Traditional vegetation indices like the normalized difference vegetation index (NDVI) can also be computed from MERIS data. The NDVI was designed to enhance vegetation signal and it is basically an indicator of the amount of vegetation and its "greenness". Due to its simplicity, this index has found a large number of applications. For instance, NDVI has been related to fAPAR (Myneni and Williams 1994), and was also used to estimate crop and forest productivity (Maselli and Chiesi 2006; Moriondo et al. 2007). For this study, the advantage of computing this index is that it can also be derived from TM data so that we can compare results at 25 m.

The MTCI, MGVI and NDVI are easy to compute and, if the selected data fusion method preserves the MERIS spectral information, they can be used to study vegetation status at a much higher spatial resolution. The best fused image, as identified based on the land cover classification accuracy, was selected to compute these vegetation indices. In addition to the vegetation indices, the spectral consistency of the best fused image was checked by comparing the average spectral signature of the training areas used during the land cover classification with the corresponding signatures of the original MERIS FR data.

The NDVI was computed as follows:

$$NDVI = \frac{L_{NIR} - L_{RED}}{L_{NIR} + L_{RED}} \qquad (4.2)$$

Where L_{NIR} and L_{RED} are the TOA radiance values of the bands located in the NIR and the red regions of the electromagnetic spectrum. In the case of MERIS, band 13 was used for L_{NIR} and band 7 for L_{RED} whereas for the TM sensor bands 4 (NIR) and 3 (red) were used.

The use of radiance data to compute the NDVI facilitates the inter-comparison exercise. Nevertheless, differences in sensor spectral configuration and sensor calibration will still play an important role when comparing indices computed using data from different sensors (Teillet et al. 1997). For instance, the TM sensor was designed to quantize the spectral information using 8 bits whereas MERIS uses a 12-bits digitization.

The computation of the MTCI and MGVI indices requires that the data is transformed from TOA radiance to TOA reflectance (also known as planetary reflectance). Eq. 4.3 shows the expression used for such a transformation. The average solar irradiance per band, S^i (W $m^{-2}\mu m^{-1}$), and the solar angle, θ_s, were obtained from the MERIS metadata.

$$R^{i}_{TOA} = \frac{\pi \cdot L^{i}_{TOA}}{S^{i} \cdot \cos(\theta_s)} \tag{4.3}$$

The MTCI was computed using Eq. 4.4 where the Rx is the TOA reflectance of the x^{th} MERIS band:

$$MTCI = \frac{R10 - R9}{R9 - R8} \tag{4.4}$$

The MGVI uses the TOA reflectance in three MERIS bands: blue (band 2), red (band 8) and near-infrared, NIR, (band 13). The information in the blue band is used to derive rectified red and NIR reflectances that are corrected for atmospheric effects. After that, the MGVI is computed as a polynomial function of the rectified red and NIR reflectances (Gobron et al. 2004).

4.4 Results and discussion

4.4.1 Land cover classification

A supervised maximum likelihood classification rule was applied to: i) the complete series of fused images, ii) the Landsat TM images (all bands and 4 bands cases) and iii) the original MERIS image resampled to 25 m using cubic convolution. First, homogeneous areas belonging to the 8 main land cover types were identified using the LGN5. These areas (< 0.4 % of the total pixels) were used to train the classifier. Subsequently, the land cover classifications were validated using the whole LGN5 (Figure 4.2) as a reference.

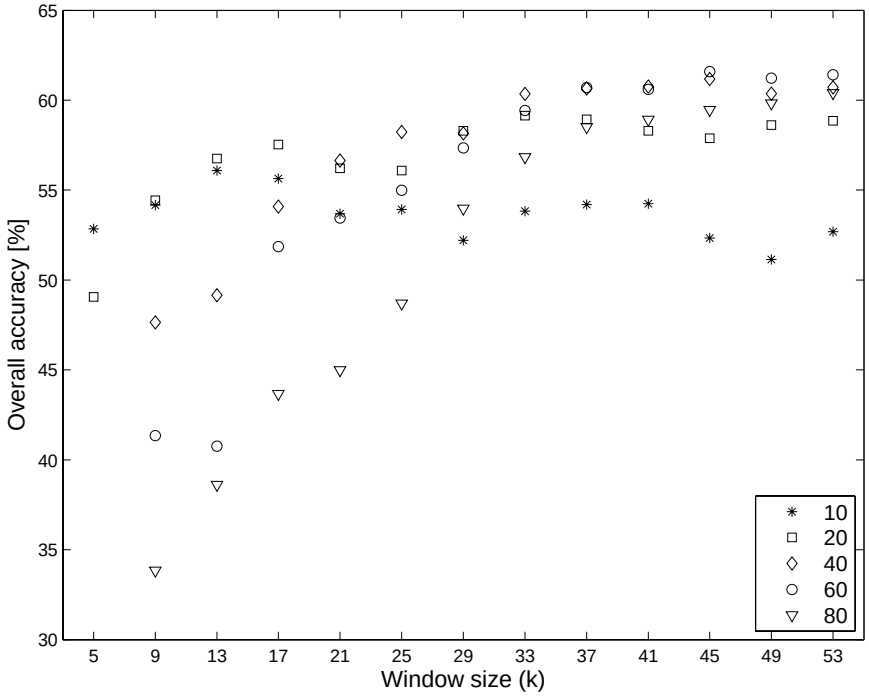

Figure 4.3. Relationship between the neighbourhood size (*k*) and the overall classification accuracy. Each symbol represents a different value of the number of classes used to classify the TM image (*nc*).

Figure 4.3 illustrates the relationship between the data fusion parameters *k* and *nc* and the overall classification accuracies. In general, the larger the neighbourhood size, the higher the classification accuracies. Nevertheless, for larger neighbourhood sizes, an asymptotic value of about 60 % is found. This indicates that increasing the window size beyond the tested values will not result in an improved overall accuracy. The poor classification results obtained for small *k* could indicate that the unmixing solutions are not stable – especially if TM has been classified in a large number of classes. The use of regularization techniques (Golub et al. 2000) might be needed in these cases.

In addition, classification accuracies for *nc* = 10 seem to be rather insensitive to the neighbourhood size and they are consistently lower than the rest of the accuracies. This could be because 10 unsupervised classes are not sufficient to properly characterize the heterogeneity of the study area.

The fused image obtained for *nc* = 60 and *k* = 45 was selected as the best fused image because it maximises the classification accuracy. Nevertheless, we recognize that other combinations of *nc* and *k* provide very similar results. This is because a number of fused images yielded classification accuracies around the asymptotic value of 60 %. Figure 4.4 shows an RGB colour composite of the best fused image and of a 25 × 25 MERIS FR pixels subset together with the original TM and MERIS FR images. The selected subset corresponds to the north-western corner of the study area (Flevoland), where the individual agricultural fields can easily be identified at 25 m but not at 300 m.

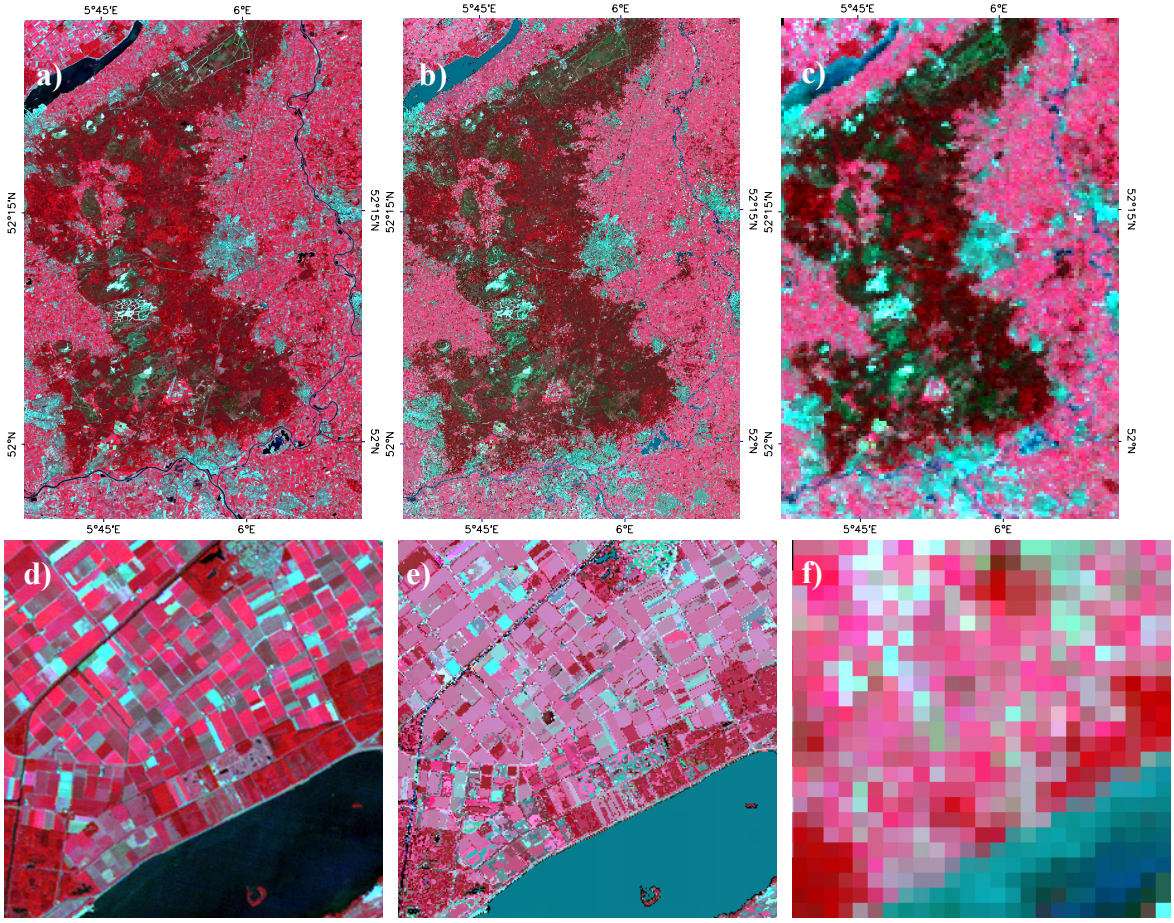

Figure 4.4. RGB color composite of bands 4, 3 and 2 of the TM image (a, d), bands 13, 7 and 5 of the fused image for *nc* = 60 and *k* = 45 (b, e) and bands 13, 7 and 5 of the original MERIS FR image (c, f). Upper row shows the whole study area, whereas the lower row shows a 25 by 25 pixel subset.

Table 4-2 summarises the overall accuracy and kappa coefficient of the best fused image as well as the ones obtained for the TM and the MERIS cubic convolution resampled images. Classification accuracies are moderate to good, especially considering the fact that the study area is very heterogeneous (even at the spatial resolution provided by the TM sensor).

Table 4-2. Classification results.

	O.A. [%]	K
Best fused image (*nc* = 60; *k* = 45)	61.59	0.519
Landsat TM 6 bands	63.32	0.550
Landsat TM bands 1 to 4	57.98	0.484
MERIS 25 m cubic convolution	40.57	0.295

O.A. = overall classification accuracy; K = kappa coefficient

The overall classification accuracy and the kappa coefficients of the original TM image were slightly better than the ones obtained for the best fused image. However, the

classification results of the TM image without the SWIR bands were worse than the ones obtained for the best fused image. This indicates that 1) the SWIR bands, which are missing in MERIS, play an important role in the final classification accuracy and 2) that the MERIS spectral configuration offers an increased class separability with respect to TM (visible and NIR).

The best fused image performed much better than the cubic convolution resampling of the original MERIS FR image. This shows that the selected data fusion approach is very useful to downscale MERIS data. Figure 4.5 shows the classification results obtained with the best fused image and with the Landsat TM (all bands). The map produced using the best fused image offers a good representation of the main landscape features.

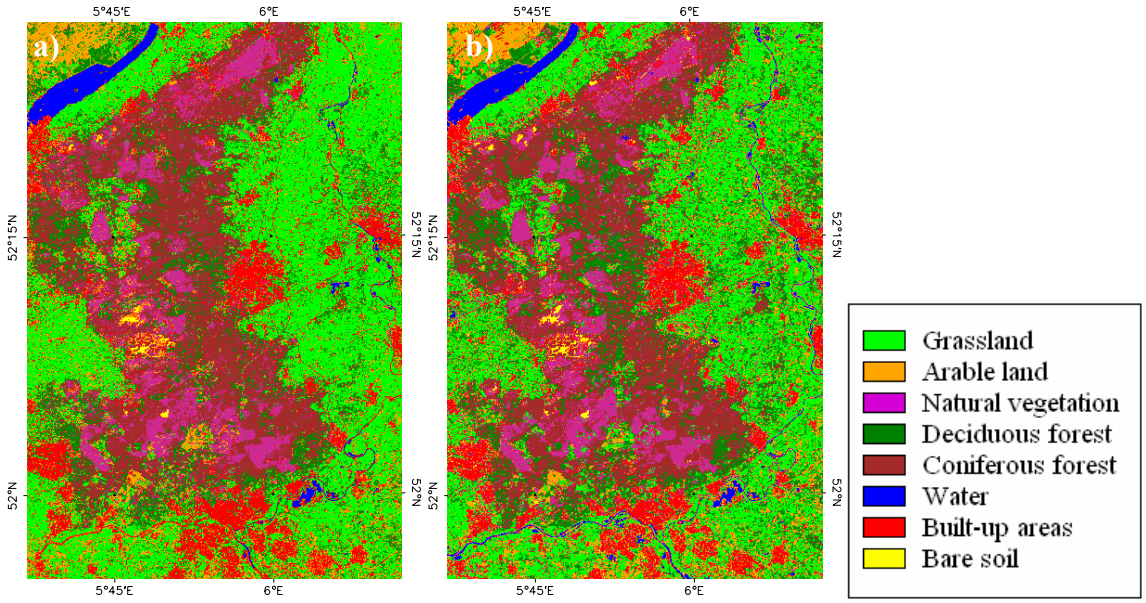

Figure 4.5. Classification results for the fused (a), and the Landsat TM (b) images.

Finally, Table 4-3 provides detailed information on the classification results of the best fused image through its full confusion matrix. In comparison, the full confusion matrix for the TM image with all 6 reflective bands is provided in Table 4-4. In both cases still a lot of confusions between classes are occurring, explaining the moderate overall classification accuracies and kappa coefficients in Table 4-2. However, this is the order of magnitude of these accuracies to be expected if no multitemporal satellite data and no ancillary information is used (Hazeu 2005). In most cases, confusion is quite similar for the fused image and for the TM image. Noticeable are the low user's and producer's accuracies for arable land. This can be explained by the heterogeneity of the class. In July, winter cereals are already mature and will look more like bare soil or urban areas. Spring cereals and in particular crops like sugar beet and potatoes are still green. As a result, mixing of the arable land class with many of the other classes occurred. In this respect, the major difference between the fused image classification and the TM classification is that in the fused image much more arable land pixels were labelled grassland, whereas in the TM image more pixels were assigned the label deciduous forest. Another noticeable class is water. It had a very high user's accuracy,

whereas the producer's accuracy was relatively low. This indicates that a significant number of water pixels was misclassified. An explanation for this can be a remaining uncertainty in the coregistration and the presence of many narrow water bodies. In the fused image, many water pixels were classified as built-up, whereas in the classified TM image many water pixels were classified as natural vegetation and arable land and not that much as built-up. Other major differences between the classifications of the best fused image and of TM are in particular the number of correctly classified pixels for the classes deciduous forest and bare soil (although the latter is a rather small class). For the bare soil class much more pixels have been labelled as arable land in the classified fused image than in the classified TM image, at least relative to the size of this class.

4.4.2 Assessing vegetation status

Figure 4.6 illustrates the average spectral signatures of the areas used as training areas for the land cover classification. Figure 4.6a was prepared using the best fused image while Figure 4.6b shows the signature of the corresponding areas in the original MERIS FR image. These signatures can be compared, since the training areas were taken from large homogeneous areas that correspond to "pure" pixels at the original MERIS scale. The general shape of these spectral signatures corresponds to typical spectra of the respective classes. The first few bands show relatively high values due to atmospheric scattering in the blue. Bands 11 and 15 show low TOA reflectance values due to the oxygen and water absorption features located near those bands. Figure 4.6 confirms that the spectral differences between the best fused image and MERIS are very small. Thus, the unmixing-based data fusion approach succeeded in synthesizing the spectral characteristics of MERIS at 25 m. This should allow the calculation of vegetation indices from the fused images.

Table 4-3. Confusion matrix for the maximum likelihood classification of the best fused image (*nc* = 60; *k* = 45).

	Actual class									
Classif. class	Water	Built-up	Grasslands	Coniferous	Arable land	Deciduous	Nat. veg.	Bare soil	Total	User's acc.
Water	64542	40	669	11	24	8	0	37	65331	98.79
Built-up	29007	272294	84149	27301	30147	8256	9937	4940	466031	58.43
Grasslands	5742	64704	925884	10184	182531	37473	2389	831	1229738	75.29
Coniferous	3854	22135	34952	633418	3020	54996	22463	541	775379	81.69
Arable land	9968	82598	142704	15425	130272	20843	9203	5714	416727	31.26
Deciduous	7909	45711	115779	107860	95145	185731	5344	549	564028	32.93
Nat. vegetation	3227	36045	51514	79117	8304	7758	176726	1539	364230	48.52
Bare soil	0	2	229	95	0	0	259	5928	6513	91.02
total	124249	523529	1355880	873411	449443	315065	226321	20079	3887977	
Producer's acc.	51.95	52.01	68.29	72.52	28.99	58.95	78.09	29.52		

Table 4-4. Confusion matrix for the maximum likelihood classification of the TM image (6 bands).

	Actual class									
Classif. class	Water	Built-up	Grasslands	Coniferous	Arable land	Deciduous	Nat. veg.	Bare soil	Total	User's acc.
Water	78313	78	1037	433	106	45	104	41	80157	97.70
Built-up	7426	278608	59312	22392	18068	3658	9857	4053	403374	69.07
Grasslands	3446	41854	859289	6703	104996	19927	4164	1334	1041713	82.49
Coniferous	3624	18533	30262	655732	2673	33760	15545	419	760548	86.22
Arable land	10786	79204	129618	15704	155259	12918	1978	1084	406551	38.19
Deciduous	4509	21975	161126	110338	146015	234045	2823	413	681244	34.36
Nat. vegetation	16081	80797	110394	61491	20121	10678	190243	2397	492202	38.65
Bare soil	64	2480	4842	618	2205	34	1607	10338	22188	46.59
Total	124249	523529	1355880	873411	449443	315065	226321	20079	3887977	
Producer's acc.	63.03	53.22	63.38	75.08	34.54	74.28	84.06	51.49		

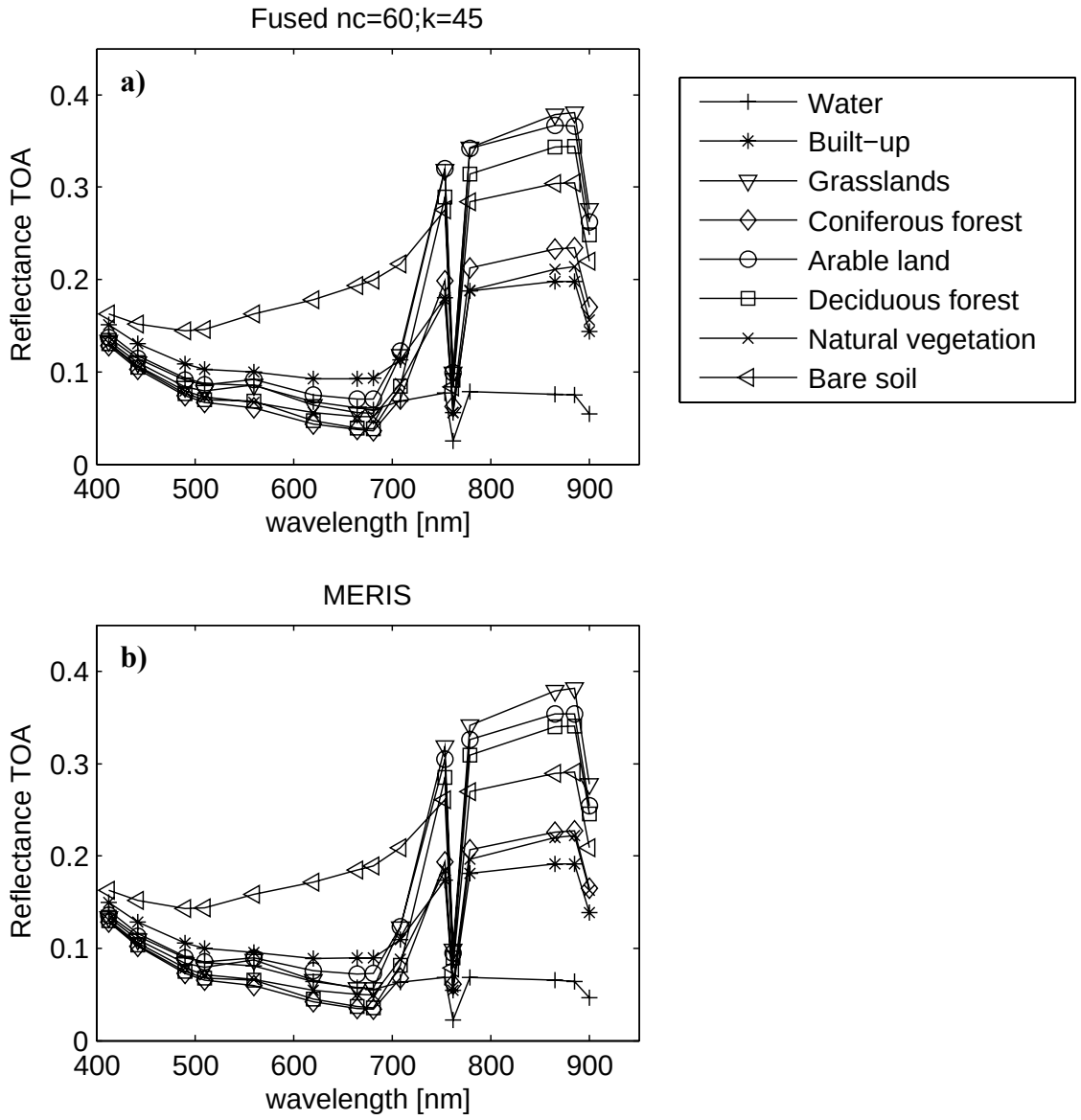

Figure 4.6. Average spectral signature for the 8 main land cover classes in The Netherlands. (a) best fused image (nc = 60; k = 45); (b) original MERIS FR data.

As an example, Figure 4.7 presents the NDVI results computed over the 25 by 25 pixels MERIS FR subset that was used in Figure 4.4. The index was computed from the TM image, from the best fused image and from the original MERIS FR image. A few negative NDVI values were identified in the NDVI images. These values, associated to bare soil, water or "edge effects" (i.e. mixed pixels in between fields or at the interface land/water), were set to zero to facilitate the interpretation of the results. Figure 4.7 illustrates that it is possible to monitor individual fields using MERIS fused images. There is a good agreement between the spatial patterns found in the fused and in the original MERIS FR image. However, the dynamic range found for the fused and the MERIS NDVI values is smaller than the one of the TM image. This can be explained by differences in band centres and bandwidths. Cross-

sensor calibration of vegetation indices is still an open issue for the remote sensing community (Fensholt et al. 2006). A detailed study by Teillet et al. (1997) identified that NDVI is very sensitive to the spectral configuration of the sensor and pointed out that the effects on the NDVI depend on the type of canopy under study. In this respect, the narrow spectral bands provided by MERIS should provide a better NDVI that the one computed using broad bands. More precisely, Teillet et al. (1997) concluded that a narrow band (less than 50 nm) located around 865 nm is optimal to compute the NDVI because this region is less sensitive to possible errors due to an improper atmospheric water vapour correction. MERIS band 13 (864.8 nm) is in the middle of this optimum region whereas TM band 4 (830 nm) is a very broad band extending outside that spectral region.

Despite the differences in sensor spectral configuration (Table 4-1), a good correlation (r = 0.76) was found between the NDVI computed from the TM and from the MERIS fused image. In a recent study, Busetto et al. (2008) found a correlation of about 0.85 using NDVI computed from TM and fused MODIS images but these sensors have a much more compatible spectral configuration than TM and MERIS.

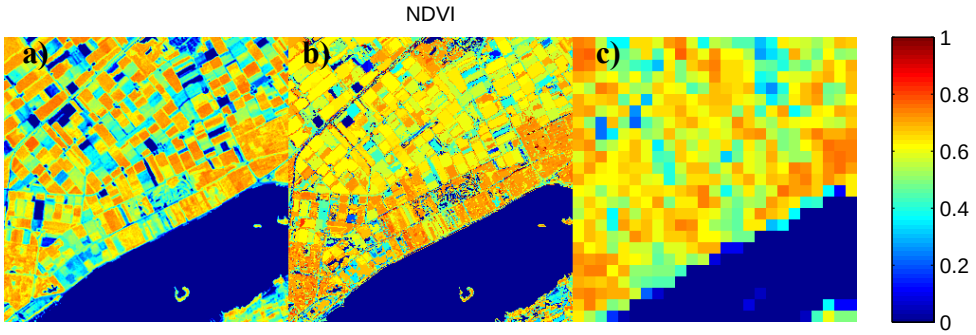

Figure 4.7. Example of the NDVI for the TM (a), the fused (b) and the MERIS FR image (c) for a 25 × 25 MERIS FR pixels subset of the study area.

Finally, Figure 4.8 shows the results for the MTCI and the MGVI vegetation indices. Notice that these indices were not computed for the large water body present in the scene since its MTCI and MGVI values are meaningless. For the land pixels, a small proportion (<1 %) of unfeasible index values, or "outliers", were identified and removed from the MTCI and MGVI images computed from the fused image. In this case, the outliers are defined as pixels that are exceeding more than 10 % of the maximum or minimum index values as found in the original MERIS FR images (i.e. we assume that pixels at 25 m might have index values outside of the range found at 300 m, because at the MERIS original scale the signal is smoothed due to the mixed pixels). The "outliers" mainly correspond with narrow linear features (e.g. roads or edges between agricultural plots). In Figure 4.8a and Figure 4.8c, they can be seen as dark blue pixels because they were set to zero. These pixels could easily be removed using, for instance, a median filter. The appearance of these unfeasible index values might be attributed to errors during the unmixing because of residual errors in the co-registration and/or because of the ill-posedness of the unmixing problem. In addition, the uncertainty of unmixing classes that have a very small fractional coverage inside the MERIS neighbourhood is inherently higher than the unmixing of classes that cover a large proportion of the neighbourhood (Zhukov et al. 1999).

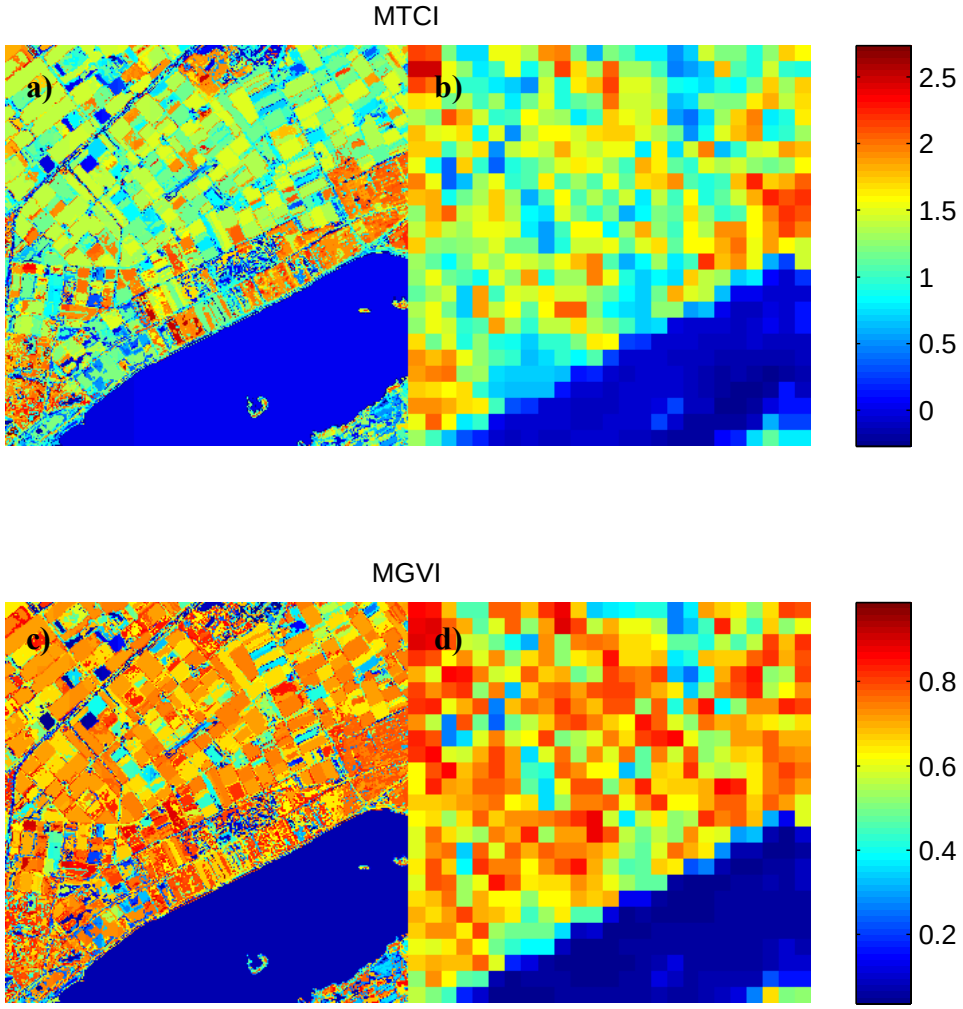

Figure 4.8. Example of the MTCI for the fused image (a) and the MERIS FR image (b) and of the MGVI for the fused image (c) and the MERIS FR image (d) for a 25 × 25 MERIS FR pixels subset of the study area.

This example clearly illustrates the potential of monitoring individual fields using the fused products, whereas this is not possible using the original MERIS image. In the MERIS FR image each pixel seems to be a mixed pixel. In the fused images mixed pixels can still be observed at object boundaries, but individual fields are clearly identifiable.

4.5 Conclusions and recommendations

In this paper we have assessed the potential of MERIS-TM fused images to derive spatially improved MERIS land products. These fused images have the spatial resolution of TM, whereas the spectral and radiometric properties are solely coming from MERIS. The selected implementation of the unmixing-based data fusion approach requires the optimisation of two parameters: the number of classes used to classify the TM image, *nc*, and the size of the MERIS neighbourhood, *k*, used to solve the unmixing. Here, a series of fused images generated with various combinations of *nc* and *k* were used to produce land cover maps of the 8 main classes of The Netherlands. The image generated with *nc* = 60 and *k* = 45 was chosen

as the best fused image based on the land cover classification results. Classification results for the TM image and for the best fused image were very similar (overall accuracies of 63.32 % and 61.59 %, respectively). However, the fused images outperformed the classification accuracies of a spectrally similar TM image (i.e. an image without the SWIR bands). This indicates that the fine spectral resolution of MERIS is better than a coarse spectral resolution for land cover mapping and that the SWIR region plays an important role in the final classification accuracy. Classification accuracies might be further improved by making use of the changing phenology of some of the classes during the year. This would require a multitemporal data fusion and classification approach.

The potential of the MERIS fused images to assess vegetation status was also evaluated in this paper. The NDVI, MTCI and the MGVI vegetation indices were computed from the best fused image (25 m) and from the original MERIS FR image (300 m). Results indicate that the best fused image can be used to successfully downscale these continuous variables. Despite differences in the spectral configuration of the TM and MERIS sensors, a good correlation ($r = 0.76$) was found between the NDVI computed from TM and from the MERIS fused image. In addition, vegetation indices computed from the fused image were spatially consistent with patterns obtained from the original MERIS FR image. Moreover, the use of fused images allows studying vegetation status of individual fields. This is not possible using original MERIS FR data over heterogeneous landscapes where most of the MERIS pixels are mixed pixels. Unsatisfactory vegetation index values are still obtained at object boundaries, because the data source for defining the object classes (a TM image), has many mixed pixels at these instances. This affected the TM unsupervised classification and resulted in deviating class labels from their neighbourhood. These deviating class labels yield deviating index values. This problem of mixed pixels at object boundaries may be solved by using an existing land cover map instead of a remote sensing image for defining the thematic classes.

Another major advantage of using a land cover map is that MERIS images of multiple dates may be fused with the same land cover map. In the current study, classes were obtained from a TM image and its classification will be different if an image from a different season is used. If the number of useful TM images is limited by cloud cover, the applicability of the proposed technique is also limited. However, the presented methodology also can be used with an existing, up-to-date land cover map. This should be implemented as a next step.

Because of the spatial, spectral and temporal resolutions of MERIS fused images, we believe that they are particularly interesting to monitor processes in both heterogeneous and frequently clouded areas. Further validation is, however, required in order to completely assess the possibilities and limitations of this data fusion method.

Acknowledgements

The contribution of R. Zurita-Milla is granted through the Dutch SRON GO programme (EO-061).

CHAPTER 5

Downscaling time series of MERIS FR data to monitor vegetation seasonal dynamics*

* Based on: Zurita-Milla, R., Kaiser, G., Clevers, J.G.P.W., Schneider, W. and Schaepman, M.E. (2008). Downscaling time series of MERIS FR data to monitor vegetation seasonal dynamics. *Remote Sensing of Environment* (In review).

Downscaling time series of MERIS FR data to monitor vegetation seasonal dynamics

Abstract

Monitoring vegetation dynamics is fundamental for improving Earth system models and for increasing our understanding of the terrestrial carbon cycle and the interactions between biosphere and climate. Medium spatial resolution sensors, like MERIS, exhibit a significant potential to study these dynamics over large areas because of their spatial, spectral and temporal resolution. However, the spatial resolution provided by MERIS (300 m in full resolution mode) is not appropriate to monitor heterogeneous landscapes, where typical length scales of these dynamics rarely reach 300 m. We, therefore, motivate the use of data fusion techniques to downscale medium spatial resolution data (MERIS full resolution, FR) to a Landsat-like spatial resolution (25 m). An unmixing-based data fusion approach was applied to a time series of MERIS FR images acquired over The Netherlands. The selected data fusion approach is based on the linear mixing model and uses a high spatial resolution land use database to produce images having the spectral and temporal resolution as provided by MERIS, but a Landsat-like spatial resolution. A quantitative assessment of the quality of the fused images was done in order to test the validity of the proposed method and to evaluate the radiometric characteristics of the MERIS fused images. The resulting series of fused images was subsequently used to compute two vegetation indices specifically designed for MERIS: the MERIS terrestrial chlorophyll index (MTCI) and the MERIS global vegetation index (MGVI). These indices represent continuous fields of canopy chlorophyll (MTCI) and of the fraction of photosynthetically active radiation absorbed by the canopy (MGVI). Results indicate that the selected data fusion approach can be successfully used to downscale MERIS data and, therefore, to monitor vegetation dynamics at Landsat-like spatial, and MERIS-like spectral and temporal resolutions.

5.1 Introduction

Monitoring vegetation dynamics is essential to better understand how the Earth system responds to anthropogenic activities (Steffen et al. 2005). For instance, knowledge on vegetation dynamics is fundamental to fully understand the terrestrial carbon cycle and the interactions between biosphere and climate (Champeaux et al. 2000; Dickinson et al. 1998; Friend et al. 2007). Earth observation satellites provide regular and synoptic data that can be used to monitor these dynamics at different spatial, spectral and temporal resolutions. Time series of vegetation indices (i.e. combinations of two or more spectral bands) are the most common approach to monitor greenness shifts (Dorigo et al. 2007). Further, key phenological metrics like the day of green-up and vegetation senescence can be retrieved using temporal series of these vegetation indices (Moody and Johnson 2001; Myneni et al. 1997a). Other relevant uses of time series of vegetation indices are: forecasting crop yield (Genovese et al. 2001), assessing habitat destruction (Pettorelli et al. 2005) and studying epidemics (Rogers et al. 2002; Scharlemann et al. 2008).

The normalized difference vegetation index (NDVI) has been extensively used for these applications. At global and regional scales, NDVI is typically computed from the data provided by the Advanced Very High Resolution Radiometer (AVHRR) onboard National Oceanic and Atmospheric Administration (NOAA) satellites. However, the AVHRR sensor was designed for meteorological applications and its radiometric and spectral performances are, therefore, not optimal for monitoring canopies. In 1998, the VEGETATION instrument was launched aboard the Satellite Pour l'Observation de la Terre (SPOT)-4. This sensor offers an improved spectral resolution because it includes a blue channel that can be used for atmospheric correction of the red, NIR and SWIR channels, which are very useful for studying canopies (Maisongrande et al. 2004).

The advent of medium spatial resolution sensors (250 to 300 m pixel size) did not only improve the spatial resolution available for monitoring landscapes but also opened the possibilities to develop new vegetation indices optimized for vegetation studies. In the case of MODIS, the enhanced vegetation index (EVI; (Huete et al. 1997)), which was designed to minimize canopy background and atmospheric effects, is now operationally computed and distributed as the MOD13 product (Huete et al. 1999). For MERIS, two vegetation indices have been included in the official processing chain: the MERIS terrestrial chlorophyll index (MTCI; (Dash and Curran 2004)) and the MERIS global vegetation index (MGVI; (Gobron et al. 1999)).

Despite the enhanced spatial and spectral resolution of these sensors, an accurate characterization of heterogeneous landscapes still requires a higher spatial resolution than the 250 or 300 m provided by MODIS and MERIS, respectively. Landsat-like sensors (spatial resolution of 20 to 30 m) can be used to study this kind of landscapes, but their temporal resolution is not sufficient for monitoring purposes, especially in frequently clouded areas (Asner 2001; Jorgensen 2000; Kontoes and Stakenborg 1990).

Data fusion techniques could facilitate the study of heterogeneous and frequently clouded areas by offering an efficient integration of the different kinds of images that are currently available (Woodcock and Ozdogan 2004). A successful data fusion approach should result in fused images that have more information than each of the input images alone (Hall and Llinas 1997; Pohl and Van Genderen 1998).

The aim of this paper is to propose an unmixing-based data fusion approach to operationally monitor heterogeneous and frequently clouded areas using (multitemporal) MERIS data and a high spatial resolution land use dataset, which has a Landsat-like spatial resolution (25 m). Even if the precise length scales of vegetation dynamics in heterogeneous landscapes are under discussion, sensors with a Landsat-like spatial resolution have a past track record in monitoring vegetation dynamics at sufficient spatial (but, in general, not temporal) resolution (Gould 2000; Griffiths et al. 2000; Hudak et al. 2002; Vogelmann et al. 1998).

The unmixing-based data fusion approach was selected because previous studies have shown that it is able to reconstruct images with a high spectral fidelity (Zhukov et al. 1999; Zurita-Milla et al. 2008a). The use of MERIS data is justified because of its spectral configuration which allows improved vegetation monitoring capabilities with respect to other medium and low spatial resolution sensors (Curran and Steele 2005; Verstraete et al. 1999).

5.2 Unmixing-based data fusion

The unmixing-based data fusion approach uses the linear mixing model to combine two images acquired at different spatial resolutions. This model assumes that the spectrum of a mixed pixel is a linear combination of the pure spectra of the components present in that pixel weighted by their fractional coverage (Settle and Drake 1993). Despite this apparent simplicity, the linear mixing model is widely used by the remote sensing community because it has a sound physical basis and it has proven to be effective in analyzing mixed pixels (Adams and Gillespie 2006). Thus, if we have a priori knowledge about the components that might be present in a given scene and about their pure spectra, we can use this model to retrieve their sub-pixel proportions. This application is known as spectral unmixing (Adams et al. 1995; Ustin et al. 1993). The identification of materials or objects (Kemper and Sommer 2004), the derivation of continuous fields of vegetation properties (DeFries et al. 2000) and the quantification of land cover change at sub-pixel scales (Haertel et al. 2004; Kressler and Steinnocher 1999) are other applications of the linear mixing model. The success of these applications relies on the quality of the a priori knowledge with respect to the scene composition. In other words, the results of any linear spectral unmixing method heavily depend on a proper identification of the main components present in the scene and their pure spectra. This identification is difficult when the image has been acquired over very heterogeneous landscapes and/or when we work with coarse resolution data because in these cases most of the pixels are mixed (i.e. hardly any pure pixel can be found in the scene). Furthermore, the number of components that can be unmixed is limited by the number of spectral bands of the image. This implies that panchromatic images cannot be used for spectral unmixing and that hyperspectral images are preferred over multispectral ones.

If a high and a low spatial resolution image are simultaneously available over a certain study area, the linear mixing model can also be used to combine the information provided by these images. This application is known as unmixing-based data fusion and it aims at downscaling the spectral information of the low spatial resolution image to the spatial resolution provided by the high spatial resolution image. This kind of unmixing does not require a priori knowledge of the main components present in the low spatial resolution image because there is no need to identify their pure signals. In fact, these signals are the output. It is, however, essential that the high spatial resolution image allows a proper identification of

the main components present in the study area (albeit without having information on their spectral characteristics). Therefore, the unmixing-based data fusion approach can be applied even if the low resolution image only has mixed pixels or a small number of spectral bands.

The theoretical basis of the unmixing-based data fusion approach was first proposed by Zhukov et al. (1999). In this work, they downscaled TM thermal data by using the information provided by the other TM bands. The approach was validated using DAIS images and they concluded that it was possible to downscale thermal information with an error smaller than 2 Kelvin. Since then, a number of implementations of the unmixing-based data fusion algorithm have emerged. For instance, Haertel and Shimabukuro (2005) used it to extract endmembers from MODIS images using TM data as a reference. Zeng et al. (2008) used it in a similar way to characterize the sun-lit background of a forest and Minghelli-Roman et al. (2001; 2006) used it to merge MERIS and TM data for coastal water monitoring.

Recently, Zurita-Milla et al. (2008a) have presented a detailed implementation of the unmixing-based data fusion approach to combine MERIS and TM data for vegetation monitoring over heterogeneous landscapes. In a follow-up study, Zurita-Milla et al. (2008b) studied the applicability of such MERIS fused images for land cover mapping and for vegetation status assessment. Results of this analysis were promising. Classification accuracies of the MERIS fused image were higher than those of the TM image without SWIR bands and very similar when all the TM bands were used. Results also showed that vegetation indices can be computed from fused images and that the observed patterns are consistent with those observed by the TM and by the MERIS sensors. The main limitation of this study was that a TM image was used to characterize the landscape and, therefore, only MERIS images acquired at about the same date as the TM image could be downscaled.

Here we propose an improved version of the unmixing-based data fusion approach where a high spatial resolution land use map is used to characterize the landscape. This allows us to apply the method to a time series of MERIS FR images and to use the resulting fused images to monitor vegetation seasonal dynamics with high spatial, spectral and temporal resolutions.

5.3 Materials and methods

5.3.1 Study area and datasets

The study area covers approximately 2400 km^2 of the central part of The Netherlands (centered at 52.19° N, 5.91° E). The largest lowland natural area of north-western Europe lies in the center of the selected study area. This area, known as the “Veluwe”, covers about 1000 km^2 and it is characterized by a mixture of heather, woodlands (both coniferous and deciduous), natural vegetation and shifting sands. The rivers IJssel and Rhine can be seen in the eastern and southern part of the study area (Figure 5.1). In these areas, soils are predominantly composed of river clays and, therefore, the main land cover types are grasslands and agricultural lands. In the north-west corner of the study area we see a part of the province of Flevoland, where we find the largest agricultural plots of the study area, and the lake “Veluwemeer”. The selected study area also includes some relatively important urban areas: Arnhem, Ede, and Apeldoorn are cities with more than 100.000 inhabitants.

For the year 2003, three datasets are available over the study area: (i) a Landsat TM-5 image acquired on 10 July 2003, (ii) a time series of seven MERIS full resolution level 1b

images acquired between February and December 2003 and (iii) a high spatial resolution land use database.

The TM image was already geo-referenced to the Dutch national coordinate system and had a pixel size of 25 m. The MERIS FR images were corrected for the smile effect (Zurita-Milla et al. 2007a) and transformed into top of atmosphere radiances (L_{TOA}) using the metadata provided with the files. Figure 5.1 shows the study area as seen by TM and MERIS.

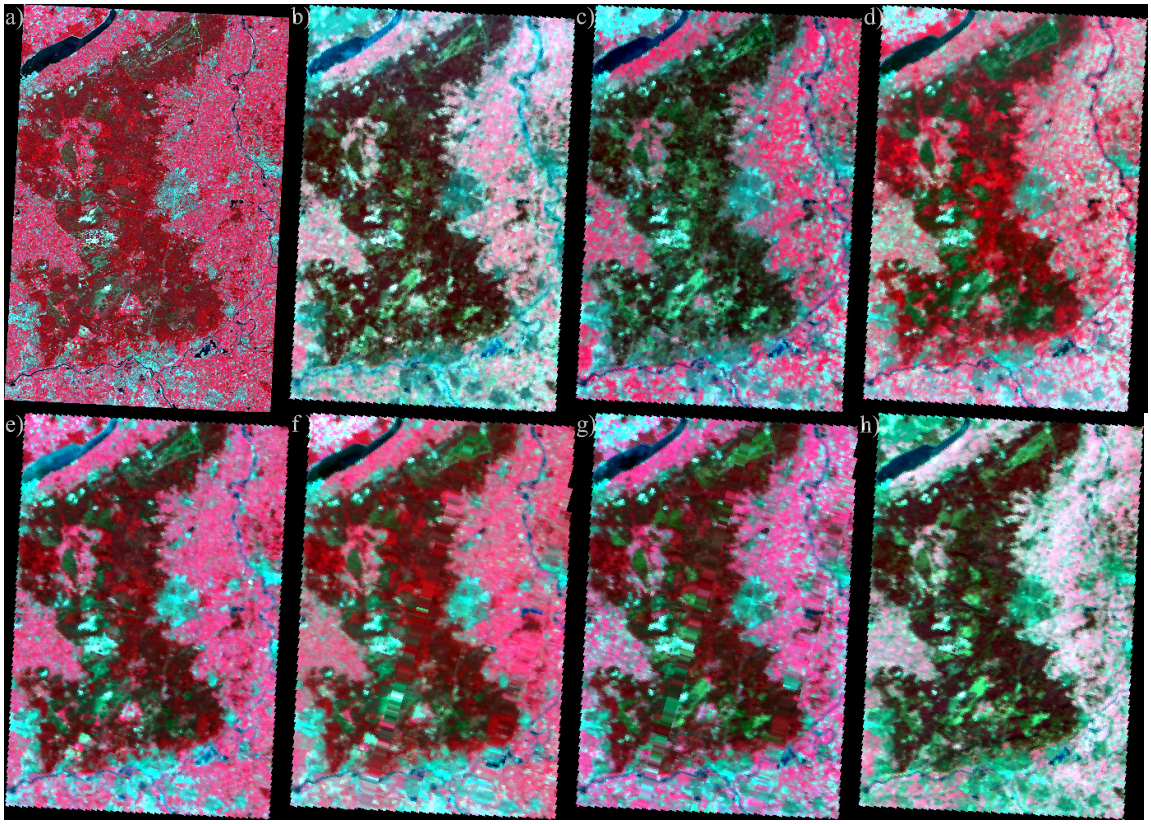

Figure 5.1. Study area as seen by Landsat TM on 10 July, 2003 (a) and by MERIS for the following dates of the same year: 18 February (b), 16 April (c), 31 May (d), 14 July (e), 6 August (f), 15 October (g) and 8 December (h).

The land use database, known in Dutch as LGN, is a geographical database that describes the main land uses in The Netherlands. The latest version, LGN5, includes the main land use/land cover types present in the country: urban areas and infrastructure, water bodies, semi-natural and natural vegetation types and various kinds of forests and agricultural classes. The LGN5 has a grid structure with a cell size of 25 m and its typical application scale is about 1:50.000. This database is based on a stratified multitemporal classification of satellite imagery of 2003 (central and eastern part of The Netherlands) and 2004 (western part of the country). In addition to satellite imagery, several sources of ancillary data are used to produce the LGN (de Wit and Clevers 2004; Hazeu 2008). The LGN5 subset that covers the study area has 30 out of the 39 original LGN classes. Table 5-1 summarizes the main classes present in the study area as well as their percentual coverage.

Table 5-1. Main land cover types in the study area after thematic aggregation into 10 classes.

Land cover	% of total area
Grasslands	34.88
Maize	5.99
Cereals	2.21
Other crops	3.36
Coniferous forest	21.68
Deciduous forest	8.10
Heather	5.81
Bare soil	0.52
Built-up areas	14.25
Water	3.20

5.3.2 Multi-temporal data fusion

As mentioned in section 5.2, the aim of the unmixing-based data fusion approach is to downscale a low spatial resolution image. For this, the low spatial resolution image (MERIS) is first co-registered with a high spatial resolution dataset (in this case the LGN5). Then, the fractional coverage of each LGN5 class is computed for each MERIS pixel. After that, each MERIS pixel is successively unmixed for each MERIS band using the corresponding LGN5 fractional coverages. In order to have enough equations a neighborhood of $k \times k$ MERIS pixels is used during the unmixing, which can be written as follows:

$$\mathbf{L}^{i,k} = \mathbf{F}^{k} \cdot \mathbf{S}^{i,k} + \mathbf{E}^{i} \tag{5.1}$$

where: $\mathbf{L}^{i,k}$ is a vector that contains the MERIS values (band i) of all pixels present in the neighborhood k. $\mathbf{F}^{k}$ is a matrix containing the corresponding LGN5 fractional coverages within the neigborhood. $\mathbf{S}^{i,k}$ is the unknown vector of spectrally downscaled MERIS values and E^{i} is a vector of unmixing residual errors.

Similar to our previous studies (Zurita-Milla et al. 2008a), a constrained least-squares method is used to solve Eq. 5.1 because $\mathbf{S}^{i,k}$ should fulfill two conditions: i) all the unmixed values should be positive and ii) they should be equal or smaller than the (per band) MERIS radiance saturation values (ESA/EO helpdesk, personal communication). The last step of the unmixing-based data fusion approach is to create a fused image by assigning the corresponding MERIS unmixed signals to each of the land cover (LGN5) classes present in the central pixel of each $k \times k$ MERIS neighborhood. The following sections provide a more detailed description on the implementation of the data fusion algorithm as well as a procedure to evaluate the fusion quality and to optimize the size of the neighborhood k.

5.3.3 Image co-registration

One prerequisite of data fusion is to have the input images perfectly co-registered. This is usually achieved by transforming the images to a common coordinate reference system. However, this transformation implies re-sampling of the images which, in turn, might have adverse effects on the quality of the fused images. The simplest and fastest re-sampling

method is nearest neighbor which preserves original pixel values but lacks geometric accuracy because the measurements are actually shifted to the nearest grid point and rotated to be aligned to the grid axes. Other techniques, such as bi-linear or bi-cubic interpolation are more accurate in respect of the geometrical transformation. However, they produce synthetic pixel values. Because of these drawbacks, we propose to use a different approach based on computing the actual ground instantaneous field of view (GIFOV) of each MERIS pixel. In order to use MERIS geo-location values that are as accurate as possible we used the AMORGOS 3.0 software (ACRI-ST 2007). This software calculates the geographic coordinates (WGS84) of the center of each pixel in the MERIS image based on satellite telemetry (ephemeredes, look angles) and a digital terrain model. Based on this information we determine the extent (i.e. the corner coordinates) of each MERIS pixel's GIFOV by two-dimensional linear interpolation.

Besides avoiding the re-projection of the data, the computation of the MERIS GIFOV allows us to determine the real number of TM pixels covered by each MERIS pixel. In our previous studies, this number was considered constant (simply by rationing the MERIS and the TM pixel sizes). With the current approach, we can study the effect of changes in viewing angles across the MERIS swath (pixels at the edge of the swath are larger).

5.3.4 Duplicates removal

The grid of the MERIS level 1b product is filled by applying a nearest neighbor re-sampling to the data acquired by the instrument. In this process a slight spatial over-sampling is used (ESA 2006). This means that the same instrument sample can be found more than once in the resulting level 1b product grid. In this case, the pixels are flagged as "duplicate" (Figure 5.2).

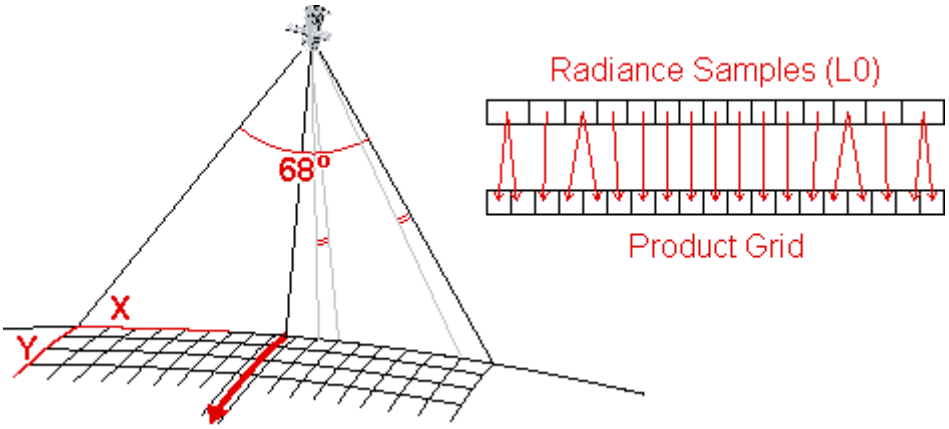

Figure 5.2. MERIS Level 1b gridding approach and MERIS duplicates. (Source: http://www.noc.soton.ac.uk/bilko/envisat/html/pop/mer_prodgrid.html).

When MERIS FR level 1b data are used as input for AMORGOS, the software runs in the so-called FSG (full-swath geo-corrected) mode. In this mode, the MERIS level 1b grid is kept (i.e. there is no restoration of the instrument geometry). This implies that duplicate pixels are not removed from the output file. However, duplicated pixels receive the same coordinates as the original MERIS pixel and therefore they can easily be located.

In our implementation of the unmixing-based data fusion approach, duplicated pixels are accounted for when computing the GIFOV. They are removed from the MERIS data so that only "real" MERIS pixels are fused with the land cover map.

In exceptional cases, three consecutive pixels may occur with identical geolocation and radiances. The reason for these 'triplets' are i) very large look angles at the edge of the swath and ii) instrument pixels being discarded from the spatial resampling for radiometric performance reasons (ESA/EO helpdesk, personal communication).

5.3.5 Fractional cover estimation

In contrast to our previous study, where a TM image was used to identify the main objects and patterns of the study area (Zurita-Milla et al. 2008a), here the LGN5 land use database is used as a reference. This approach is similar to the one proposed by Busetto et al. (2008) who used a high spatial resolution land use/land cover map to downscale MODIS NDVI values. The use of the LGN5 is justified because it reflects the objects and patterns found in the study area throughout the year and not just those of a specific date or season.

Point spread function (PSF) effects (Townshend et al. 2000) are also considered in the software implementation developed for this study. The PSF of a sensor determines how much of a signal reaching a detector element actually comes from adjacent areas outside the nominal GIFOV of the pixel and it weighs the signal over the area contributing to the detector readout (Kaiser and Schneider 2008). Therefore, when computing land cover fractions for each low spatial resolution pixel, PSF effects should be taken into account and the corresponding weights should be used to compute the fractional coverage of each class.

According to Schowengerdt (1997), the effective point spread function (PSF_{tot}) of an imaging system consists of several components: (i) the signal is blurred within the optical system (PSF_{opt}), (ii) motion of the sensor (PSF_{mot}) causes blurring in the in-track and/or cross-track direction (depending on the type of sensor), (iii) the signal is integrated over the non-zero area of the detector element (PSF_{det}) and (iv) the electronic components cause smoothing by applying a low-pass filter to reduce noise (PSF_{el}). By assuming that every component is a shift-invariant linear system, PSF_{tot} can be computed by convolution of its parts (Kaiser and Schneider 2008). For this study, the PSF was regarded as "ideal" (i.e. no blurring caused by optics, motion or electronics) because MERIS PSF effects are negligible for this kind of data fusion approach (Zurita-Milla et al. 2007d). However, it should be noted that this is not the case when using MODIS data because its triangular PSF causes 25 % of a signal recorded in a pixel to originate from adjacent areas (Kristof and Pataki, 2008; Tan et al., 2006).

As a combined effect of the heterogeneity of the landscape in the selected study area and the high thematic resolution of the LGN5 database, individual class fractions for certain MERIS pixels can be relatively small. Zhukov et al. (1999) showed that the accuracy of the retrieved signal is inversely related to the fractional coverage of the class and they suggested aggregating small fractions to increase the reliability of the solutions. In our work, a threshold of 5 % was selected. This is, classes that cover less than 5 % of a MERIS pixel are aggregated into the spectrally most similar LGN5 class present in the pixel under consideration. Several options are possible to rank the LGN5 classes according to their spectral similarity. Here we propose to use a very pragmatic approach: first, the LGN5 and the TM dataset are overlaid. Then, a class-wise average of the TM spectral signatures is computed. This operation results in 30 spectral signatures characterizing each of the LGN5 classes present in the study area.

Subsequently, the correlation coefficients between these spectral signatures are computed. Based on these results, a look-up-table of spectral similarity is created. In this case, the table has a size of 30 × 30 because there are 30 LGN5 classes in the study area.

5.3.6 Data fusion quality and optimizing the MERIS neighborhood

Assessing the quality of fused images is not straightforward because it depends on many factors like the difference in spatial or spectral resolution of the input images and the type of landscape under consideration (Thomas and Wald 2004). As a result, a number of data fusion quality indicators can be found in literature (Alparone et al. 2004; Tsai 2004; Wald et al. 1997; Wang and Bovik 2002). Wald et al. (1997) proposed a general framework for assessing the quality of fused images where it is advised to do this assessment at the original resolution of the input images. Similar to other studies (Minghelli-Roman et al. 2006; Zurita-Milla et al. 2008a), the ERGAS index (Lillo-Saavedra et al. 2005; Ranchin et al. 2003; Wald 2002) was used in this work for the data fusion quality assessment. The ERGAS index is computed as follows:

$$ERGAS = 100 \frac{h}{l} \sqrt{\frac{1}{N} \sum_{i=1}^{N} \left(RMSE_i^2 / M_i^2 \right)} \tag{5.2}$$

where: h is the pixel size of the high spatial resolution image; l is the pixel size of the low spatial resolution image; N is the number of spectral bands involved in the assessment; M_i is the mean value of the dataset used as a reference (band i) and $RMSE_i$ is the root mean square error computed between band i of the reference image and its spectrally corresponding band from the fused image.

The choice of the reference image depends on the scale at which the analysis is performed. The Landsat TM image is used for the quality analysis at 25 m and the original MERIS images are used for the analysis at 300 m (notice that the MERIS fused images should reproduce the corresponding MERIS image when degraded to the original spatial resolution).

Besides evaluating the quality of the fused images, this assessment was also used to optimize the size of the $k \times k$ MERIS neighborhood used during the unmixing (Eq. 5.1). To do so, four neighborhoods (5, 7, 9, and 11) were tested using the MERIS image of July. This MERIS image was selected because of the availability of the TM image acquired 4 days earlier which allows computing the ERGAS at 25 m and at 300 m. The neighborhood size yielding the best quality (minimum ERGAS values) will be selected as the best one and will subsequently be used for the rest of the MERIS images.

5.3.7 Vegetation seasonal dynamics

MERIS' potential for land applications (Curran and Steele 2005; Verstraete et al. 1999) has resulted in a number of semi-operational and operational MERIS land products. Currently, two vegetation indices are operationally produced to monitor vegetation status using MERIS data: the MERIS terrestrial chlorophyll index, MTCI (Dash and Curran 2004) and the MERIS global vegetation index, MGVI (Gobron et al. 1999).

Like the MERIS red-edge position (Clevers et al. 2002), the MTCI is related to the chlorophyll content of canopies. According to Dash and Curran (2004), the MTCI is more sensitive to high chlorophyll content and less sensitive to spatial resolution and atmospheric effects than the red-edge position. The MTCI is computed as follows:

$$\mathrm{MTCI} = \frac{\mathrm{R10 - R9}}{\mathrm{R9 - R8}} \tag{5.3}$$

where R8, R9 and R10 are the top of atmosphere (TOA) reflectances of the MERIS bands centered at 680.9 nm, 708.4 nm and 753.5 nm.

The MGVI has a positive linear relationship with the fraction of absorbed photosynthetically active radiation by the canopy (fAPAR). This index is computed using the TOA reflectance in three MERIS bands: blue (band 2), red (band 8) and near-infrared, NIR, (band 13). The information in the blue band is used to derive rectified (i.e. "atmospherically corrected") red and NIR reflectances. The MGVI is computed as a polynomial function of the rectified red and NIR reflectances (Gobron et al. 2004):

$$\mathrm{MGVI} = f_0(\mathrm{R8^*,R13^*}) \tag{5.4}$$

where f_0 is the polynomial function and R8* and R13* are the rectified reflectance values of bands 8 (680.9 nm) and 13 (864.8 nm) – see Gobron et al. (2004) for the polynomial coefficients of the function f_0 and for the coefficients of the polynomial function used to rectify bands 8 and 13.

Eq. 5.5 was used to convert the original TOA radiance into TOA reflectance values required to compute the above mentioned vegetation indices. The average solar irradiance per band, S^i ($\mathrm{Wm^{-2}\ \mu m^{-1}}$), and the solar angle, θ_s, were obtained from the metadata available in each MERIS level 1b dataset.

$$\mathrm{R^{i}_{TOA}} = \frac{\pi \cdot L^i_{TOA}}{S^i \cdot \cos(\theta_s)} \tag{5.5}$$

5.4 Results and discussion

5.4.1 Co-registration accuracy

The LGN5 and the time series of MERIS images were co-registered without re-sampling the data. To do this, the ground instantaneous field of view (GIFOV) of each MERIS pixel was computed. Figure 5.3 shows an overlay of the MERIS image from July (band 13, NIR) over the TM image of July (band 4, NIR). Notice that since the TM image used in this study was one of the images used to create the LGN5, the co-registration between this image and the LGN5 was perfect. The GIFOV of each MERIS pixel is represented as a polygon in Figure 5.3. The small irregularities that can be observed in the shape of these polygons are

caused by topography and by the satellite position and look angle. In addition, an increase of the GIFOV was observed when moving from nadir to the edge of the swath. Accounting for this effect is, therefore, essential to properly determine the fractional composition of each MERIS pixel. Figure 5.3 can also be used to visually assess the co-registration accuracy: the color gradient of the MERIS pixels corresponds well with the fraction of water within these pixels. Furthermore, under the assumption that pure water and pure land pixels have a constant MERIS band 13 (NIR) value in the vicinity of the land-water-boundary, a linear regression model was used to assess co-registration accuracy numerically. For this purpose, we determined fractional water coverage by digitizing the land-water-boundary (red line in Figure 5.3) in the co-registered Landsat TM image. Then, the area fractions of water were plotted against the corresponding MERIS pixel values in band 13 (Figure 5.4). A correlation coefficient of 0.95 was found between these variables. This clearly supports the selected method to compute the LGN5 fractional coverages inside each MERIS pixel. Besides this, Figure 5.3 and Figure 5.4 clearly show that the use of AMORGOS to compute the MERIS geo-location values resulted in a good co-registration accuracy. This supports the findings of Arino et al. (2008), who found a root mean square error of about 0.25 MERIS FR pixels when using the AMORGOS software.

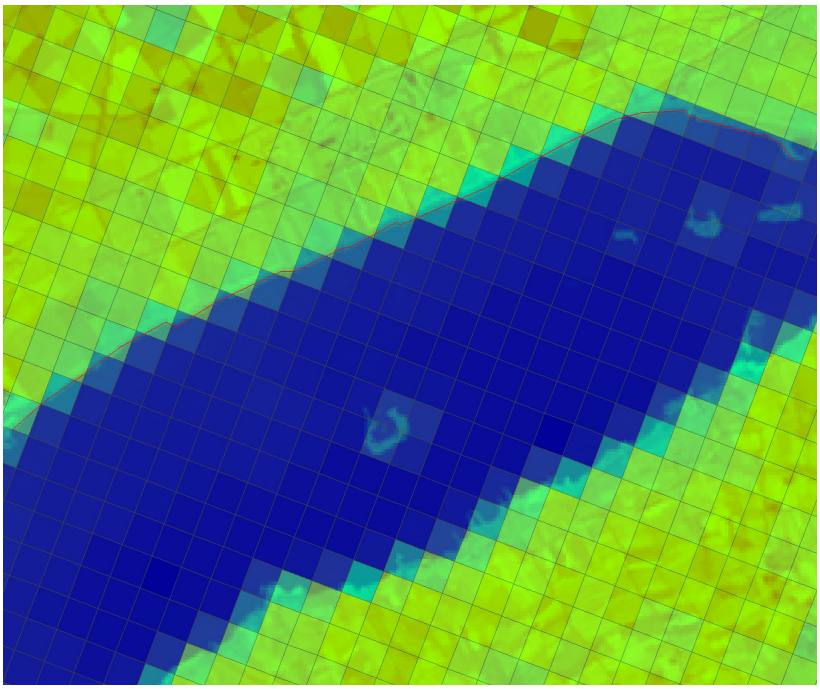

Figure 5.3. Co-registration of the MERIS and TM images of July: MERIS band 13 is depicted using a blue-green-red color table and TM is shown as semi-transparent background. The red line north of the water body shows the land-water-boundary as obtained from the TM image.

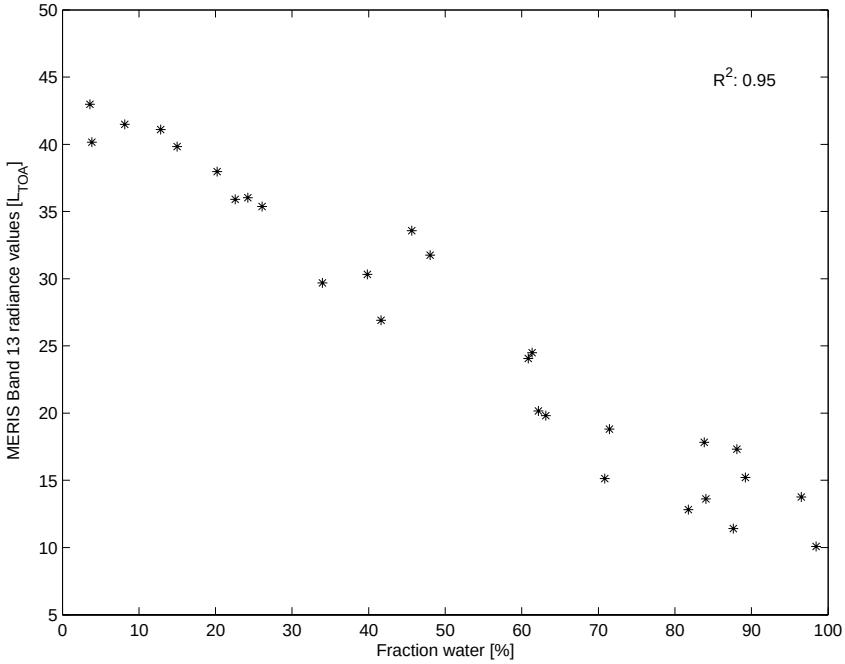

Figure 5.4. Fraction of water present in a selection of MERIS pixels (14 July 2003) and corresponding MERIS band 13 (864.8 nm) radiance values.

5.4.2 Effect of neighborhood size on data fusion quality

Figure 5.5 summarizes the quality assessment of the fused images for the month of July. For comparison purposes we present both the results of the fusion with no aggregation and the results of the fusion after re-assigning the fractions that cover less than 5 % of the pixel to the spectrally most similar class. Notice that because the ERGAS index is an error-based index, the lower its value the better the quality of the fused images. Three observations can be made from Figure 5.5:

There is a trade-off between the reconstruction of the image at 25 m and at 300 m: for increasing values of *k*, the ERGAS values at 25 m become smaller whereas the ERGAS values at 300 m steadily increase.

Aggregation of fractions that covered less than 5 % of the pixel resulted in an improvement of the data fusion quality at 25 m and in a small degradation of the data fusion quality at 300 m. This is because the aggregation of classes stabilizes the unmixing (i.e. in general, it reduces the ill-posedness of the problem) and, as a consequence the solution at 25 m is better than when using the original fractions. However, aggregating classes reduces the spectral variability of the fused image and this explains why the ERGAS at 300 m is slightly worse than when using the original fractions.

The ERGAS values at 25 m reach an asymptotic value at about 2. This means that testing neighborhood sizes larger than 11 will not improve the fusion quality.

Studying the various fused images in detail, the aggregation changed less than 0.6 % of the LGN5 pixels when re-labeling the classes that covered less than 5 % of a MERIS pixel. Moreover, all 30 classes present in the study area remained in the aggregated result (i.e. no classes disappeared during the aggregation). Considering that the fused images will be used at

25 m and the fact that the range of ERGAS values at 300 m is very small, the value of $k = 9$ was selected as the best neighborhood size. This size was then applied for the fusion of all MERIS images with the LGN5 database.

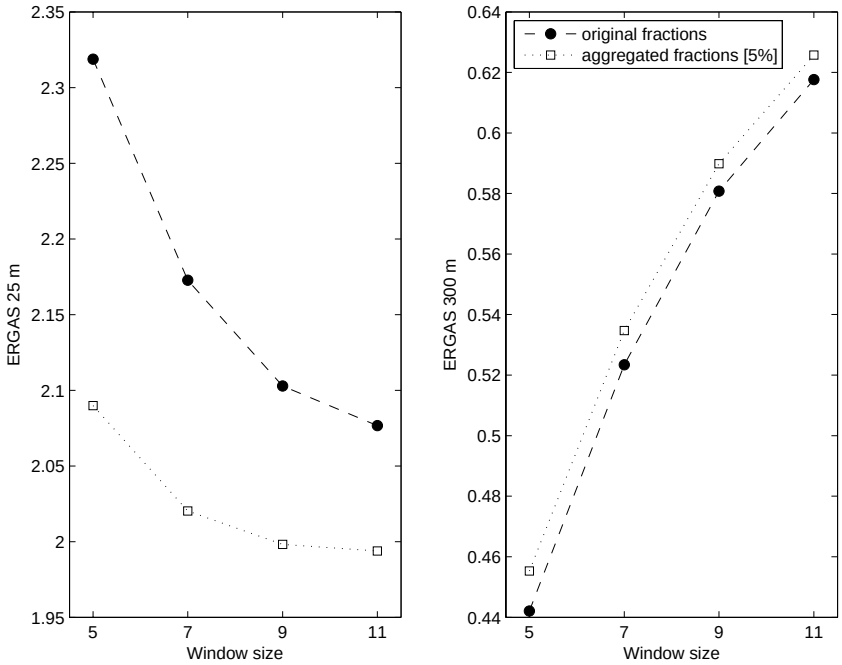

Figure 5.5. ERGAS values for the fused images of 14 July at 25 m (left) and 300 m (right).

The MERIS images were fused with the LGN5 to produce a series of MERIS fused images using the best configuration (i.e. aggregation of fractions and neighborhood size of 9 by 9 MERIS pixels). Figure 5.6, shows the resulting ERGAS values at 300 m. As expected, the values are rather constant for all dates. The only exception is the value for the image of October. This could be explained by the presence of "triplets" (i.e. 3 pixels having the same value) in this image. These triplets are probably due to a problem with a detector element since the study area is not situated at the edge of any of the selected MERIS images. Triples were not treated separately in the current implementation and, therefore, they worsen the quality of the fused images. Despite this, the ERGAS 300 m values found in this study are about a factor two smaller than the ones found in our previous study (Zurita-Milla et al. 2008a).

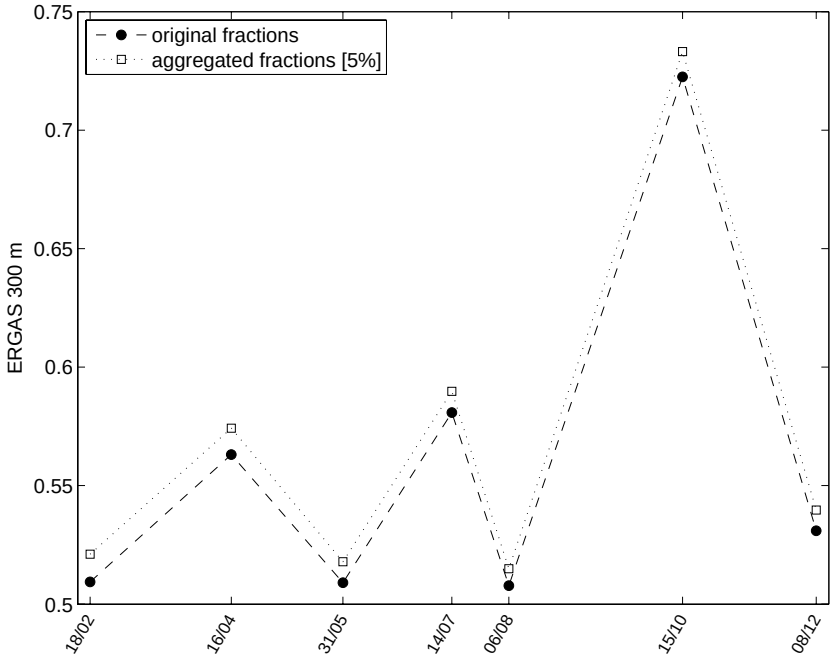

Figure 5.6. Comparison of ERGAS values at 300 m for the time series of fused images. These values correspond to the fused images created with original and with aggregated (5 %) LGN5 fractions.

5.4.3 Vegetation dynamics

The series of fused images was used to compute the MERIS terrestrial chlorophyll index (MTCI) and the MERIS global vegetation index (MGVI). A 300 by 300 TM pixels subset located in the northwest of the study area was selected for illustration so that the spatial enhancement of the fused images could clearly be visualized. Figure 5.7 shows the results for the MTCI whereas Figure 5.8 shows the results for the MGVI. The large water body situated in the middle of the selected subset was masked out before computing the vegetation indices because its MTCI and MGVI values are meaningless. Similar to our previous work (Zurita-Milla et al. 2008b), some outlier pixels (i.e. pixels with unfeasible index values) were identified at the edges of field plots and for non-vegetated areas (e.g. roads, bare soil plots, built-up, etc). These values were masked out from the images (shown as zero values in dark blue).

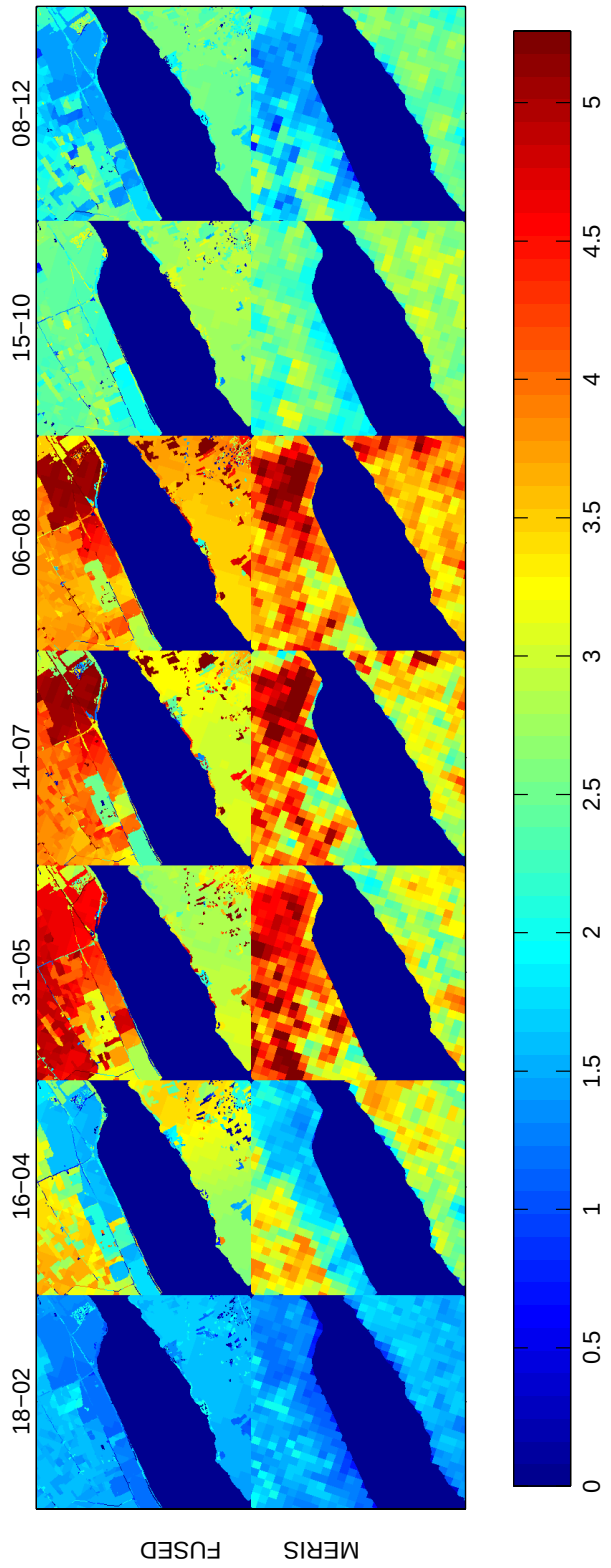

Figure 5.7. Temporal evolution of MTCI values for fused (top) and MERIS (bottom) data.

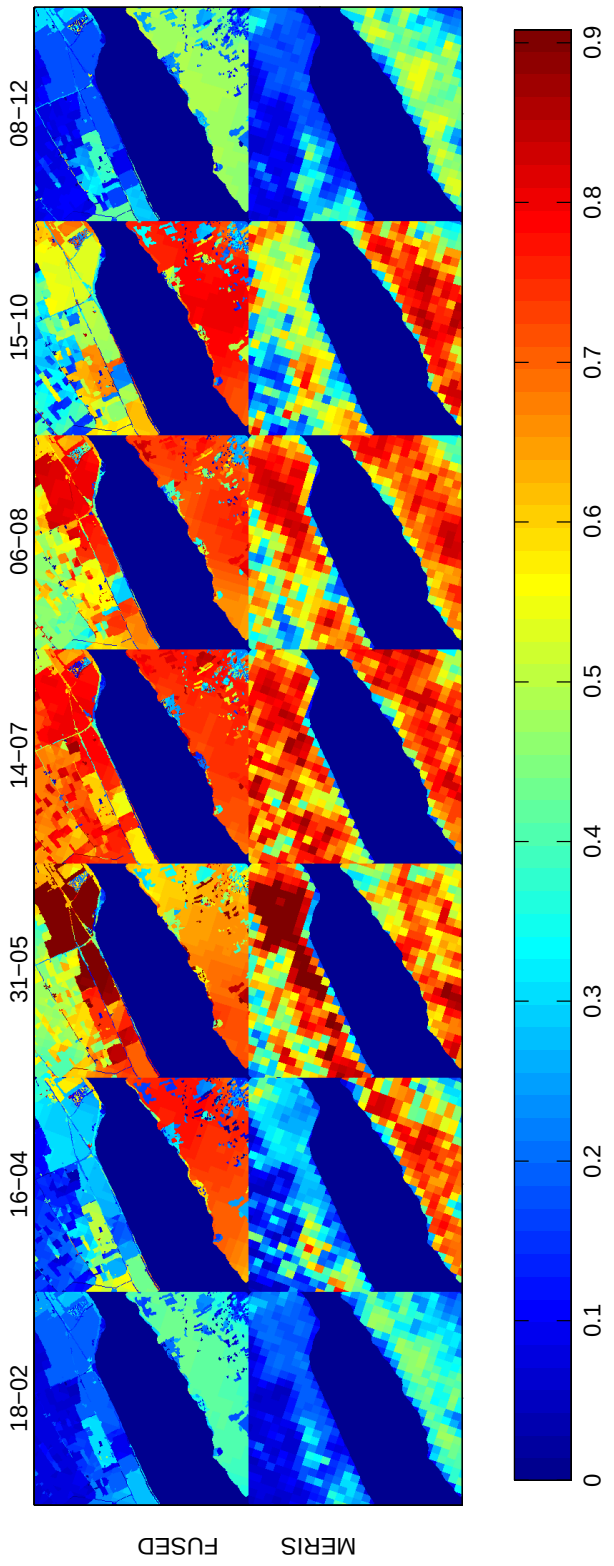

Figure 5.8. Temporal evolution of MGVI values for fused (top) and MERIS (bottom) data.

Vegetation dynamics are visible in both images: low vegetation index values are found at the beginning and at the end of the series (which correspond to the winter months) and high vegetation index values are found in the middle of the series (spring and summer). The fused images preserve the information contained in the original MERIS images (i.e. general spatial patterns are consistent at the original MERIS scale) whilst showing additional spatial details. This shows the potential of fused images for monitoring individual fields.

Using the LGN5 as a reference, pixels belonging to the main land cover types present in the study area were selected to study their temporal evolution. These land cover types are: heather, coniferous and deciduous forest (the main natural vegetation types of the "Veluwe" area) and grasslands, cereals and maize (the main agricultural types present in the study area). With respect to the 10 main land cover types (Table 5-1), only four land cover types are not considered. Other crops is a small class where several crops were aggregated in order to prepare the summary table of main land cover types and the three other classes are non-vegetated (bare soil, built-up and water) and, therefore, their MTCI and MGVI values are, in principle, meaningless. Figure 5.9 and Figure 5.10 respectively illustrate the MTCI and the MGVI profiles computed using the fused and the original MERIS images. Pixels located in homogeneous areas were used to prepare these profiles so that results at 25 and at 300 m could be compared. Results show that the profiles are similar when computed from the fused and from the original MERIS images. In addition, they point out the phenological variation of each land cover class. Most of the vegetated classes show a greenness/chlorophyll peak for the image of July (Figure 5.9). Coniferous forest and heather have their chlorophyll content peak in August. Grasslands have a more fluctuating profile caused by biomass fluctuations during the growing season due to mowing and grazing regimes. With respect to the MGVI values, the fAPAR is also reaching its highest value in summer. Heather presents lower fAPAR values than the rest of the land cover classes because it is a less leafy canopy.

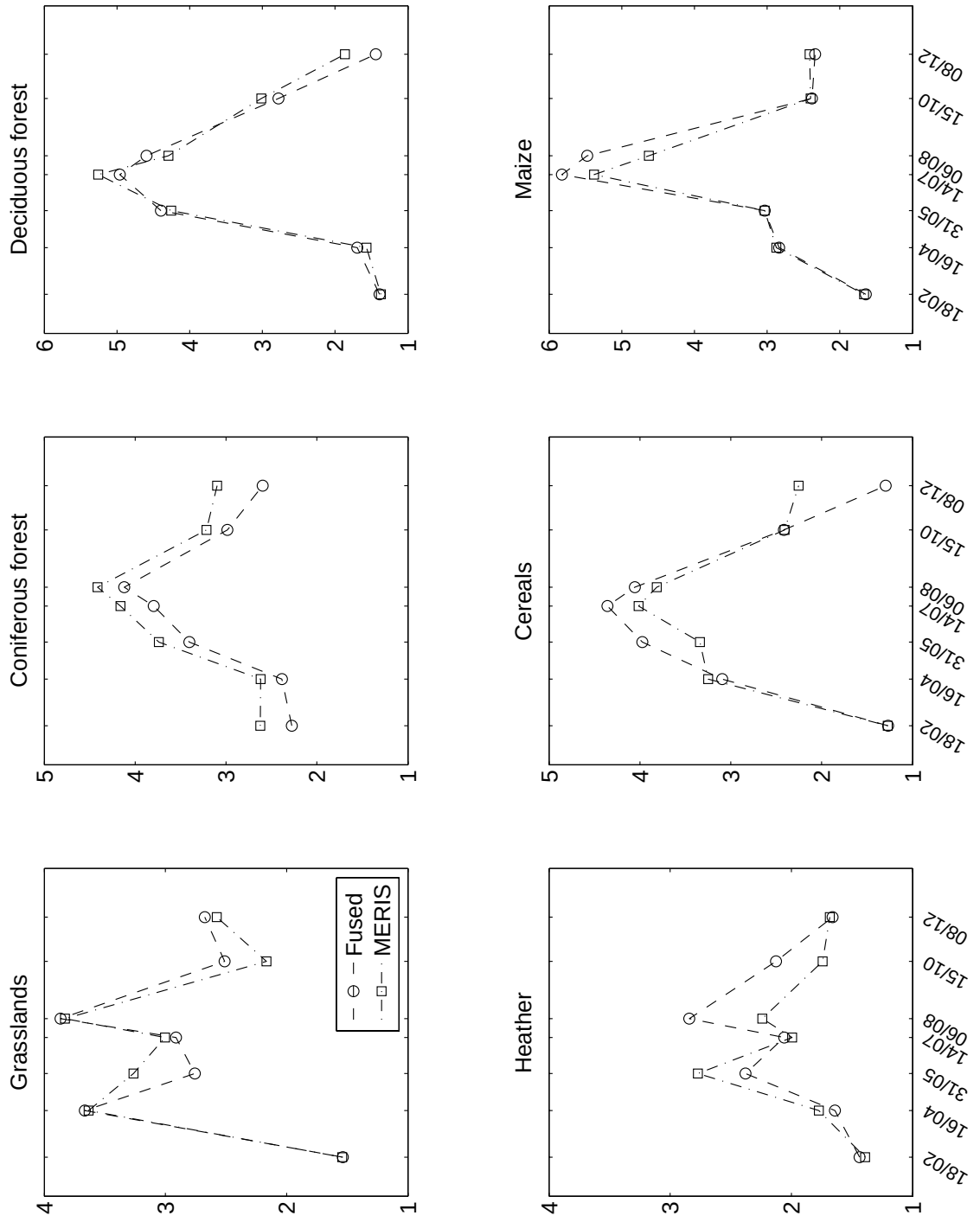

Figure 5.9. Comparison of temporal MTCI profiles of fused and MERIS FR data for the 6 main land cover types present in the study area.

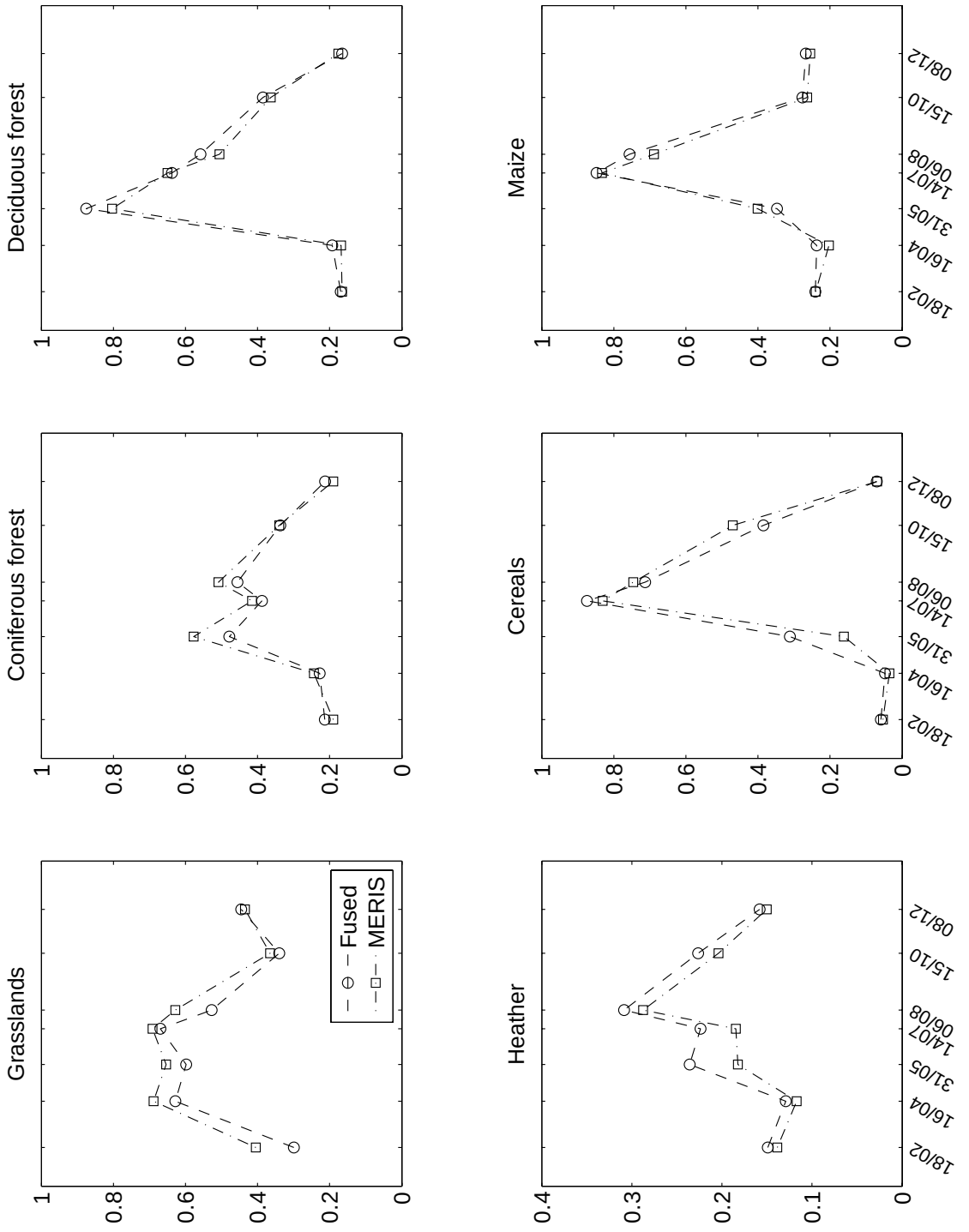

Figure 5.10. Comparison of temporal MGVI profiles of fused and MERIS FR data for the 6 main land cover types present in the study area.

5.5 Conclusions

In this work the linear mixing model is used to downscale time series of MERIS FR images (300 m pixel size) to a Landsat-like spatial resolution (25 m). A heterogeneous and fragmented landscape located in the central part of The Netherlands was selected to illustrate the performance and applicability of the proposed method. Seven MERIS FR images were available over this area covering the period comprised between the months of February and December 2003. Because of the characteristics of the landscape under study, most of the MERIS pixels were mixed pixels (i.e. more than one land cover type per pixel). The Dutch land use database of the same year (LGN5) was used to derive the fractional composition of each MERIS pixel. To do so, the ground instantaneous field of view (GIFOV) of each MERIS pixel was computed using the AMORGOS software to obtain accurate MERIS geo-location values. In this way, there was no need to re-project the images and we avoided processing errors (e.g. geometric errors due to the use of nearest neighbor resampling). Subsequently, each MERIS pixel was successively unmixed for each MERIS band using the corresponding LGN5 fractions and a MERIS neighborhood (needed to get sufficient equations to solve the unmixing equations). A quantitative data fusion quality assessment of the fused image of July was used to identify the optimal size of this neighborhood. The ERGAS index computed at 25 m and at 300 m was used for this assessment. The results of the ERGAS index at 300 m, confirmed that the proposed improvements in the data fusion approach presented in this paper enhance the quality of the fused images.

Two vegetation indices specifically designed for the MERIS sensor were computed from the series of fused images and their corresponding MERIS images. These indices are the MERIS terrestrial chlorophyll index (MTCI) and the MERIS global vegetation index (MGVI). Results showed that vegetation indices computed from the fused images yielded consistent spatial patterns as those found when computing the indices with original MERIS images. However, the use of fused images provided much more spatial details. MTCI and MGVI profiles were extracted from the fused and the MERIS images for the 6 main land cover types present in the study area (heather, coniferous and deciduous forest, grasslands, cereals and maize). The profiles showed a consistent temporal evolution. These results confirmed the potential of fused images to monitor individual vegetation patches or agricultural fields.

In summary, this work has shown that the unmixing-based data fusion approach can be used to successfully downscale time series of MERIS data to a relevant spatial resolution that allows studying vegetation processes in heterogeneous landscapes. This creates new opportunities to monitor vegetation dynamics (phenology) at high spatial, spectral *and* temporal resolutions. Sub-pixel MTCI and MGVI time series can be computed from the fused images and accurate temporal profiles can be derived for individual vegetation patches or agricultural fields. These profiles can subsequently be used for a number of applications like crop yield estimation, net primary production mapping or parameterization of vegetation models. These results are particularly relevant to map and monitor frequently clouded, heterogeneous and/or highly fragmented landscapes where the use of medium or low spatial resolution data is required in order to increase the chance of getting cloud free images.

Acknowledgements

The contribution of R. Zurita-Milla is granted through the Dutch SRON GO programme (EO-061). Financial support by the Austrian Science Foundation (*Fonds zur Förderung der wissenschaftlichen Forschung*, FWF), grant no. P17647-N04, is acknowledged.

CHAPTER 6

Synthesis

6.1 Conclusions

The main objective of this thesis is to develop a multi-sensor and multi-resolution data fusion approach that allows mapping and monitoring of heterogeneous and highly fragmented landscapes using medium spatial resolution satellite data. Each of the chapters of this thesis concentrates on answering one of the research questions proposed in section 1.5. Here we summarize our answers to the research questions of this thesis.

A. What is the radiometric quality of MERIS data and what are the potential impacts of miscalibration on MERIS land products?

In chapter 2, we studied the smile effect and the vicarious calibration corrections for the MERIS instrument and their impact on radiometry and product accuracy. The implications of applying different levels of radiometric correction were evaluated using two approaches: regional land cover mapping using spectral unmixing and the assessment of vegetation status using three MERIS land products: the MERIS terrestrial chlorophyll index (MTCI), the MERIS global vegetation index (MGVI) that is linearly related to the fraction of absorbed photosynthetically active radiation (fAPAR) and the normalized difference vegetation index (NDVI), which is related to vegetation greenness.

Our analysis showed that both the smile and the vicarious corrections are very small for the MERIS instrument (i.e. the correction factors are close to 1). Therefore, if the endmembers used for the spectral unmixing are selected from the image, the level of calibration is not very critical. However, if endmembers coming from other sources (e.g. spectral libraries) are to be used, then knowledge on their calibration level becomes essential. In this respect, all recommended correction factors must be systematically applied to MERIS data in order to preserve the highest possible classification accuracy.

For the MERIS products, relevant differences were observed when using data at different calibration levels. More precisely, we noticed that the magnitude of the smile correction factors can be locally very important and that inappropriate or incomplete corrections might lead to striping effects in the final MERIS products.

B. Can we use the linear mixing model to downscale MERIS FR data to a Landsat-like spatial resolution? What is the quality of the resulting fused images?

Chapter 3 illustrates the use of the linear mixing model to downscale MERIS FR images acquired over a (typical) heterogeneous and fragmented European landscape. The selected method, known as unmixing-based data fusion, requires the use of a high spatial resolution image to characterize the spatial patterns of the area under study. In this case, a Landsat TM image acquired four days earlier than the MERIS FR image was used to characterize the landscape by means of an unsupervised classification. Then, each MERIS pixel was successively unmixed for each band using the fractional coverage derived from the TM image and the original MERIS spectral information. The resulting fused images have the spatial resolution provided by TM and the MERIS spectral resolution (i.e. images at 25 m and with 15 spectral bands).

Two parameters need to be optimized in this method namely the number of classes, *nc*, used to classify the TM image and the size of the MERIS neighborhood, *k*, used to solve the unmixing equations. A quantitative data fusion analysis based on the ERGAS index was used both to check the quality of the resulting images and to assist with the identification of the best set of *nc* and *k* values. The results of this analysis indicate that: a) the unmixing-based data fusion approach succeeded in preserving the spectral information of MERIS (low ERGAS values) and b) there is a trade-off between the quality of the fused images at the TM and the original MERIS spatial resolutions (the ERGAS indices at the TM and at the MERIS spatial resolutions are inversely correlated). Because of this trade-off, the use of a specific application (e.g. land cover mapping) is suggested as a means to identify the best fused image.

Special attention should be paid to the co-registration of the high and low spatial resolution images and to the criteria used to select the best fused image because the quality of the image greatly depends on the choice of the two parameters that need to be optimized. In addition, it is important to study the effects that (possible) landscape changes between the acquisition dates of the TM and the MERIS images might have on the quality of the fused images. Finally, it is important to realize that fused images are only an approximation of what the MERIS sensor would be measuring if it had a Landsat-like spatial resolution.

C. Can we use MERIS fused images to derive spatially improved MERIS land products like land cover and vegetation status maps?

Chapter 4 explores the use of MERIS fused images to produce land cover maps and to assess vegetation status. The series of fused images generated in chapter 3 for different combinations of *nc* and *k* are used as an input here. First, all the fused images were classified into the 8 main land cover types of The Netherlands using a maximum likelihood classification rule. Based on the classification results, the image generated with $nc = 60$ and $k = 45$ was chosen as the best fused image. Classification results for the TM and for this fused image were very similar (overall accuracies of 63.32 % and 61.59 %, respectively). However, the best fused image outperformed the classification accuracies of a spectrally similar TM image (i.e. an image without the SWIR bands). This indicates that the fine spectral resolution of MERIS is better than a coarse spectral resolution (TM) for land cover mapping and that the SWIR region plays an important role in the final classification accuracy.

With respect to the assessment of vegetation status, the best fused image was used to compute the same three vegetation indices used in chapter 2: the MGVI, the MTCI and the NDVI. For comparison purposes, these three indices were computed for the MERIS FR (300 m) image and the NDVI was also computed for the TM image (25 m). Results indicate that MERIS fused images can be used to successfully downscale these three vegetation indices. Despite differences in the spectral configuration of the TM and MERIS sensors, a good correlation ($r = 0.76$) was found between the NDVI computed from TM and from the MERIS fused image. In addition, the vegetation indices computed from the fused image were spatially consistent with the patterns observed in the original MERIS FR image, but they provide much more spatial details. This allows us to study vegetation status of individual fields. Nevertheless, a few unsatisfactory vegetation index values were found at object boundaries. This is probably because the unsupervised classification of the TM image is not very consistent at those instances because TM pixels are also mixed at that scale. This problem may be solved by using an existing land cover map instead of a remote sensing image for

defining the thematic classes or simply by filtering the unsupervised TM or the MERIS fused image.

D. Can we use downscaled time series of MERIS data to monitor heterogeneous and fragmented landscapes with a high spatial, spectral and temporal resolution?

Chapter 5 focuses on exploiting the high temporal resolution provided by the MERIS sensor. The unmixing-based data fusion approach is used to downscale a time series of MERIS FR images (300 m pixel size). Seven MERIS FR images were available over the study area (the central part of The Netherlands) covering the period between February and December 2003. The Dutch land use database of the same year, known as the LGN5, was used to derive the fractional composition of each MERIS pixel. This was done by computing the ground instantaneous field of view (GIFOV) of each MERIS pixel. No re-projection was needed and, therefore, geometric or radiometric errors due to the use of nearest neighbor or cubic convolution resampling were avoided.

Because the LGN5 is used as a reference, we only need to optimize the k parameter (i.e. the size of the MERIS neighborhood used to get enough equations to solve the unmixing). Similar to chapter 3, the ERGAS index was used to assist with the identification of the best k value. Because of the availability of the TM image acquired in July, the MERIS image of the same month was selected for the ERGAS analysis. In this case, a value of $k = 9$ was selected as the best one. This value is significantly lower than the one found in chapter 3 but one has to realize that the number of classes used to characterize the landscape was also smaller (30 LGN5 classes vs. 60 unsupervised TM classes).

Here, only the two vegetation indices specifically designed for the MERIS sensor were considered: the MTCI and the MGVI. These vegetation indices were computed for the series of fused images and their corresponding MERIS images. Results showed that: a) vegetation indices computed from the fused images yield consistent spatial patterns with those found when computing them from the original MERIS images and b) the use of fused images provides much more spatial details.

Finally, MTCI and MGVI profiles were extracted from the fused and the MERIS images. The profiles showed a consistent temporal evolution for each of the land cover types under investigation. These results confirm the potential of fused images to monitor individual fields or vegetation patches. This creates new opportunities to monitor vegetation dynamics (phenology) at high spatial, spectral and temporal resolution. Sub-pixel MTCI and MGVI time series can be used for a number of applications like crop yield estimation, net primary production mapping or parameterization of vegetation models. These results are particularly relevant to map and monitor frequently clouded, heterogeneous and/or highly fragmented landscapes where the use of medium or low spatial resolution data is required in order to increase the chance of getting cloud free images.

General conclusions:

Based on the studies in the four previous chapters it can be concluded that:

- MERIS delivers data with a high radiometric quality (the smile and the vicarious calibration corrections are very small). However, some undesired effects were observed when using MERIS data without the smile correction. Therefore we recommend to systematically monitor the radiometric quality of this sensor and to apply all the necessary corrections to generate stable MERIS time series that can subsequently be used to obtain products with the highest possible quality.

- The linear mixing model can be successfully used to downscale MERIS data to a Landsat-like spatial resolution. This process, known as unmixing-based data fusion, requires the use of a high spatial resolution dataset (e.g. a Landsat classified image) to characterize the landscape. The resulting fused images have the spatial resolution of this high spatial resolution dataset and the spectral resolution provided by MERIS.

- The quality of fused images needs to be assessed in order to complete the data fusion process. This task is not straightforward because there is no universal way to assess the quality of fused images. In this work, the ERGAS index in combination with an application-based assessment were used to assess the quality of the fused images. Results indicate that MERIS fused images can be used to derive spatially improved land cover maps and continuous fields of vegetation properties.

- The high temporal resolution of MERIS can be used to generate time series of fused images that can be used to monitor vegetation dynamics at high spatial, spectral and temporal resolution. More precisely, downscaling MERIS images to a Landsat-like resolution allows the study of individual fields and relatively small vegetation patches. This creates new opportunities to monitor heterogeneous and fragmented landscapes that suffer from frequent cloud coverage.

6.2 Outlook

In this section we put our findings into perspective and we outline possible improvements to the proposed data fusion approach as well as further lines of research that could be derived from this thesis.

Medium spatial resolution sensors were designed to fill the gap between the data provided by high spatial resolution (Landsat-like) and coarse spatial resolution (NOAA-like) sensors. Because of their unprecedented spatial, spectral and temporal resolutions, a large number of (semi-)operational products are currently derived from MERIS and MODIS data (Curran and Steele 2005; Masuoka et al. 1998). These products are substantially supporting Earth system science research at regional to global scales (Running et al. 2004; Schmullius and Hese 2003; Zhan et al. 2002). However, the spatial resolution provided by these sensors (250 to 500 m) is

not sufficient to capture all the variability present in heterogeneous and fragmented landscapes (Addink et al. 2006; Garrigues et al. 2008; Tarnavsky et al. 2008).

High spatial resolution sensors have a past track record in mapping and monitoring heterogeneous and fragmented landscapes but, in general, they do not provide an appropriate temporal resolution. A constellation of high spatial resolution sensors has been suggested as a solution to the trade-off between the spatial, spectral and temporal resolution of Earth observation sensors (Wulder et al. 2008). However, the use of high spatial resolution data does not completely eliminate the mixed pixel problem: it shifts it towards smaller spatial scales, for instance, mixtures of photosynthetic and non-photosynthetic materials (Malenovsky et al. 2008; Verrelst et al. 2007) or mixtures of sunlit and shadowed materials (Fitzgerald et al. 2005; Malenovsky et al. 2007). In this respect, spectral mixture analysis (SMA) will always be relevant to understand what is inside a pixel (Fisher 1997). Sub-pixel methods are, therefore, useful when working with low, medium and high spatial resolution imagery. In the case of MERIS, spectral unmixing has been used to map land cover fractional composition (Zurita-Milla et al. 2007b; Zurita-Milla et al. 2005) and forest fire severtity (Gonzalez-Alonso et al. 2007). Nevertheless, the selection of appropriate training areas (or endmembers), the validation and the operationalization of the unmixing of medium spatial resolution data acquired over complex landscapes still remains a challenge.

In this thesis, we have demonstrated that it is possible to downscale MERIS FR data to a Landsat-like spatial resolution (provided that a high spatial resolution dataset is available over the area covered by MERIS). The Netherlands, having a population density of 480 inhabitants/km^2 (about four times higher than the European average; (CBS 2008)) was selected as the main study site because it presents a typical example of landscapes heavily shaped by anthropogenic activities. Because of this anthropogenic pressure, there is a continuous need to map and monitor Dutch landscapes (VROM 1999). Moreover, mapping and monitoring The Netherlands using optical sensors is also a challenge because of the persistent cloud coverage throughout the year. In this respect, the use of MERIS fused images increases the chance of getting cloud free images and it allows to map and monitor individual fields and (small) vegetation patches with a higher temporal resolution than the one provided by Landsat-like sensors. Other applications that benefit from this kind of data fusion approach are: land cover change detection (Gutman et al. 2004), proper retrieval of biophysical and biochemical parameters (Simic et al. 2004), designing reliable soil-vegetation-atmosphere models (Bormann 2008) or, even to evaluate the history of a given landscape (Motzkin et al. 1999) and the socio-cultural and environmental services that it can provide (Altieri 1999; Solon 1995).

Despite the potential of the selected data fusion method and of the resulting MERIS fused images, a few issues still require further work before the method can become operational. The next sections discuss these issues that have been grouped according to the spatial, spectral and temporal dimensions.

6.2.1 Spatial dimension

A few issues related to the spatial dimension of MERIS data will be discussed in this section. These issues are: co-registration, fusion extent, use of contextual information and appropriate spatial scale.

Co-registration

A good co-registration is a critical prerequisite of all the remote sensing data fusion methods that use data acquired by different sensors or at different scales. Manual image-to-image co-registration is possible when the difference in spatial scale is not large and when the images have a similar acquisition date (otherwise it might be difficult to locate adequate ground control points). An automatic co-registration, like the one proposed in chapter 5, facilitates the operationalization of the fusion. For the unmixing-based data fusion approach, a co-registration accuracy of 0.1-0.2 low spatial resolution pixels is recommended (Zhukov et al. 1999). In this respect, current MERIS geo-location accuracy is about 0.25 MERIS FR pixels (Arino et al. 2008). This has been achieved thanks to the continuous improvement on the determination of ENVISAT's position that has led to the development of the AMORGOS geo-location software (Saunier et al. 2006).

Fusion extent

As discussed in chapter 1, high spatial resolution images have a smaller swath than medium and coarse spatial resolution sensors. Therefore, one limitation of combining data acquired at different spatial resolutions is that the fusion can only be performed over the common area. The use of readily available land use/land cover datasets can overcome this limitation (e.g. chapter 5). However, these datasets often contain features not directly derived from spectral images (like roads, etc). Furthermore, these datasets are "static" (i.e. they map field boundaries at a certain time of the year) and they neglect within-class variability. Thus, additional research effort should be put on investigating these issues.

Contextual information

The unmixing-based data fusion approach operates at the measurement (i.e. pixel) level. Contextual information is only used to extract enough equations to solve the unmixing. However, within-class heterogeneity can be considerably large due to environmental factors. Therefore, a smarter use of the contextual information should be investigated. For instance, the shape of the neighbourhood used to solve the unmixing could be relaxed to account for within-class heterogeneity (Busetto et al. 2008).

Appropriate spatial scale

The proposed data fusion method should be tested at other scales and with other datasets because a single combination of sensors and scales cannot sufficiently capture the complexity of heterogeneous landscapes. Complementary strategies that focus on determining the best pixel size for a given application should also be supported (Hengl 2006; Woodcock and Strahler 1987).

6.2.2 Spectral dimension

The use of regularization methods and the spectral quality of the MERIS and of the fused images are briefly discussed in this section.

Solving the mixing equations

Both the linear and the non-linear unmixing are typical examples of ill-posed problems because the solution does not continuously depend on the data. In other words, a small perturbation in the input data can result in a largely different output (Combal et al. 2002).

In the case of the linear mixing the ill-posedness can be evaluated by the so-called condition number of the matrix of endmembers (spectral unmixing) or the matrix of proportions (unmixing-based data fusion). When the rows or columns of this matrix are linearly independent the condition number equals 1. If the matrix contains a pair of rows or columns that is linearly dependent the condition number is infinite. High condition numbers are associated with ill-posed problems and require the use of regularization techniques (Hansen 2001). For the non-linear unmixing, the ill-posedness is more difficult to evaluate. Further work is, therefore, needed to assess the pros and cons of linear versus non-linear approaches. The use of radiative transfer models can assist in understanding how the signals are mixed at different spatial resolutions and for different levels of landscape complexity.

Spectral quality

In order to obtain high quality spectral images, the data collected by Earth observation sensors need to be corrected for instrument and atmospheric effects. In this thesis we have explored the effects of MERIS calibration and studied the smile and vicarious calibration corrections. For operational reasons, little attention was paid here to the atmospheric correction (the atmospheric effects were considered homogenous over the study area or minimized by the use of vegetation indices like the MGVI). However, we realize that performing a full atmospheric correction is very important for a number of applications (e.g. retrieval of biophysical properties by inverting a radiative transfer model). The atmospheric correction algorithm proposed by Guanter et al. (2008) was tested for MERIS images acquired over The Netherlands. Some adjustments were needed because this algorithm works for land surfaces whereas water bodies and coastal areas are very important in The Netherlands. Preliminary results were promising (Zurita-Milla et al. 2007c), but further work is needed to assess this and other MERIS atmospheric correction methods. In this respect, calibration and validation activities should be further encouraged. Operational atmospheric correction methods, monitoring sensor spectral shifts, comparing data acquired by different sensors and implementing data assimilation schemes are essential to produce stable long-term series of remote sensing images as well as products (Goryl et al. 2007; Lyapustin et al. 2007).

Spectral data fusion quality

In this thesis we have consistently evaluated the quality of fused images using the ERGAS index. Although this index represents a state-of-the-art method of assessment, the use of other data fusion quality indicators should be explored for comparison purposes. A preliminary

study was done with the images presented in chapter 5. The so-called Skill index (Taylor 2001) was used with the fused images of 14 July 2003. This index ranges between 0 and 1 and the higher its value, the better the quality of the fused images.

$$S^i = \frac{\left(1+R^i\right)^4}{\left(\frac{\mu^i_{fused}}{\mu^i_{ref}}+\frac{\mu^i_{ref}}{\mu^i_{fused}}\right)^2\left(\frac{\sigma^i_{fused}}{\sigma^i_{ref}}+\frac{\sigma^i_{ref}}{\sigma^i_{fused}}\right)^2} \tag{6.1}$$

where: R^i is the correlation coefficient between the i^{th} band of the fused image and its spectrally correspondent TM band, μ^i_{fused} and μ^i_{ref} are the mean values of those bands, and σ^i_{fused} and σ^i_{ref} are the corresponding standard deviations.

The first four TM bands and their spectrally correspondent MERIS bands (i.e. the bands used for the ERGAS at 25 m) were used to compute the Skill. Subsequently, the per-band Skill values were averaged to obtain a representative data fusion quality value for each fused image (Figure 6.1). These results are consistent with those obtained by the ERGAS index (see Figure 5.5).

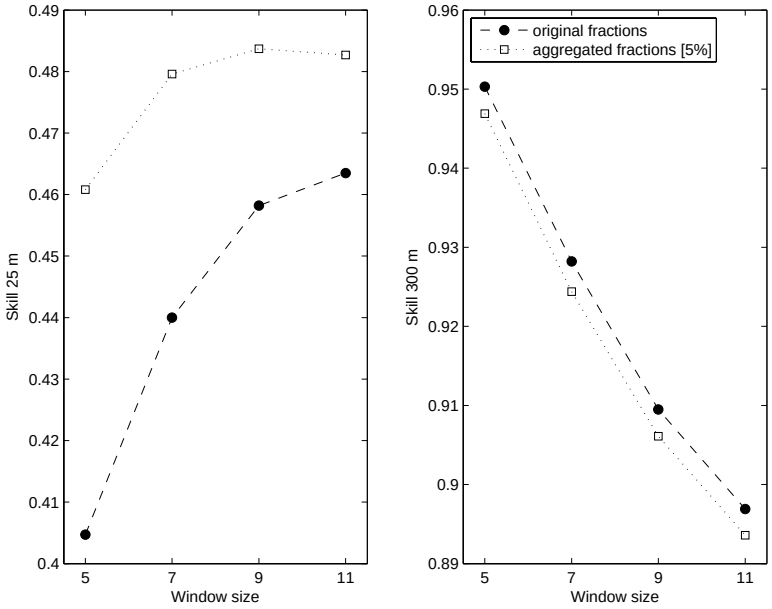

Figure 6.1. Average Skill values for the fused image of 14 July 2003 at 25 m (left) and 300 m (right).

6.2.3 Temporal dimension

Three issues, namely cloud masking, factors to consider in multi-temporal studies and the optimum temporal resolution will be discussed in this section.

Cloud masking

Figure 6.2 shows the temporal series of MERIS FR images used in this thesis. As we can see, clouds hamper the operational use of images acquired by optical sensors. Therefore, an automatic and efficient cloud screening algorithm is required to facilitate the elaboration of remote sensing based products.

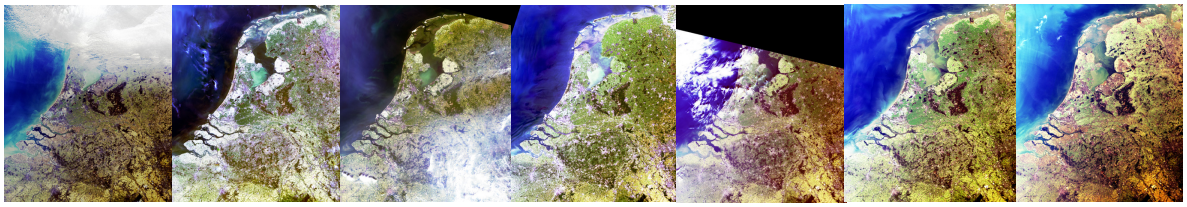

Figure 6.2. Time series of MERIS FR images for the year 2003.

The use of an unmixing-based data screening algorithm (Gómez-Chova et al. 2007a) has been tested over this time series of MERIS FR images (Gómez-Chova et al. 2007b; Zurita-Milla et al. 2007c). Figure 6.3 shows the cloud screening results for the first image of the series and the cloud free days that are available for each MERIS FR pixel. These results are still preliminary and extra effort should be put on the detection and appropriate masking of thin clouds and cloud shadows.

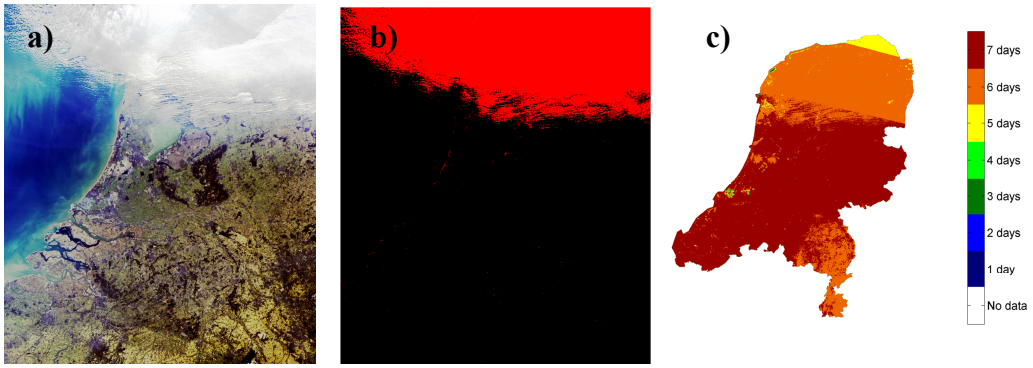

Figure 6.3. MERIS image of 18 February 2003 (a), corresponding cloud mask (b) and per-pixel number of cloud-free dates (c).

Multi-temporal studies

Multi-temporal studies typically require that the images are perfectly co-registered, corrected for atmospheric effects, for solar and viewing angles (BRDF effects) and for

possible shifts in the spectral calibration of the instrument (Lillesand and Kiefer 2000). In heterogeneous landscapes, it is also very important to realize that images acquired from different orbits do not have congruent pixels (i.e. the pixels do not have the same ground instantaneous field of view, GIFOV). This is illustrated in Figure 6.4 where we show an RGB composite of the MGVI computed from three MERIS dates (16 April, 14 July and 15 October). In this figure, the 25 m LGN5 grid is filled using the GIFOV of each MERIS pixel for each of the dates under consideration. The small irregularities in the shape of the MERIS pixels are explained by the resolution of the reference grid, possible topographic effects and the MERIS viewing angle (recall that the size of the GIFOV varies along the MERIS swath).

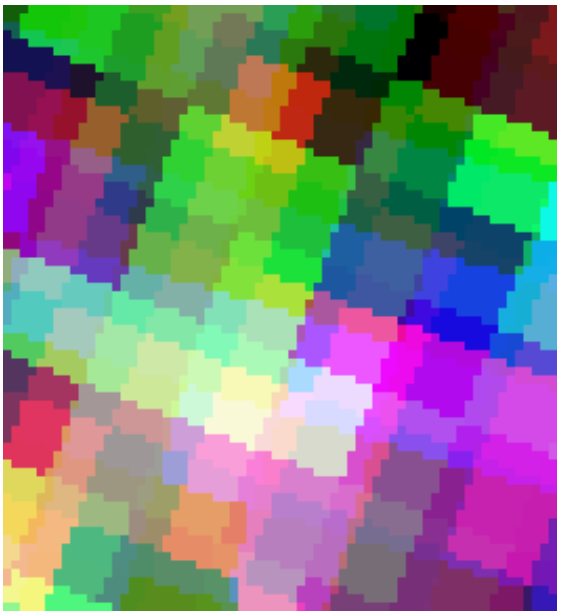

Figure 6.4. Detail of the ground instantaneous field of view for three MERIS MGVI images (16 April, 14 July and 15 October) displayed as an RGB color composite.

These effects should be considered when performing land cover change studies and when linking ground and satellite measurements (e.g. product validation).

Optimum temporal resolution

Finally, it is important to study the optimum temporal resolution for monitoring vegetation status because the information provided by images acquired at consecutive days is highly correlated. This optimum resolution should consider the phenological heterogeneity of the vegetation present in a certain area and account for the probability of getting cloud-free images over that area (Alexandridis et al. 2008).

In this thesis it was demonstrated that data fusion methods can be used to successfully bridge the spectral, spatial and temporal scaling gaps. This opens two future lines of work. On the one hand certain scaling gaps can be filled by combining existing Earth observation instruments so that the continuity of historical and present data records is improved. On the other hand, data fusion can substantially contribute to future products and instrument design by facilitating a multi-scale and multi-sensor framework where different instruments can be optimally integrated.

References

Abdou, W.A., Bruegge, C.J., Helmlinger, M.C., Conel, J.E., Pilorz, S.H., Ledeboer, W., Gaitley, B.J., & Thome, K.J. (2002). Vicarious calibration experiment in support of the multi-angle imaging spectroradiometer. *IEEE Transactions on Geoscience and Remote Sensing, 40*, 1500-1511.

Acerbi-Junior, F.W., Clevers, J.G.P.W., & Schaepman, M.E. (2006). The assessment of multi-sensor image fusion using wavelet transforms for mapping the Brazilian Savanna. *International Journal of Applied Earth Observation and Geoinformation, 8*, 278-288.

ACRI-ST (2007). AMORGOS v. 3.0 Software User Manual & Interface Control Document, rev. 0A.

Adams, J.B., & Gillespie, A.R. (2006). *Remote sensing of landscapes with spectral images. A physical modeling approach*. New York: Cambridge University Press.

Adams, J.B., Sabol, D.E., Kapos, V., Almeida, R., Roberts, D.A., Smith, M.O., & Gillespie, A.R. (1995). Classification of Multispectral Images Based on Fractions of Endmembers - Application to Land-Cover Change in the Brazilian Amazon. *Remote Sensing of Environment, 52*, 137-154.

Addink, E.A., Clevers, J.G.P.W., de Jong, S.M., Epema, G.F., van der Meer, F.D., Skidmore, A.K., & Bakker, W.H. (2006). The 'Stained Glass Procedure', a new method to compare classification performance of images acquired with different pixel sizes. *International Journal of Applied Earth Observation and Geoinformation, 8*, 237-245.

Alexandridis, T.K., Gitas, I.Z., & Silleos, N.G. (2008). An estimation of the optimum temporal resolution for monitoring vegetation condition on a nationwide scale using MODIS/Terra data. *International Journal of Remote Sensing, 29*, 3589-3607.

Alparone, L., Baronti, S., Garzelli, A., & Nencini, F. (2004). A global quality measurement of pan-sharpened multispectral imagery. *IEEE Geoscience and Remote Sensing Letters, 1*, 313-317.

Altieri, M.A. (1999). The ecological role of biodiversity in agroecosystems. *Agriculture, Ecosystems and Environment, 74*, 19-31.

Aplin, P. (2004). Remote sensing as a means of ecological investigation. In: M.O. Altan (Ed.) *Proceedings of the XXth congress of the International Society for Photogrammetry and Remote Sensing: geo-imagery bridging continents.* (pp. 325-333). Istanbul, Turkey: ISPRS.

Aplin, P. (2006). On scales and dynamics in observing the environment. *International Journal of Remote Sensing, 27*, 2123-2140.

Arino, O., Gross, D., Ranera, F., Leroy, M., Bicheron, P., Brockman, C., Defourny, P., Vancutsem, C., Achard, F., Durieux, L., Bourg, L., Latham, J., Di Gregorio, A., Witt, R., Herold, M., Sambale, J., Plummer, S., & Weber, J.L. (2008). GlobCover: ESA service for Global land cover from MERIS. In: *Proceedings of the International Geoscience and Remote Sensing Symposium (IGARSS)* (pp. 2412-2415). Barcelona, Spain: IEEE.

Arino, O., Trebossen, H., Achard, F., Leroy, M., Brockman, C., Defourny, P., Witt, R., Latham, J., Schmullius, C., Plummer, S., Laur, H., Goryl, P., & Houghton, N. (2005). The globcover initiative. In: *Proceedings of the MERIS (A)ATSR Workshop 2005* (pp. 171-175). Salzburg, Austria: ESA.

Asner, G.P. (2001). Cloud cover in Landsat observations of the Brazilian Amazon. *International Journal of Remote Sensing, 22*, 3855-3862.

Atkinson, P.M. (2004). Resolution Manipulation and Sub-Pixel Mapping. In: S.M. de Jong & F.D. van der Meer (Eds.), *Remote Sensing Image Analysis: Including the Spatial Domain,* (pp. 51-70). Dordrecht, The Netherlands: Kluwer Academic Publishers.

Atkinson, P.M. (2007). The importance of scale in remote sensing and GIS and its implications for data integration In: V. Mesev (Ed.), *Integration of GIS and Remote Sensing* (p. 296). Chichester, West Sussex, UK: Wiley.

Atkinson, P.M., Pardo-Iguzquiza, E., & Chica-Olmo, M. (2008). Downscaling cokriging for super-resolution mapping of continua in remotely sensed images. *IEEE Transactions on Geoscience and Remote Sensing, 46*, 573-580.

Aussedat, O., & Gobron, N. (2004). fAPAR processor plug-in for BEAM.

Bacour, C., Baret, F., Beal, D., Weiss, M., & Pavageau, K. (2006). Neural network estimation of LAI, fAPAR, fCover and LAIxCab, from top of canopy MERIS reflectance data: Principles and validation. *Remote Sensing of Environment, 105*, 313-325.

Baret, F., Morissette, J.T., Fernandes, R.A., Champeaux, J.L., Myneni, R.B., Chen, J., Plummer, S., Weiss, M., Bacour, C., Garrigues, S., & Nickeson, J.E. (2006). Evaluation of the representativeness of networks of sites for the global validation and intercomparison of land biophysical products: Proposition of the CEOS-BELMANIP. *IEEE Transactions on Geoscience and Remote Sensing, 44*, 1794-1802.

Bastin, L. (1997). Comparison of fuzzy c-means classification, linear mixture modelling and MLC probabilities as tools for unmixing coarse pixels. *International Journal of Remote Sensing, 18*, 3629-3648.

Berk, A., Bernstein, L.S., Anderson, G.P., Acharya, P.K., Robertson, D.C., Chetwynd, J.H., & Adler-Golden, S.M. (1998). MODTRAN cloud and multiple scattering upgrades with application to AVIRIS. *Remote Sensing of Environment, 65*, 367-375.

Bézy, J.-L., Delwart, S., & Rast, M. (1998). The ESA medium resolution imaging spectrometer MERIS. In: W.L. Barnes (Ed.) *Proceedings of SPIE - Earth Observing Systems III* (pp. 594-604)

Bézy, J.-L., Gourmelon, G., Bessudo, R., Baudin, G., Sontag, H., & Weiss, S. (1999). ENVISAT Medium Resolution Imaging Spectrometer (MERIS). In: *Proceedings of the International Geoscience and Remote Sensing Symposium (IGARSS)* (pp. 1432-1434). Hamburg, Germany: IEEE.

Boardman, J.W. (1990). Inversion of high spectral resolution data. In: G. Vane (Ed.) *Proceedings of SPIE - Imaging Spectroscopy of the Terrestrial Environment* (pp. 222-233). Orlando, USA: SPIE.

Boegh, E., Thorsen, M., Butts, M.B., Hansen, S., Christiansen, J.S., Abrahamsen, P., Hasager, C.B., Jensen, N.O., van der Keur, P., Refsgaard, J.C., Schelde, K., Soegaard, H., & Thomsen, A. (2004). Incorporating remote sensing data in physically based distributed agro-hydrological modelling. *Journal of Hydrology, 287*, 279-299.

Borel, C.C., & Gerstl, S.A.W. (1994). Nonlinear spectral mixing models for vegetative and soil surfaces. *Remote Sensing of Environment, 47*, 403-416.

Bormann, H. (2008). Sensitivity of a soil-vegetation-atmosphere-transfer scheme to input data resolution and data classification. *Journal of Hydrology, 351*, 154-169.

Boschetti, L., Flasse, S.P., & Brivio, P.A. (2004). Analysis of the conflict between omission and commission in low spatial resolution dichotomic thematic products: The Pareto Boundary. *Remote Sensing of Environment, 91*, 280-292.

Boucher, A., & Kyriakidis, P.C. (2006). Super-resolution land cover mapping with indicator geostatistics. *Remote Sensing of Environment, 104*, 264-282.

Burnett, C., & Blaschke, T. (2003). A multi-scale segmentation/object relationship modelling methodology for landscape analysis. *Ecological Modelling, 168*, 233-249.

Burrough, P.A., & McDonnell, R.A. (1998). *Principles of Geographical Information Systems*. Oxford: Oxford University Press, UK

Busetto, L., Meroni, M., & Colombo, R. (2008). Combining medium and coarse spatial resolution satellite data to improve the estimation of sub-pixel NDVI time series. *Remote Sensing of Environment, 112*, 118-131.

CBS (2008). Demografische informatie http://www.cbs.nl/nl-NL/menu/themas/bevolking/beschrijving/default.htm [accessed 22nd May 2008].

Champeaux, J.L., Arcos, D., Bazile, E., Giard, D., Goutorbe, J.P., Habets, F., Noilhan, J., & Roujean, J.L. (2000). AVHRR-derived vegetation mapping over Western Europe for use in Numerical Weather Prediction models. *International Journal of Remote Sensing, 21*, 1183-1199.

Chander, G., & Markham, B. (2003). Revised Landsat-5 TM radiometric calibration procedures and postcalibration dynamic ranges. *IEEE Transactions on Geoscience and Remote Sensing, 41*, 2674-2677.

Chang, C.I., & Heinz, D.C. (2000). Constrained subpixel target detection for remotely sensed imagery. *IEEE Transactions on Geoscience and Remote Sensing, 38*, 1144-1159.

Chen, X.X., & Vierling, L. (2006). Spectral mixture analyses of hyperspectral data acquired using a tethered balloon. *Remote Sensing of Environment, 103*, 338-350.

Chikara, R.S. (1984). Effect of mixed (boundary) pixels on crop proportion estimation *Remote Sensing of Environment, 14*, 207-218.

Christensen, N.L., Bartuska, A.M., Brown, J.H., Carpenter, S., D'Antonio, C., Francis, R., Franklin, J.F., MacMahon, J.A., Noss, R.F., Parsons, D.J., Peterson, C.H., Turner, M.G., & Woodmansee, R.G. (1996). The report of the ecological society of america committee on the scientific basis for ecosystem management. *Ecological Applications, 6*, 665-691.

Cleveland, W.S. (1985). *The elements of graphing data*: Wadsworth Publ. Co.

Clevers, J.G.P.W., de Jong, S.M., Epema, G.F., van der Meer, F., Bakker, W.H., Skidmore, A.K., & Addink, E.A. (2001). MERIS and the red-edge position. *International Journal of Applied Earth Observation and Geoinformation, 3*, 313-320.

Clevers, J.G.P.W., de Jong, S.M., Epema, G.F., van der Meer, F.D., Bakker, W.H., Skidmore, A.K., & Scholte, K.H. (2002). Derivation of the red edge index using the MERIS standard band setting. *International Journal of Remote Sensing, 23*, 3169-3184.

Clevers, J.G.P.W., Schaepman, M.E., Mücher, C.A., de Wit, A.J.W., Zurita-Milla, R., & Bartholomeus, H.M. (2007). Using MERIS on Envisat for land cover mapping in the Netherlands. *International Journal of Remote Sensing, 28*, 637-652.

Clevers, J.G.P.W., Zurita Milla, R., Schaepman, M.E., & Bartholomeus, H.M. (2005). Using MERIS on ENVISAT for land cover mapping. . In: *Proceedings of the 2004 Envisat & ERS Symposium* (pp. 771-780). Salzburg, Austria: ESA.

Combal, B., Baret, F., Weiss, M., Trubuil, A., Macé, D., Pragnere, A., Myneni, R.B., Knyazikhin, Y., & Wang, L. (2002). Retrieval of biophysical variables from bidirectional reflectance: using prior information to solve the ill-posed inverse problem. *Remote Sensing of Environment, 84*, 1-15.

Courrèges-Lacoste, G.B., Schaarsberg, J.G., Sprik, R., & Delwart, S. (2003). Modeling of spectralon diffusers for radiometric calibration in remote sensing. *Optical Engineering, 42*, 3600-3607.

Cross, A.M., Settle, J.J., Drake, N.A., & Paivinen, R.T.M. (1991). Subpixel measurement of tropical forest cover using AVHRR data. *International Journal of Remote Sensing, 12*, 1119-1129.

Curran, P.J., & Steele, C.M. (2005). MERIS: The re-branding of an ocean sensor. *International Journal of Remote Sensing, 26*, 1781-1798.

Dash, J., & Curran, P.J. (2004). The MERIS terrestrial chlorophyll index. *International Journal of Remote Sensing, 25*, 5403-5413.

de Wit, A.J.W., & Clevers, J.G.P.W. (2004). Efficiency and accuracy of per-field classification for operational crop mapping. *International Journal of Remote Sensing*, 4091-4112.

DeFries, R.S., Hansen, M.C., & Townshend, J.R.G. (2000). Global continuous fields of vegetation characteristics: A linear mixture model applied to multi-year 8 km AVHRR data. *International Journal of Remote Sensing, 21*, 1389-1414.

DeFries, R.S., & Townshend, J.R.G. (1994). NDVI-derived land cover classifications at a global scale. *International Journal of Remote Sensing, 15*, 3567-3586.

DeFries, R.S., & Townshend, J.R.G. (1999). Global land cover characterization from satellite data: From research to operational implementation? *Global Ecology and Biogeography, 8*, 367-379.

Delwart, S., & Bourg, L. (2003). MERIS 1st Year: Early Calibration Results. In: *Proceedings of the International Geoscience and Remote Sensing Symposium (IGARSS)* (pp. 1591-1593). Toulouse, France: IEEE.

Dickinson, R.E., Shaikh, M., Bryant, R., & Graumlich, L. (1998). Interactive canopies for a climate model. *Journal of Climate, 11*, 2823-2836.

Dorigo, W.A., Zurita-Milla, R., de Wit, A.J.W., Brazile, J., Singh, R., & Schaepman, M.E. (2007). A review on reflective remote sensing and data assimilation techniques for enhanced agroecosystem modeling. *International Journal of Applied Earth Observation and Geoinformation, 9*, 165-193.

Du, Q., & Chang, C.I. (2004). Linear mixture analysis-based compression for hyperspectal image analysis. *IEEE Transactions on Geoscience and Remote Sensing, 42*, 875-891.

Dubuisson, P., Borde, R., Dessailly, D., & Santer, R. (2003). In-flight spectral calibration of the oxygen A-band channel of MERIS. *International Journal of Remote Sensing, 24*, 1177-1182.

Ehlers, M. (1991). Multisensor image fusion techniques in remote sensing. *ISPRS Journal of Photogrammetry & Remote Sensing, 46*, 19-30.

ESA (2006). MERIS Product Handbook. http://envisat.esa.int/handbooks/meris/ [accessed 2nd March 2007].

ESA EOHelpdesk (personal communication) (2006). MERIS Lsat values over land.

European Commission (2003). *Council Directive 92/43/CEE of 21 May 1992 on the conservation of natural habitats and of wild fauna and flora. As amended by the Accession Act of Austria, Finland and Sweden (1995) and the Accession Act of the Czech Republic, the Republic of Estonia, the Republic of Cyprus, the Republic of Latvia, the Republic of Lithuania, the Republic of Hungary, the Republic of Malta, the Republic of Poland, the Republic of Slovenia and the Slovak Republic (2003)*. Brussels (BE): European Commission 1992/95/2003.

Fensholt, R., Sandholt, I., & Stisen, S. (2006). Evaluating MODIS, MERIS, and VEGETATION - Vegetation indices using in situ measurements in a semiarid environment. *IEEE Transactions on Geoscience and Remote Sensing, 44*, 1774-1786.

Fernandes, R., Fraser, R., Latifovic, R., Cihlar, J., Beaubien, J., & Du, Y. (2004). Approaches to fractional land cover and continuous field mapping: A comparative assessment over the BOREAS study region. *Remote Sensing of Environment, 89*, 234-251.

Fisher, P. (1997). The pixel: A snare and a delusion. *International Journal of Remote Sensing, 18*, 679-685.

Fitzgerald, G.J., Pinter, P.J., Hunsaker, D.J., & Clarke, T.R. (2005). Multiple shadow fractions in spectral mixture analysis of a cotton canopy. *Remote Sensing of Environment, 97*, 526-539.

Foley, J.A., DeFries, R., Asner, G.P., Barford, C., Bonan, G., Carpenter, S.R., Chapin, F.S., Coe, M.T., Daily, G.C., Gibbs, H.K., Helkowski, J.H., Holloway, T., Howard, E.A., Kucharik, C.J., Monfreda, C., Patz, J.A., Prentice, I.C., Ramankutty, N., & Snyder, P.K. (2005). Global consequences of land use. *Science, 309*, 570-574.

Foody, G.M. (2002). Status of land cover classification accuracy assessment. *Remote Sensing of Environment, 80*, 185-201.

Foody, G.M. (2004). Sub-Pixel Methods in Remote Sensing. In: S.M. de Jong & F.D. van der Meer (Eds.), *Remote Sensing Image Analysis: Including the Spatial Domain,* (pp. 37-49). Dordrecht, The Netherlands: Kluwer Academic Publishers.

Fraser, R.H., Abuelgasim, A., & Latifovic, R. (2005). A method for detecting large-scale forest cover change using coarse spatial resolution imagery. *Remote Sensing of Environment, 95*, 414-427.

Fraser, R.H., Li, Z., & Cihlar, J. (2000). Hotspot and NDVI differencing synergy (HANDS): A new technique for burned area mapping over boreal forest. *Remote Sensing of Environment, 74*, 362-376.

Friend, A.D., Arneth, A., Kiang, N.Y., Lomas, M., Ogée, J., Rödenbeck, C., Running, S.W., Santaren, J.D., Sitch, S., Viovy, N., Ian Woodward, F., & Zaehle, S. (2007). FLUXNET and modelling the global carbon cycle. *Global Change Biology, 13*, 610-633.

Gallego, F.J. (2004). Remote sensing and land cover area estimation. *International Journal of Remote Sensing, 25*, 3019-3047.

Gardner, B.L. (2005). Causes of rural economic development. *Agricultural Economics, 32*, 21-41.

Garrigues, S., Allard, D., Baret, F., & Morisette, J. (2008). Multivariate quantification of landscape spatial heterogeneity using variogram models. *Remote Sensing of Environment, 112*, 216-230.

Garrigues, S., Allard, D., Baret, F., & Weiss, M. (2006). Influence of landscape spatial heterogeneity on the non-linear estimation of leaf area index from moderate spatial resolution remote sensing data. *Remote Sensing of Environment, 105*, 286-298.

Genovese, G., Vignolles, C., Negre, T., & Passera, G. (2001). A methodology for a combined use of normalised difference vegetation index and CORINE land cover data for crop yield monitoring and forecasting. A case study on Spain. *Agronomie, 21*, 91-111.

Gobron, N., Aussedat, A., Pinty, B., Taberner, M., & Verstraete, M. (2004). Medium Resolution Imaging Spectrometer (MERIS). Level 2 Land Surface Product. Algorithm Theoretical Basis Document. Institute for Environment and Sustainability. Joint Research Centre. EUR 21387 EN Ispra, Italy

Gobron, N., Pinty, B., Verstraete, M., & Govaerts, Y. (1999). The MERIS Global Vegetation Index (MGVI): description and preliminary application. *International Journal of Remote Sensing, 20*, 1917-1927.

Golub, G.H., Hansen, P.C., & O'Leary, D.P. (2000). Tikhonov Regularization and Total Least Squares. *SIAM Journal of Matrix Analysis and Applications, 21*, 185-194.

Gómez-Chova, L., Camps-Valls, G., Calpe-Maravilla, J., Guanter, L., & Moreno, J. (2007a). Cloud-screening algorithm for ENVISAT/MERIS multispectral images. *IEEE Transactions on Geoscience and Remote Sensing, 45*, 4105-4118.

Gómez-Chova, L., Zurita-Milla, R., Camps-Valls, G., Guanter, L., Clevers, J., Calpe, J., Schaepman, M.E., & Moreno, J. (2007b). Cloud screening and multitemporal unmixing of MERIS FR data. In: *Proceedings of Envisat Symposium*. Montreux, Switzerland: ESA

Gonzalez-Alonso, F., Merino-De-Miguel, S., Roldan-Zamarron, A., Garcia-Gigorro, S., & Cuevas, J.M. (2007). MERIS full resolution data for mapping level-of-damage caused by forest fires: The Valencia de Alcantara event in August 2003. *International Journal of Remote Sensing, 28*, 797-809.

González-Audícana, M., Otazu, X., Fors, O., & Alvarez-Mozos, J. (2006). A low computational-cost method to fuse IKONOS images using the spectral response function of its sensors. *IEEE Transactions on Geoscience and Remote Sensing, 44*, 1683-1691.

Goodenough, D.G., Dyk, A., Murdoch, M., West, C., Niemann, K.O., Chen, H., Han, T., & Pearlman, J.S. (2003). Processing Hyperion and ALI for forest classification. *IEEE Transactions on Geoscience and Remote Sensing, 41*, 1321-1331.

Goryl, P., Brockmann, C., Block, T., Riazanoff, S., & Santer, R. (2007). The EO calval portal. In: *Proceedings of Envisat Symposium*. Montreux, Switzerland: ESA.

Goryl, P., & Huot, J.P. (2003). Overview of the Envisat Meris and AATSR data quality, calibration and validation program. In: *Proceedings of the International Geoscience and Remote Sensing Symposium (IGARSS)* (pp. 1588-1590). Toulouse, France: IEEE.

Gould, W. (2000). Remote sensing of vegetation, plant species richness, and regional biodiversity hotspots. *Ecological Applications, 10*, 1861-1870.

Govaerts, Y.M., & Clerici, M. (2004). Evaluation of radiative transfer simulations over bright desert calibration sites. *IEEE Transactions on Geoscience and Remote Sensing, 42*, 176-187.

Griffiths, G.H., Lee, J., & Eversham, B.C. (2000). Landscape pattern and species richness; regional scale analysis from remote sensing. *International Journal of Remote Sensing, 21*, 2685-2704.

Guanter, L., Alonso, L., Gómez-Chova, L., Amorós-López, J., Vila, J., & Moreno, L. (2007). Estimation of solar-induced vegetation fluorescence from space measurements. *Geophysical Research Letters, 34, L08401*

Guanter, L., Gomez-Chova, L., & Moreno, J. (2008). Coupled retrieval of aerosol optical thickness, columnar water vapor and surface reflectance maps from ENVISAT/MERIS data over land. *Remote Sensing of Environment, 112*, 2898-2913.

Gutman, G., Janetos, A.C., Justice, C.O., Moran, E.F., Mustard, J.F., Rindfuss, R.R., Skole, D., Turner II, B.L., & Cochrane, M.A. (Eds.) (2004). *Land Change Science*. Dordrecht (The Netherlands): Kluwer Academic Publishers.

Haertel, V., Shimabukuro, Y.E., & Almeida-Filho, R. (2004). Fraction images in multitemporal change detection. *International Journal of Remote Sensing, 25*, 5473-5489.

Haertel, V.F., & Shimabukuro, Y.E. (2005). Spectral linear mixing model in low spatial resolution image data. *IEEE Transactions on Geoscience and Remote Sensing, 43*, 2555-2562.

Hall, D.L., & Llinas, J. (1997). An introduction to multisensor data fusion. In: *Proceedings of the International Geoscience and Remote Sensing Symposium (IGARSS)* (pp. 6-23). Toronto, Canada: IEEE.

Hall, F.G., Shimabukuro, Y.E., & Huemmrich, K.F. (1995). Remote-Sensing of Forest Biophysical Structure Using Mixture Decomposition and Geometric Reflectance Models. *Ecological Applications, 5*, 993-1013.

Hall, F.G., Strebel, D.E., & Sellers, P.J. (1988). Linking knowledge among spatial and temporal scales: Vegetation, atmosphere, climate and remote sensing. *Landscape Ecology, 2*, 3-22.

Hall, S.S. (1992). *Mapping the next millenium: The discovery of new geographies*. New York, USA: Random House.

Hansen, P.C. (2001). Regularization Tools Version 3.1 for Matlab 6.0. *Numerical Algorithms, 6*, 1-35.

Hapke, B. (1981). Bidirectional reflectance spectroscopy I. Theory. *Journal of Geophysical Research, 86*, 3039-3054.

Hay, G.J., Blaschke, T., Marceau, D.J., & Bouchard, A. (2003). A comparison of three image-object methods for the multiscale analysis of landscape structure. *ISPRS Journal of Photogrammetry and Remote Sensing, 57*, 327-345.

Hazeu, G. (2004). The Dutch Land Use Database LGN http://www.alterra.wur.nl/UK/cgi/LGN/ [accessed: 3rd July 2004].

Hazeu, G. (2005). The Dutch Land Use Database LGN. [web page] http://www.lgn.nl/ [accessed 22nd February 2006].

Hazeu, G. (2008). The land use database of The Netherlands. http://www.alterra.wur.nl/UK/research/Specialisation+Geo-Information/LGN [accessed: 21 March 2008].

Hengl, T. (2006). Finding the right pixel size. *Computers & Geosciences, 32*, 1283-1298.

Horler, D.N.H., Dockray, M., & Barber, J. (1983). The red edge of plant leaf reflectance. *International Journal of Remote Sensing, 4*, 273-288.

Hu, Y.H., Lee, H.B., & Scarpace, F.L. (1999). Optimal linear spectral unmixing. *IEEE Transactions on Geoscience and Remote Sensing, 37*, 639-644.

Hudak, A.T., Lefsky, M.A., Cohen, W.B., & Berterretche, M. (2002). Integration of lidar and Landsat ETM+ data for estimating and mapping forest canopy height. *Remote Sensing of Environment, 82*, 397-416.

Huete, A.R., Justice, C.O., & van Leeuwen, W. (1999). MODIS vegetation index (MOD13) algorithm theoretical basis document version 3.

Huete, A.R., Liu, H.Q., Batchily, K., & van Leeuwen, W. (1997). A comparison of vegetation indices over a global set of TM images for EOS-MODIS. *Remote Sensing of Environment, 59*, 440-451.

Ichoku, C., & Karnieli, A. (1996). A Review of Mixture Modeling Techniques for Sub-Pixel Land Cover Estimation. *Remote Sensing Reviews, 13*, 161-186.

Jacquemoud, S., & Baret, F. (1990). Prospect - a Model of Leaf Optical-Properties Spectra. *Remote Sensing of Environment, 34*, 75-91.

Janetos, A.C., & Justice, C.O. (2000). Land cover and global productivity: A measurement strategy for the NASA programme. *International Journal of Remote Sensing, 21*, 1491-1512.

Jorgensen, P.V. (2000). Determination of cloud coverage over Denmark using Landsat MSS/TM and NOAA-AVHRR. *International Journal of Remote Sensing, 21*, 3363-3368.

Ju, J., Gopal, S., & Kolaczyk, E.D. (2005). On the choice of spatial and categorical scale in remote sensing land cover classification. *Remote Sensing of Environment, 96*, 62-77.

Kaiser, G., & Schneider, W. (2008). Estimation of sensor point spread function by spatial subpixel analysis. *International Journal of Remote Sensing, 29*, 2137-2155.

Kemper, T., & Sommer, S. (2004). Use of airborne hyperspectral data to estimate residual heavy metal contamination and acidification potential in the Guadiamar flood plain Andalusia, Spain after the Aznacollar mining accident. In: M. Ehlers, F. Posa, H.J. Kaufmann, U. Michel & G. De Carolis (Eds.), *Proceedings of SPIE - Remote Sensing for Environmental Monitoring, GIS Applications, and Geology IV* (pp. 224-234). Maspalomas, Spain: SPIE.

Khlopenkov, K.V., & Trishchenko, A.P. (2008). Implementation and Evaluation of Concurrent Gradient Search Method for Reprojection of MODIS Level 1B Imagery. *IEEE Transactions on Geoscience and Remote Sensing, (In press)*

Kneisys, F.X., Abreu, L.W., Anderson, G.P., Chetwynd, J.H., Shettle, E.P., Berk, A., Bernstein, L.S., Robertson, D.C., Acharya, P.K., Rothman, L.S., J.E.A., S., Gallery, W.O., & Clough, S.A. (1995). The MODTRAN 2/3 and LOWTRAN 7 Model. North Andover, MA: Ontar Corporation

Kneubuehler, M., Schaepman, M.E., Schläpfer, D., & Thome, K.J. (2004). MERIS/ENVISAT Vicarious Calibration Over Land. In: R. Meynart, S.P. Neeck, H. Shimoda, J.B. Lurie & M.L. Aten (Eds.), *Proceedings of SPIE - Sensors, Systems, and Next-Generation Satellites VII* (pp. 614-623). Barcelona, Spain: SPIE.

Kneubuehler, M., Schaepman, M.E., & Thome, K. (2003). MERIS/ENVISAT Vicarious Calibration Results at Railroad Valley Playa (NV). In: M. Habermeyer (Ed.) *Proceedings of the 3rd EARSeL Workshop on Imaging Spectroscopy* (pp. 88-94). Herrsching (Germany)

Kneubuehler, M., Schaepman, M.E., Thome, K., Baret, F., & Mueller, A. (2002). Calibration and validation of MERIS, part 1: Vicarious calibration at Railroad Valley Playa (NV). In: *Proceedings of the Envisat validation workshop*. Frascati, Italy: ESA.

Kontoes, C., & Stakenborg, J. (1990). Availability of cloud-free Landsat images for operational projects. The analysis of cloud-cover figures over the countries of the European Community. *International Journal of Remote Sensing, 11*, 1599-1608.

Kressler, F.P., & Steinnocher, K.T. (1999). Detecting land cover changes from NOAA-AVHRR data by using spectral mixture analysis. *International Journal of Applied Earth Observation and Geoinformation, 1999*, 21-26.

Kristof, D., Pataki, R., Neidert, D., Nagy, Z., & Pinter, K. (2007). Integrating temporal and spectral information from low-resolution MODIS and high-resolution optical satellite images: Two Hungarian case studies. In: C.M.U. Neale, M. Owe & G. D'Urso (Eds.), *Proceedings of SPIE - Remote Sensing for Agriculture, Ecosystems, and Hydrology IX*. Florence, Italy

Lauer, D.T., Morain, S.A., & Salomonson, V.V. (1997). The Landsat program: Its origins, evolution, and impacts. *Photogrammetric Engineering and Remote Sensing, 63*, 831-838.

Laur, H., Kohlhammer, G., Desnos, Y.L., & Coulson, S. (2002). The ENVISAT mission: access to the data. In: *Proceedings of the International Geoscience and Remote Sensing Symposium (IGARSS)* (pp. 617-619). Toronto, Canada: IEEE.

Legg, C.A. (1991). A Review of Landsat Mss Image Acquisition over the United-Kingdom, 1976-1988, and the Implications for Operational Remote-Sensing. *International Journal of Remote Sensing, 12*, 93-106.

Liang, S.L., & Townshend, J.R.G. (1996). A modified Hapke model for soil bidirectional reflectance. *Remote Sensing of Environment, 55*, 1-10.

Lillesand, T.M., & Kiefer, R.W. (2000). *Remote Sensing and Image Interpretation*. New York, USA: John Wiley and Sons, Fourth Edition.

Lillo-Saavedra, M., & Gonzalo, C. (2006). Spectral or spatial quality for fused satellite imagery? A trade-off solution using the wavelet à trous algorithm. *International Journal of Remote Sensing, 27*, 1453–1464.

Lillo-Saavedra, M., & Gonzalo, C. (2007). Multispectral images fusion by a joint multidirectional and multiresolution representation. *International Journal of Remote Sensing, 28*, 4065 - 4079.

Lillo-Saavedra, M., Gonzalo, C., Arquero, A., & Martinez, E. (2005). Fusion of multispectral and panchromatic satellite sensor imagery based on tailored filtering in the Fourier domain. *International Journal of Remote Sensing, 26*, 1263-1268.

Louet, J. (2001). The Envisat mission and system. In: *European Space Agency Bulletin, 106.*

Lyapustin, A., Wang, Y., Kahn, R., Xiong, J., Ignatov, A., Wolfe, R., Wu, A., Holben, B., & Bruegge, C. (2007). Analysis of MODIS-MISR calibration differences using surface albedo around AERONET sites and cloud reflectance. *Remote Sensing of Environment, 107*, 12-21.

Maisongrande, P., Duchemin, B., & Dedieu, G. (2004). VEGETATION/SPOT: An operational mission for the Earth monitoring; presentation of new standard products. *International Journal of Remote Sensing, 25*, 9-14.

Malenovsky, Z., Martin, E., Homolova, L., Gastellu-Etchegorry, J.P., Zurita-Milla, R., Schaepman, M.E., Pokorny, R., Clevers, J.G.P.W., & Cudlin, P. (2008). Influence of woody elements of a Norway spruce canopy on nadir reflectance simulated by the DART model at very high spatial resolution. *Remote Sensing of Environment, 112*, 1-18.

Malenovsky, Z., Zurita-Milla, R., Homolova, L., Martin, E., Schaepman, M.E., Gastellu-Etchegory, J.P., Pokorny, R., & Clevers, J.G.P.W. (2007). Retrieval of coniferous canopy chlorophyll content from high spatial resolution hyperspectral data In: M.E. Schaepman, S. Liang, N.E. Groot & M. Kneubühler (Eds.), *Proceedings of the 10th International Symposium on Physical Measurements and Spectral Signatures in Remote Sensing (ISPMSRS'07)* (pp. 108-113). Davos, Switzerland: ISPRS.

Marshall, G.J., Dowdeswell, J.A., & Rees, W.G. (1994). The Spatial and Temporal Effect of Cloud Cover on the Acquisition of High-Quality Landsat Imagery in the European Arctic Sector. *Remote Sensing of Environment, 50*, 149-160.

Martinez, P.J., Perez, R.M., Plaza, A., Aguilar, P.L., Cantero, M.C., & Plaza, J. (2006). Endmember extraction algorithms from hyperspectral images. *Annals of Geophysics, 49*, 93-101.

Maselli, F., & Chiesi, M. (2005). Integration of high- and low-resolution satellite data to estimate pine forest productivity in a Mediterranean coastal area. *IEEE Transactions on Geoscience and Remote Sensing, 43*, 135-143.

Maselli, F., & Chiesi, M. (2006). Integration of multi-source NDVI data for the estimation of Mediterranean forest productivity. *International Journal of Remote Sensing, 27*, 55-72.

Masuoka, E., Fleig, A., Wolfe, R.E., & Patt, F. (1998). Key characteristics of MODIS data products. *IEEE Transactions on Geoscience and Remote Sensing, 36*, 1313-1323.

Millennium Ecosystem Assessment (2005). *Ecosystems and Human Well-being: Synthesis.* Washington D.C., USA: Island Press.

Minghelli-Roman, A., Mangolini, M., Petit, M., & Polidori, L. (2001). Spatial resolution improvement of MeRIS images by fusion with TM images. *IEEE Transactions on Geoscience and Remote Sensing, 39*, 1533-1536.

Minghelli-Roman, A., Polidori, L., Mathieu-Blanc, S., Loubersac, L., & Cauneau, F. (2006). Spatial resolution improvement by merging MERIS-ETM images for coastal water monitoring. *IEEE Geoscience and Remote Sensing Letters, 3*, 227-231.

Moody, A., & Johnson, D.M. (2001). Land-surface phenologies from AVHRR using the discrete fourier transform. *Remote Sensing of Environment, 75*, 305-323.

Moriondo, M., Maselli, F., & Bindi, M. (2007). A simple model of regional wheat yield based on NDVI data. *European Journal of Agronomy, 26*, 266-274.

Motzkin, G., Wilson, P., Foster, D.R., & Allen, A. (1999). Vegetation patterns in heterogeneous landscapes: The importance of history and environment. *Journal of Vegetation Science, 10*, 903-920.

Mouroulis, P., Green, R.O., & Chrien, T.G. (2000). Design of Pushbroom Imaging Spectrometers for Optimum Recovery of Spectroscopic and Spatial Information. *Applied Optics, 39*, 2210-2220.

Myneni, R.B., Keeling, C.D., Tucker, C.J., Asrar, G., & Nemani, R.R. (1997a). Increased plant growth in the northern high latitudes from 1981 to 1991. *Nature, 386*, 698-702.

Myneni, R.B., Nemani, R.R., & Running, S.W. (1997b). Estimation of global leaf area index and absorbed par using radiative transfer models. *IEEE Transactions on Geoscience and Remote Sensing, 35*, 1380-1393.

Myneni, R.B., & Williams, D.L. (1994). On the relationship between FAPAR and NDVI. *Remote Sensing of Environment, 49*, 200-211.

Napelka, R.P., & Hyde, P.D. (1972). Classifying unresolved objects from simulated space data. In: *Proceedings of the 8th International Symposium on Remote Sensing of Environment* (pp. 935-949). Ann Arbor, USA

Nieke, J., Hori, M., Aoki, T., Tanikawa, T., Motoyoshi, H., & Nakajima, Y. (2003). Cross-calibration of satellite sensors over snow fields. In: W.L. Barnes (Ed.) *Proceedings of SPIE - Earth Observing Systems VIII* (pp. 406-414). San Diego, USA

Nielsen, A.A. (2001). Spectral mixture analysis: Linear and semi-parametric full and iterated partial unmixing in multi- and hyperspectral image data. *International Journal of Computer Vision, 42*, 17-37.

North, P.R.J. (2002). Estimation of fAPAR, LAI, and vegetation fractional cover from ATSR-2 imagery. *Remote Sensing of Environment, 80*, 114-121.

Otazu, X., Gonzalez-Audicana, M., Fors, O., & Nunez, J. (2005). Introduction of sensor spectral response into image fusion methods. application to wavelet-based methods. *IEEE Transactions on Geoscience and Remote Sensing, 43*, 2376-2385.

Peddle, D.R., Brunke, S.P., & Hall, F.G. (2001). A comparison of spectral mixture analysis and ten vegetation indices for estimating boreal forest biophysical information from airborne data. *Canadian Journal of Remote Sensing, 27*, 627-635.

Peddle, D.R., Hall, F.G., & LeDrew, E.F. (1999). Spectral mixture analysis and geometric-optical reflectance modeling of boreal forest biophysical structure. *Remote Sensing of Environment, 67*, 288-297.

Pellemans, A.H.J.M., Jordans, R.W.L., & Allewijn, R. (1993). Merging multispectral and panchromatic SPOT images with respect to the radiometric properties of the sensor. *Photogrammetric Engineering & Remote Sensing, 59*, 81-87.

Pettorelli, N., Vik, J.O., Mysterud, A., Gaillard, J.-M., Tucker, C.J., & Stenseth, N.C. (2005). Using the satellite-derived NDVI to assess ecological responses to environmental change. *Trends in Ecology & Evolution, 20*, 503-510.

Pielke Sr., R.A. (2005). Land use and climate change. *Science, 310*, 1625-1626.

Plaza, A., Martinez, P., Perez, R., & Plaza, J. (2004). A quantitative and comparative analysis of endmember extraction algorithms from hyperspectral data. *IEEE Transactions on Geoscience and Remote Sensing, 42*, 650-663.

Plaza, J., Plaza, A., Pérez, R., & Martínez, P. (2005). Automated generation of semi-labeled training samples for nonlinear neural network-based abundance estimation in hyperspectral data. In: *Proceedings of the International Geoscience and Remote Sensing Symposium (IGARSS)* (pp. 1261-1264). Seoul, Korea: IEEE.

Pohl, C., & Van Genderen, J.L. (1998). Multisensor image fusion in remote sensing: Concepts, methods and applications. *International Journal of Remote Sensing, 19*, 823-854.

Quattrochi, D.A., & Goodchild, M.F. (Eds.) (1997). *Scale in Remote Sensing and GIS*. Boca Raton, USA: Lewis publishers. CRC press.

Ramsey, M.S., & Christensen, P.R. (1998). Mineral abundance determination: Quantitative deconvolution of thermal emission spectra. *Journal of Geophysical Research B: Solid Earth, 103*, 577-596.

Ranchin, T., Aiazzi, B., Alparone, L., Baronti, S., & Wald, L. (2003). Image fusion - The ARSIS concept and some successful implementation schemes. *ISPRS Journal of Photogrammetry and Remote Sensing, 58*, 4-18.

Rast, M., & Bézy, J.L. (1990). ESA's medium resolution imaging spectrometer (MERIS). Mission, system and applications. In: G. Vane (Ed.) *Proceedings of SPIE - Imaging Spectroscopy of the Terrestrial Environment* (pp. 114-126). Orlando, USA: SPIE.

Rast, M., Bézy, J.L., & Bruzzi, S. (1999). The ESA Medium Resolution Imaging Spectrometer MERIS - a review of the instrument and its mission. *International Journal of Remote Sensing, 20*, 1681-1702.

Richards, J.A. (1986). *Remote Sensing Digital Image Analysis. An introduction*. Berlin Heidelberg: Springer-Verlag.

Roberts, D.A., Smith, M.O., & Adams, J.B. (1993). Green vegetation, nonphotosynthetic vegetation, and soils in AVIRIS data. *Remote Sensing of Environment, 44*, 255-269.

Rogers, D.J., Randolph, S.E., Snow, R.W., & Hay, S.I. (2002). Satellite imagery in the study and forecast of malaria. *Nature, 415*, 710-715.

Running, S.W., Loveland, T.R., Pierce, L.L., Nemani, R.R., & Hunt, E.R. (1995). A remote sensing based vegetation classification logic for global land cover analysis. *Remote Sensing of Environment, 51*, 39-48.

Running, S.W., Nemani, R.R., Heinsch, F.A., Zhao, M.S., Reeves, M., & Hashimoto, H. (2004). A continuous satellite-derived measure of global terrestrial primary production. *BioScience, 54*, 547-560.

Salomonson, V.V., Barnes, W.L., Maymon, P.W., Montgomery, H.E., & Ostrow, H. (1992). MODIS: advanced facility instrument for studies of the earth as a system. *IEEE Transactions on Geoscience and Remote Sensing, v*, 145-153.

Saunier, S., Goryl, P., Delwart, S., & Ludovic, B. (2006). Meris full resolution products, geometry aspects. In: *Proceedings of the 2nd Working Meeting on MERIS and AATSR Calibration and Geophysical Validation (MAVT-2006)*. Frascati, Italy: ESA.

Schaepman, M., Zurita Milla, R., Kneubühler, M., Clevers, J.G.P.W., & Delwart, S. (2004). Assessment of long-term vicarious calibration efforts of MERIS on land product quality. In: R. Meynart, S.P. Neeck & H. Shimoda (Eds.), *Proceedings of SPIE - Sensors, Systems, and Next-Generation Satellites VIII* (pp. 363-371). Maspalomas, Spain: SPIE.

Schaepman, M.E., & Dangel, S. (2000). Solid laboratory calibration of a nonimaging spectroradiometer. *Applied Optics, 39*, 3754-3764.

Scharlemann, J.P.W., Benz, D., Hay, S.I., Purse, B.V., Tatem, A.J., Wint, G.R.W., & Rogers, D.J. (2008). Global data for ecology and epidemiology: A novel algorithm for temporal fourier processing MODIS data. *PLoS ONE, 3*

Schmullius, C., & Hese, S. (2003). SIBERIA-II: Sensor Systems and Data Products for Greenhouse Gas Accounting. In: *Proceedings of the International Geoscience and Remote Sensing Symposium (IGARSS)* (pp. 1499-1501). Toulouse, France: IEEE.

Schowengerdt, R.A. (1997). *Remote Sensing. Models and Methods for Image Processing; Second Ed.*: Academic Press. .

Schreier, G., & Dech, S. (2005). High resolution earth observation satellites and services in the next decade-a European perspective. *Acta Astronautica, 57*, 520-533.

Settle, J.J., & Drake, N.A. (1993). Linear Mixing and the Estimation of Ground Cover Proportions. *International Journal of Remote Sensing, 14*, 1159-1177.

Shi, W., Zhu, C., Tian, Y., & Nichol, J. (2005). Wavelet-based image fusion and quality assessment. *International Journal of Applied Earth Observation and Geoinformation, 6*, 241-251.

Shimabukuro, Y.E., & Smith, J.A. (1991). The Least-Squares Mixing Models to Generate Fraction Images Derived from Remote-Sensing Multispectral Data. *IEEE Transactions on Geoscience and Remote Sensing, 29*, 16-20.

Simic, A., Chen, J.M., Liu, J., & Csillag, F. (2004). Spatial scaling of net primary productivity using subpixel information. *Remote Sensing of Environment, 93*, 246-258.

Solon, J. (1995). Anthropogenic disturbance and vegetation diversity in agricultural landscapes. *Landscape & Urban Planning, 31*, 171-180.

Steffen, W., Sanderson, A., Tyson, P.D., Jäger, J., Matson, P.A., Moore III, B., Oldfield, F., Richardson, K., Schellnhuber, H.J., Turner II, B.L., & Wasson, R.J. (2005). *Global Change and the Earth System. A Planet Under Pressure* Würzburg (DE): Springer Berlin Heidelberg

Steven, M.D., Malthus, T.J., Baret, F., Xu, H., & Chopping, M.J. (2003). Intercalibration of vegetation indices from different sensor systems. *Remote Sensing of Environment, 88*, 412-422.

Tan, B., Hu, J., Zhang, P., Huang, D., Shabanov, N., Weiss, M., Knyazikhin, Y., & Myneni, R.B. (2005). Validation of Moderate Resolution Imaging Spectroradiometer leaf area

index product in croplands of Alpilles, France. *Journal of Geophysical Research D: Atmospheres, 110*, 1-15.

Tan, B., Woodcock, C.E., Hu, J., Zhang, P., Ozdogan, M., Huang, D., Yang, W., Knyazikhin, Y., & Myneni, R.B. (2006). The impact of gridding artifacts on the local spatial properties of MODIS data: Implications for validation, compositing, and band-to-band registration across resolutions. *Remote Sensing of Environment, 105*, 98-114.

Tarnavsky, E., Garrigues, S., & Brown, M.E. (2008). Multiscale geostatistical analysis of AVHRR, SPOT-VGT, and MODIS global NDVI products. *Remote Sensing of Environment, 112*, 535-549.

Tate, N.J., & Atkinson, P.M. (Eds.) (2001). *Modelling Scale in Geographical Information Science*. Chichester, West Sussex, UK: Wiley

Tatem, A.J., Lewis, H.G., Atkinson, P.M., & Nixon, M.S. (2003). Increasing the spatial resolution of agricultural land cover maps using a Hopfield neural network. *International Journal of Geographical Information Science, 17*, 647-672.

Taylor, K.E. (2001). Summarizing multiple aspects of model performance in a single diagram. *Journal of Geophysical Research-Atmospheres, 106*, 7183-7192.

Teillet, P.M., Staenz, K., & Williams, D.J. (1997). Effects of spectral, spatial, and radiometric characteristics on remote sensing vegetation indices of forested regions. *Remote Sensing of Environment, 61*, 139-149.

Thomas, C., & Wald, L. (2004). Assessment of the quality of fused products. In: M. Oluic (Ed.) *Proceedings of the 24th EARSeL Symposium, New Strategies for European Remote Sensing* (pp. 317-326). Dubrovnik, Croatia: EARSeL.

Thome, K.J. (2002). Ground-look radiometric calibration approaches for remote sensing images in the solar reflective. In: *Proceedings of the ISPRS Commission I Mid-Term Symposium in conjunction with Pecora 15/Land Satellite Information IV* (p. 6). Denver, USA: ISPRS.

Tian, Y., Dickinson, R.E., Zhou, L., Zeng, X., Dai, Y., Myneni, R.B., Knyazikhin, Y., Zhang, X., Friedl, M., Yu, H., Wu, W., & Shaikh, M. (2004). Comparison of seasonal and spatial variations of leaf area index and fraction of absorbed photosynthetically active radiation from Moderate Resolution Imaging Spectroradiometer (MODIS) and Common Land Model. *Journal of Geophysical Research D: Atmospheres, 109*, D01103.

Townshend, J., Justice, C., Wei, L., Gurney, C., & McManus, J. (1991). Global land cover classification by remote sensing: present capabilities and future possibilities. *Remote Sensing of Environment, 35*, 243-255.

Townshend, J.R.G., Huang, C., Kalluri, S.N.V., Defries, R.S., Liang, S., & Yang, K. (2000). Beware of per-pixel characterization of land cover. *International Journal of Remote Sensing, 21*, 839-843.

Tsai, V.J.D. (2004). Evaluation of multiresolution image fusion algorithms. In: *Proceedings of the International Geoscience and Remote Sensing Symposium (IGARSS)* (pp. 621-624). Anchorage, USA: IEEE.

Turner, W., Spector, S., Gardiner, N., Fladeland, M., Sterling, E., & Steininger, M. (2003). Remote sensing for biodiversity science and conservation. *Trends in Ecology & Evolution, 18*, 306-314.

United Nations (1992). *Convention on Biological Diversity. Environmental Law and Institutions Programme Activity Centre*. New York: United Nations Environment Programme.

United Nations (2007). *World Population Prospects: The 2006 Revision, Highlights (Working Paper No. ESA/P/WP 202)*: Department of Economic and Social Affairs, Population Division.

Ustin, S.L., Smith, M.O., & Adams, J.B. (1993). Remote sensing of ecological processes: a strategy for developing and testing ecological models using spectral mixture analysis. In: J.R. Ehleringer & C.B. Field (Eds.), *Scaling physiological processes: leaf to globe* (p. 388). San Diego, CA, USA: Academic Press.

Verhoef, W. (1984). Light-Scattering by Leaf Layers with Application to Canopy Reflectance Modeling - the Sail Model. *Remote Sensing of Environment, 16*, 125-141.

Verrelst, J., Zurita-Milla, R., Koetz, B., Clevers, J.G.P.W., & Schaepman, M.E. (2007). Angular unmixing of photosynthetic and non-photosynethetic vegetation within a coniferous forest using CHRIS-PROBA. In: M.E. Schaepman, S. Liang, N.E. Groot & M. Kneubühler (Eds.), *Proceedings of the 10th International Symposium on Physical Measurements and Spectral Signatures in Remote Sensing (ISPMSRS'07)* (pp. 355-360). Davos, Switzerland: ISPRS.

Verstraete, M.M., Pinty, B., & Curran, P.J. (1999). MERIS potential for land applications. *International Journal of Remote Sensing, 20*, 1747-1756.

Vogelmann, J.E., Helder, D., Morfitt, R., Choate, M.J., Merchant, J.W., & Bulley, H. (2001). Effects of Landsat 5 Thematic Mapper and Landsat 7 Enhanced Thematic Mapper plus radiometric and geometric calibrations and corrections on landscape characterization. *Remote Sensing of Environment, 78*, 55-70.

Vogelmann, J.E., Sohl, T.L., Campbell, P.V., & Shaw, D.M. (1998). Regional land cover characterization using Landsat thematic mapper data and ancillary data sources. *Environmental Monitoring and Assessment, 51*, 415-428.

VROM (1999). Planning the Netherlands: Strategic Principles for a New Spatial Planning Policy. The Hague, The Netherlands: Netherlands National Spatial Planning Agency

Wald, L. (1998). A European proposal for terms of reference in data fusion. *International Archives of Photogrammetry and Remote Sensing, 32*, 651-654.

Wald, L. (1999). Some terms of reference in data fusion. *IEEE Transactions on Geoscience and Remote Sensing, 37*, 1190-1193.

Wald, L. (2002). *Data Fusion Definitions and Architectures: Fusion of Images of Different Spatial Resolutions*. Paris: Ecole des Mines Pres.

Wald, L., Ranchin, T., & Mangolini, M. (1997). Fusion of satellite images of different spatial resolutions: Assessing the quality of resulting images. *Photogrammetric Engineering and Remote Sensing, 63*, 691-699.

Wang, Z., & Bovik, A.C. (2002). A universal image quality index. *IEEE Signal Processing Letters, 9*, 81-84.

Widlowski, J.L., Taberner, M., Pinty, B., Bruniquel-Pinel, V., Disney, M., Fernandes, R., Gastellu-Etchegorry, J.P., Gobron, N., Kuusk, A., Lavergne, T., Leblanc, S., Lewis, P.E., Martin, E., Mottus, M., North, P.R.J., Qin, W., Robustelli, M., Rochdi, N., Ruiloba, R., Soler, C., Thompson, R., Verhoef, W., Verstraete, M.M., & Xie, D. (2007). Third Radiation Transfer Model Intercomparison (RAMI) exercise: Documenting progress in canopy reflectance models. *Journal of Geophysical Research-Atmospheres, 112*, D09111.

Wigjey, T.M.L. (1998). The Kyoto Protocol: CO2, CH4 and climate implications. *Geophysical Research Letters, 25*, 2285-2288.

Woodcock, C.E., & Ozdogan, M. (2004). Trends in land cover mapping and monitoring. In: G. Gutman, A.C. Janetos, C.O. Justice, E.F. Moran, J.F. Mustard, R.R. Rindfuss, D. Skole, B.L. Turner II & M.A. Cochrane (Eds.), *Land Change Science: Observing, Monitoring and Understanding Trayectories of Change on the Earth's Surface* (pp. 367-377). Dordrecht, The Netherlands: Kluwer Academic Publishers.

Woodcock, C.E., & Strahler, A.H. (1987). The Factor of Scale in Remote-Sensing. *Remote Sensing of Environment, 21*, 311-332.

Wulder, M.A., White, J.C., Goward, S.N., Masek, J.G., Irons, J.R., Herold, M., Cohen, W.B., Loveland, T.R., & Woodcock, C.E. (2008). Landsat continuity: Issues and opportunities for land cover monitoring. *Remote Sensing of Environment, 112*, 955-969.

Xiong, X., Che, N., Barnes, W., Xie, Y., Wang, L., & Qu, J. (2006). Status of aqua MODIS spatial characterization and performance. In: R. Meynart, S.P. Neeck & H. Shimoda (Eds.), *Proceedings of SPIE - Sensors, Systems, and Next-Generation Satellites X* (p. 63610T). Stockholm, Sweden

Yang, C., Everitt, J.H., & Bradford, J.M. (2007). Using multispectral imagery and linear spectral unmixing techniques for estimating crop yield variability. *Transactions of the American Society of Agricultural and Biological Engineers (ASABE), 50*, 667-674.

Yu, Z., van Genderen, J.L., & Jixian, Z. (2006). Comparison and analysis of remote sensing data fusion techniques at feature and decision levels. In: *ISPRS mid-term symposium 2006 remote sensing : from pixels to processes* (p. 5p.). 8-11 May 2006, Enschede, the Netherlands.: ISPRS.

Zeng, Y., Schaepman, M.E., Wu, B., Clevers, J.G.P.W., & Bregt, A.K. (2008). Quantative forest canopy structure assessment using an inverted geometric-optical model and up-scaling. *International Journal of Remote Sensing*, in press.

Zhan, X., Sohlberg, R.A., Townshend, J.R.G., DiMiceli, C., Carroll, M.L., Eastman, J.C., Hansen, M.C., & DeFries, R.S. (2002). Detection of land cover changes using MODIS 250 m data. *Remote Sensing of Environment, 83*, 336-350.

Zhang, Y. (2002). Problems in the fusion of commercial high-resolution satelitte images as well as Landsat 7 images and initial solutions. *International Archives of Photogrammetry and Remote Sensing, 34*

Zhang, Y. (2004). Understanding image fusion. *Photogrammetric Engineering and Remote Sensing, 70*, 657-661.

Zhukov, B., Oertel, D., Lanzl, F., & Reinhackel, G. (1999). Unmixing-based multisensor multiresolution image fusion. *IEEE Transactions on Geoscience and Remote Sensing, 37*, 1212-1226.

Zurita-Milla, R., Clevers, J.G.P.W., & Schaepman, M.E. (2008a). Unmixing-based Landsat TM and MERIS FR data fusion. *IEEE Geoscience and Remote Sensing Letters, 5*, 453-457.

Zurita-Milla, R., Clevers, J.G.P.W., Schaepman, M.E., & Kneubuehler, M. (2007a). Effects of MERIS L1b radiometric calibration on regional land cover mapping and land products. *International Journal of Remote Sensing, 28*, 653-673.

Zurita-Milla, R., Clevers, J.G.P.W., Schaepman, M.E., & Plaza, A.J. (2007b). Retrieving sub-pixel land cover composition through an effective integration of the spatial, spectral and temporal dimensions of MERIS imagery. *Journal of Remote Sensing, 11*, 659-668.

Zurita-Milla, R., Clevers, J.G.P.W., van Gijsel, J.A.E., & Schaepman, M.E. (2008b). Using MERIS fused images for land cover mapping and vegetation status assessment in heterogeneous landscapes. *International Journal of Remote Sensing*, (In review).

Zurita-Milla, R., Gómez-Chova, L., Clevers, J.G.P.W., Schaepman, M.E., & Camps-Valls, G. (2007c). Multitemporal unmixing of MERIS FR data. In: *Proceedings of the 10th International Symposium on Physical Measurements and Spectral Signatures in Remote Sensing (ISPMSRS'07)* (pp. 238-243). Davos, Switzerland: ISPRS.

Zurita-Milla, R., Kaiser, G., Clevers, J.P.G.W., Schneider, W., & Schaepman, M.E. (2007d). Spatial unmixing of MERIS data for monitoring vegetation dynamics. In: *Proceedings of Envisat Symposium*. Montreux, Switzerland: ESA.

Zurita-Milla, R., Schaepman, M.E., & Clevers, J.G.P.W. (2005). Possibilities of MERIS for sub-pixel regional land cover mapping. In: M. Owe & G. D'Urso (Eds.), *Proceedings of SPIE - Remote Sensing for Agriculture, Ecosystems, and Hydrology VII* (pp. 264-273). Bruges, Belgium: SPIE.

Summary

Our environment is continuously undergoing change. This change takes place at several spatial and temporal scales and it is largely driven by anthropogenic activities. In order to protect our environment and to ensure a sustainable use of natural resources, a wide variety of national and international initiatives have been established. In this context, Earth observation sensors can provide a substantial amount of information about the biotic and abiotic conditions of our planet. For instance, high spatial resolution sensors, like Landsat TM, deliver data that can be used to produce maps of canopy properties and of land cover types. However, the use of this kind of sensors is not feasible for obtaining full coverage of large areas. Furthermore, high spatial resolution sensors generally do not provide sufficient temporal resolution for monitoring vegetation development during the year. This is especially true for areas having severe cloud coverage throughout the year. In this respect, coarse spatial resolution sensors, which deliver nearly daily data, have a higher chance of encountering cloud free areas. This facilitates large scale monitoring studies but at the expense of a lower spatial resolution providing images with potentially many mixed pixels.

Recent developments in imaging devices resulted into a new kind of sensor that works at a medium spatial resolution while providing high temporal and spectral resolutions. The MEdium Resolution Imaging Spectrometer (MERIS) aboard the European Space Agency's ENVISAT platform belongs to this category. MERIS measures the solar radiation reflected from the Earth's surface in 15 narrow spectral bands and it has a revisit time of 2-3 days. This unprecedented spectral and temporal resolution has resulted in several land, water and atmospheric products. In addition, two vegetation indices have been specifically designed to monitor vegetated canopies using this sensor: the MERIS Terrestrial Chlorophyll index (MTCI) and the MERIS Global Vegetation Index (MGVI). However, the spatial resolution provided by this sensor – 300 m in full resolution (FR mode) – is not sufficient to accurately map and monitor heterogeneous and fragmented landscapes. This is why the synergic use of high spatial resolution and MERIS data is investigated in this thesis. More precisely, the objective of this thesis is to develop a multi-sensor and multi-resolution data fusion approach that allows mapping and monitoring of heterogeneous and highly fragmented landscapes using MERIS data. The Netherlands is selected as study area because of its mixed landscapes where patches of arable land, natural vegetation, forests, and water bodies can be found next to each other. Besides this, The Netherlands also suffers from frequent cloud coverage, which severely hampers operational mapping and monitoring with both high spatial and high temporal resolution.

Chapter 1 outlines the challenges of mapping and monitoring heterogeneous and fragmented landscapes using data from the current optical Earth observing missions, sketches the core concepts of data fusion and linear spectral (un)mixing and, after that, lists the research objectives of this PhD thesis.

Chapter 2 presents the calibration scheme of the MERIS sensor and subsequently focuses on the smile effect and on the vicarious calibration corrections. The effects of these corrections on regional land cover mapping and vegetation status assessment are studied. Our analysis showed that MERIS delivers data with a very high radiometric quality. Nevertheless, some effects were observed when using MERIS data without the smile correction. Therefore, we recommend to systematically apply all the necessary corrections to generate stable long-term series of MERIS data.

Chapter 3 introduces a data fusion technique that can be used to generate images with the spatial resolution provided by Landsat TM and the spectral resolution provided by MERIS. The method is based on the linear mixing model and requires the use of a high spatial resolution dataset (in this case, a Landsat TM image) to downscale the information collected by MERIS. Two parameters need to be optimized in this implementation of the unmixing-based data fusion approach: the number of classes used to classify the TM image and the size of the MERIS neighbourhood used to solve the unmixing equations. A quantitative data fusion quality analysis was used to assist with the identification of the best combination of these two parameters. The results of this analysis demonstrated that it is possible to downscale MERIS FR images to a Landsat-like spatial resolution (25 m).

Chapter 4 elaborates in more detail on the potential of MERIS fused images for land cover mapping and vegetation status assessment in heterogeneous and fragmented landscapes. First, the fused images are used to produce land cover maps, which are validated using a high spatial resolution dataset. Then, the fused image with the highest overall classification accuracy is selected as the best fused image. Subsequently, this image is used to compute three vegetation indices: the normalized difference vegetation index (NDVI), which is an indicator of vegetation amount and its 'greenness', and the two vegetation indices specifically designed to monitor vegetation status using MERIS data (i.e. the MTCI and the MGVI). Classification results for the best fused image and for the TM image used to downscale MERIS are very similar and when comparing spectrally similar images (i.e. no SWIR bands in the TM image), the results of the best fused image outperform those of TM. With respect to the vegetation indices, a good correlation was found between the NDVI computed from TM and from the best fused image (in spite of their different spectral configuration). For the MTCI and the MGVI, the spatial patterns found when using MERIS fused images were consistent with those found in MERIS. The main advantage of using fused images is the possibility of monitoring individual agricultural fields and small vegetation patches. This is not possible when using the original MERIS FR images.

Chapter 5 investigates the use of the unmixing-based data fusion approach to downscale time series of MERIS FR data. In this case, a high spatial resolution land use database is used to characterize the landscape composition. Because of this, only the size of the MERIS neighbourhood used for the unmixing needs to be optimized. In this chapter, the AMORGOS 3.0 software was used to ensure working with the best possible MERIS geo-location values. This allowed an automatic image co-registration and the calculation of the actual ground instantaneous field of view (GIFOV) of each MERIS pixel which, in turn, allows us to determine the real number of TM pixels covered by each MERIS pixel without having to re-project the datasets. Similar to chapter 2, a quantitative data fusion assessment was performed in order to test the validity of the proposed method and to identify the best neighbourhood size. After that, the series of fused images was used to compute the MTCI and the MGVI. Finally, MTCI and MGVI temporal profiles were extracted for the main land cover types present in the study area. Results indicate that the selected data fusion approach can be successfully used to downscale time series of MERIS FR data and, therefore, to monitor vegetation dynamics at high spatial, spectral and temporal resolutions.

Chapter 6 contains the final conclusions and gives recommendations for further research. The overall conclusion is that the selected unmixing-based data fusion approach is able to downscale MERIS FR data to a Landsat-like resolution with little compromises on the spectral quality. This allows mapping and monitoring heterogeneous and fragmented

landscapes that suffer from frequent cloud coverage. The results presented in this thesis should, therefore, encourage further research on multi-sensor and multi-resolution data fusion approaches as a means to bridge spatial, spectral and temporal scaling gaps in current and future Earth observation missions.

Samenvatting

Onze leefomgeving is continu onderhevig aan veranderingen. Deze veranderingen vinden plaats op verschillende ruimtelijke en temporele schalen en worden voornamelijk gedreven door antropogene activiteiten. Om ons milieu te beschermen en om een duurzaam gebruik van natuurlijke hulpbronnen te garanderen, is een grote verscheidenheid aan nationale en internationale initiatieven gestart. In deze context kunnen sensoren voor aardobservatie een substantiële hoeveelheid informatie over de biotische en a-biotische condities van onze planeet verschaffen. Sensoren met een hoge ruimtelijke resolutie zoals Landsat TM leveren bijvoorbeeld data die gebruikt kunnen worden om kaarten te produceren van planteigenschappen en van landgebruik. Met dit type sensoren kunnen echter geen data voor de volledige dekking van grote gebieden verkregen worden. Bovendien is met zulke hoge ruimtelijke resolutie sensoren in het algemeen een onvoldoende hoge temporele resolutie beschikbaar voor het monitoren van de ontwikkeling van vegetatie. Dit is met name het geval in gebieden met een hoge bewolkingsgraad gedurende het hele jaar. In dit opzicht is er een grotere kans om onbewolkt te kunnen meten met sensoren die een lage ruimtelijke resolutie hebben, maar wel vrijwel dagelijks data leveren. Dit bevordert het op grote schaal monitoren maar gaat ten koste van de hoge ruimtelijke resolutie waardoor deze metingen veel gemengde pixels kunnen bevatten.

Recente ontwikkelingen in beeldopnameapparatuur hebben er toe geleid dat er een nieuw soort sensoren ontwikkeld is die een middelmatige ruimtelijke resolutie hebben terwijl ze een hoge temporele en spectrale resolutie leveren. MERIS (MEdium Resolution Imaging Spectrometer) aan boord van de ENVISAT satelliet van de Europese ruimtevaartorganisatie (ESA) valt in deze categorie. MERIS meet de straling gereflecteerd door het aardoppervlak in 15 smalle spectrale banden en passeert hetzelfde gebied elke twee tot drie dagen. Deze unieke spectrale en temporele resoluties hebben geleid tot de ontwikkeling van verschillende producten gerelateerd aan land, water en atmosferische eigenschappen. Daarnaast zijn er twee vegetatie-indices speciaal ontwikkeld voor deze sensor: de MTCI (MERIS Terrestrial Chlorophyll Index) en de MGVI (MERIS Global Vegetation Index). De ruimtelijke resolutie van de MERIS data (300 m in hoge-resolutiemodus; hierna MERIS FR) is echter niet voldoende hoog om heterogene en gefragmenteerde landschappen nauwkeurig te kunnen karteren en monitoren. Om deze reden is het synergetisch gebruik van informatie met een hoge ruimtelijke resolutie in combinatie met MERIS data bestudeerd in dit proefschrift. De doelstelling van dit proefschrift is om een methodologie te ontwikkelen waarin multi-sensor- en multi-resolutie-data gefuseerd worden waarmee heterogene en sterk gefragmenteerde landschappen gekarteerd en gemonitord kunnen worden. Nederland is gekozen als studiegebied vanwege haar gevarieerde landschappen waarin landbouwgronden, natuurgebieden, bossen en oppervlaktewater elkaar veelvuldig afwisselen. Daarnaast heeft Nederland ook frequent een hoge bewolkingsgraad, wat operationele kartering en monitoring met zowel hoge ruimtelijke resolutie als hoge temporele resolutie bemoeilijkt.

Hoofdstuk een beschrijft de uitdagingen voor het karteren en monitoren van heterogene en gefragmenteerde landschappen bij gebruik van data van de huidige optische aardobservatiesensoren. Verder worden de concepten van datafusie en lineaire spectrale (de)compositie beschreven en de onderzoeksvragen van dit promotieonderzoek gepresenteerd.

In hoofdstuk twee wordt het calibratieschema van de MERIS sensor gepresenteerd en vervolgens richt dit hoofdstuk zich op het zogenoemde ‘smile effect’ en op indirecte

('vicarious') calibratiecorrecties. De effecten van deze correcties op de kartering van regionaal landgebruik en op de bepaling van de vegetatiestatus zijn bestudeerd. Onze analyses laten zien dat de MERIS data geleverd worden met een hoge radiometrische kwaliteit, maar daarentegen zijn er wel enkele effecten zichtbaar wanneer de correctie voor het 'smile effect' niet worden toegepast. Daarom bevelen wij aan om systematisch alle nodige correcties toe te passen om zo stabiele tijdseries van MERIS data te genereren.

In hoofdstuk drie wordt een datafusietechniek geïntroduceerd die kan worden gebruikt om beelden te produceren met de ruimtelijke resolutie van Landsat TM en de spectrale resolutie van MERIS. De methode is gebaseerd op het lineaire mixmodel en vereist de beschikbaarheid van een dataset met een hoge ruimtelijke resolutie (in dit geval een Landsat TM opname) om de MERIS-data te schalen naar een hogere resolutie. In deze implementatie van de op decompositie gebaseerde datafusie dienen twee parameters geoptimaliseerd te worden: het aantal klassen dat gebruikt is om de Landsat TM data te classificeren en de grootte van het MERIS venster dat gebruikt is om de decompositievergelijkingen op te lossen. De kwaliteit van de datafusie wordt gekwantificeerd als onderdeel van de identificatie van de beste combinatie van deze twee parameters. De resultaten van deze analyse demonstreren dat het mogelijk is om MERIS FR data naar een Landsat-achtige ruimtelijke resolutie (25 m) te brengen.

In hoofdstuk vier wordt in meer detail ingegaan op de toepassingsmogelijkheden van gefuseerde MERIS beelden voor landgebruikskartering en de bepaling van de vegetatiestatus in heterogene en gefragmenteerde landschappen. Allereerst worden de gefuseerde data geclassificeerd om een landgebruikskaart te produceren welke gevalideerd wordt met een bestaande landgebruikskaart (LGN) met een hoge ruimtelijke resolutie. Vervolgens wordt de gefuseerde dataset waarvan de classificatie het meest overeenkomt met LGN geselecteerd om drie vegetatie-indices te berekenen: de NDVI (normalised difference vegetation index; een indicator van de hoeveelheid groene vegetatie) en de twee indices speciaal ontwikkeld voor MERIS (MTCI en MGVI). Classificatieresultaten met de geselecteerde dataset zijn vergelijkbaar met de resultaten voor de TM data die gebruikt zijn om de hoge resolutie informatie te verkrijgen. Wanneer in spectraal opzicht vergelijkbare data (d.w.z. TM zonder SWIR) vergeleken worden, zijn de resultaten beter voor de gefuseerde dataset dan voor TM. Met betrekking tot de vegetatie-indices wordt een goede correlatie gevonden tussen de NDVI berekend van TM en die van de beste gefuseerde dataset ondanks de verschillen in spectrale configuraties van de sensoren. Voor de MTCI en de MGVI zijn de ruimtelijke patronen van het gefuseerde beeld consistent met die van MERIS op 300 m. Het belangrijkste voordeel van het gebruik van gefuseerde data is de mogelijkheid om individuele agrarische velden en kleine stukken natuurlijke begroeiing te monitoren. Dit is niet mogelijk wanneer originele MERIS FR data gebruikt worden.

In hoofdstuk vijf wordt het gebruik van de datafusiemethode gebaseerd op decompositie onderzocht om een tijdserie van MERIS FR data te schalen naar een hogere ruimtelijke resolutie. In deze studie wordt een landgebruiksdatabase met hoge ruimtelijk resolutie gebruikt om de landschapscompositie te karakteriseren. Hierdoor hoeft enkel nog de grootte van het MERIS venster tijdens de decompositie geoptimaliseerd te worden. In dit hoofdstuk wordt gebruikt gemaakt van de AMORGOS 3.0 software om de beste MERIS geolocatiewaarden te verkijgen. Hierdoor wordt automatische beeldcoregistratie mogelijk gemaakt en kan voor elke MERIS pixel het instantane gezichtsveld bepaald worden, waarmee vervolgens het aantal TM pixels die corresponderen met deze MERIS pixel kan worden

bepaald zonder de datasets te hoeven herprojecteren. Vergelijkbaar met hoofdstuk twee wordt een kwantitatieve beoordeling van de datafusie gedaan om de geldigheid van de voorgestelde methode te testen en om de optimale venstergrootte te bepalen. Hierna wordt met de tijdserie van gefuseerde datasets de MTCI en de MGVI berekend en vervolgens worden hieruit de temporele profielen voor de voornaamste landgebruiksklassen in het studiegebied bepaald. De resultaten wijzen er op dat de methode succesvol kan worden toegepast om tijdseries van MERIS FR data te schalen naar een hogere ruimtelijke resolutie en daarmee om vegetatiedynamiek te monitoren op hoge ruimtelijke, spectrale en temporele resoluties.

Hoofdstuk zes bevat de eindconclusies en presenteert aanbevelingen voor verder onderzoek. De algemene conclusie is dat de geselecteerde op decompositie gebaseerde datafusiemethode MERIS FR data naar een hogere ruimtelijke resolutie (vergelijkbaar met die van Landsat) kan schalen met behoud van de spectrale kwaliteit. Hierdoor kunnen nu heterogene en gefragmenteerde landschappen, die tevens frequent een hoge bewolkingsgraad hebben, gekarteerd en gemonitord worden. De resultaten die gepresenteerd zijn in dit proefschrift zouden daarom vervolgstudies moeten stimuleren zich te richten op multi-sensor- en multi-resolutie-datafusiemethodes als een middel om spectrale, ruimtelijke en temporele hiaten in huidige en toekomstige aardobservatiemissies te overbruggen.

Resumen

Nuestro planeta esta continuamente experimentando cambios. Estos cambios, en gran parte motivados por actividades antropogénicas, tienen lugar a varias escalas espaciales y temporales. Con el fin de proteger nuestro medio ambiente y de garantizar un uso sostenible de los recursos naturales, en los últimos años se han puesto en marcha una amplia variedad de iniciativas nacionales e internacionales para el seguimiento de estos cambios.

En este contexto, los sensores de observación de la Tierra ofrecen una gran cantidad de datos que, adecuadamente procesados, se convierten en información sobre las condiciones bióticas y abióticas de nuestro planeta. Por ejemplo, los datos recogidos por sensores de alta resolución espacial, como Landsat TM, pueden ser utilizados para producir mapas de usos del suelo y/o de diversas propiedades de la cubierta vegetal. El uso de este tipo de sensores no es operacional cuando se pretende estudiar grandes áreas; además, estos sensores no proporcionan la suficiente resolución temporal para realizar un apropiado seguimiento del desarrollo de cubiertas vegetales a lo largo del año. Esto es especialmente cierto en áreas persistentemente cubiertas por nubes, en las que sería más recomendable el uso de sensores de baja resolución espacial. Estos sensores tienen una resolución temporal casi diaria y, por consiguiente, ofrecen una mayor probabilidad de obtener imágenes libres de nubes. Por tanto, el uso de sensores de baja resolución espacial facilita los estudios de seguimiento de cubiertas vegetales a gran escala, pero a costa de trabajar con imágenes que, normalmente, contienen muchos píxeles mixtos.

Recientes avances en dispositivos para la captura de imágenes han dado como resultado el desarrollo de un nuevo tipo de sensor que trabaja a media resolución espacial y que ofrece altas resoluciones espectrales y temporales. El espectrómetro de media resolución (MERIS), a bordo de la plataforma ENVISAT de la Agencia Espacial Europea, pertenece a esta nueva categoría de sensores.

MERIS mide la radiación solar reflejada desde la superficie de la Tierra en 15 bandas estrechas (i.e. con una alta resolución espectral) y con una resolución temporal de 2 ó 3 días. Estas características permiten que MERIS pueda utilizarse en aplicaciones terrestres, acuáticas y atmosféricas. Además, dos índices de vegetación han sido específicamente diseñados para el seguimiento de cubiertas vegetales utilizando este sensor: el índice terrestre de clorofila (MTCI) y el índice global de vegetación (MGVI). Sin embargo, la resolución espacial proporcionada por MERIS - 300 m en el modo a resolución completa o “FR mode” - no es suficiente para estudiar y cartografiar paisajes heterogéneos y fragmentados.

Esto justifica que esta tesis se centre en la utilización sinérgica de imágenes de alta resolución espacial y baja resolución temporal (Landsat TM) y de imágenes MERIS. Más concretamente, el objetivo de esta tesis es el desarrollo de una metodología para la fusión de datos multi-sensor y multi-resolución que permita cartografiar y estudiar paisajes heterogéneos y fragmentados aprovechando las altas resoluciones espectrales y temporales de MERIS. Los Países Bajos han sido seleccionados como área de estudio debido a su heterogeneidad ya que en un mismo paisaje pueden encontrarse áreas de cultivo, áreas de vegetación natural, bosques y diversos tipos de masas de agua. Además, las nubes suponen un gran obstáculo para el estudio de los paisajes holandeses utilizando sólo sensores de alta resolución espacial.

El capitulo 1 discute las dificultades del estudio y cartografiado de paisajes heterogéneos y fragmentados con los sensores actuales de observación de la Tierra, ofrece una primera definición de los conceptos de fusión de datos y del modelo lineal de mezcla espectral y, por último, contiene los objetivos de esta tesis doctoral.

El capítulo 2 presenta la calibración radiométrica del sensor MERIS y, posteriormente, se centra en la corrección del llamado efecto “smile” (sonrisa) y en la corrección radiométrica derivada de un experimento de calibración vicaria. Los efectos de estas correcciones sobre productos derivados de MERIS (cartografía de uso del suelo e índices de vegetación) son estudiados en este capítulo. Los resultados muestran que MERIS ofrece datos con una alta calidad radiométrica aunque se identificaron algunos artefactos cuando se usaron datos MERIS sin la corrección del efecto “smile”. Por consiguiente, recomendamos aplicar sistemáticamente todas las correcciones radiométricas necesarias para generar series estables de datos MERIS.

El capítulo 3 introduce una técnica de fusión de datos que puede ser usada para generar imágenes con la resolución espacial de Landsat TM y la resolución espectral de MERIS. El método se basa en el modelo lineal de mezcla espectral y requiere el uso de una fuente de datos de alta resolución espacial (en este caso, una imagen Landsat TM) para aumentar la resolución espacial de la imagen MERIS. Esta técnica de fusión de datos requiere la optimización de dos parámetros: el número de clases usado para clasificar la imagen Landsat TM y el tamaño de ventana de MERIS usado para resolver las ecuaciones que separan la información espectral recogida en cada píxel MERIS (“desmezclado espectral”). Una evaluación cuantitativa de la calidad de las imágenes fusionadas se utilizó para ayudar a identificar la mejor combinación de estos dos parámetros. Los resultados de este estudio muestran que es posible bajar la resolución espacial de imágenes MERIS (300 m) hasta una resolución espacial de tipo Landsat (25 m).

El capítulo 4 ofrece un estudio detallado de las posibilidades de las imágenes fusionadas MERIS (15 bandas espectrales y píxel de 25 m) para cartografiar usos del suelo y evaluar el estado de la vegetación en paisajes heterogéneos y fragmentados. En primer lugar, se usaron una serie de imágenes fusionadas MERIS/Landsat TM para producir mapas de usos del suelo que fueron validados usando una base de datos de alta resolución espacial (25 m). La imagen con una mayor precisión de la clasificación se seleccionó como mejor imagen y se usó para calcular tres índices de vegetación: el índice de vegetación de la diferencia normalizada (NDVI), que es un indicador de la cantidad de vegetación y de su "verdor", y los dos índices de vegetación específicamente diseñados para el seguimiento de la vegetación usando datos MERIS (el MTCI y el MGVI). Los resultados de este estudio muestran que la clasificación de usos del suelo de la mejor imagen fusionada y la obtenida a partir de datos TM son muy similares. Mas aún, cuando se comparan imágenes espectralmente similares (es decir, se elimina la banda SWIR de la imagen TM), la precisión de la clasificación de la imagen fusionada supera a la de la imagen TM. Con respecto a los índices de vegetación, el NDVI calculado a partir de datos fusionados está altamente correlacionado con el calculado a partir de datos TM (a pesar de las diferencias espectrales entre estos sensores). Además, los patrones espaciales encontrados en las imágenes de MTCI y MGVI calculadas con la mejor imagen fusionada son compatibles con los encontrados al calcular estos índices usando las imágenes MERIS. Esto demuestra el gran potencial de las imágenes fusionadas para estudiar pequeñas parcelas y/o áreas de vegetación lo que en general no es posible cuando se utiliza MERIS a su resolución espacial original.

El capítulo 5 profundiza en el estudio de la técnica de fusión de datos basada en el "desmezclado espectral" de imágenes de media resolución. Esta técnica se aplicó a una serie temporal de datos MERIS FR y, en este caso, se usó una base de datos de usos del suelo para caracterizar la composición del paisaje con una alta resolución espacial. En consecuencia, sólo el tamaño de la ventana de pixeles MERIS usados para resolver las ecuaciones que separan la información espectral necesita ser optimizado. Además, en este capitulo se usó el programa AMORGOS 3.0 para obtener las coordenadas geográficas de cada píxel MERIS de la manera más precisa posible. Esto permitió co-registrar las imágenes de forma automática y calcular el área proyectada de cada píxel MERIS (lo que a su vez permite calcular el número de píxeles de alta resolución que hay "dentro" de cada píxel MERIS) sin necesidad de re-proyectar las imágenes. Al igual que en el capítulo 2, se utilizó un método cuantitativo para evaluar la validez de la fusión y para determinar el tamaño óptimo de la ventana de pixeles MERIS. A continuación, se calcularon los índices de vegetación MTCI y MGVI a partir de la las imágenes fusionadas y de las imágenes MERIS originales y se extrajeron perfiles temporales de estos índices para los principales tipos de usos del suelo presentes en el área de estudio. Los resultados indican que la fusión de datos propuesta en esta tesis puede ser usada con éxito para mejorar la resolución espacial de series temporales de datos MERIS FR. En otras palabras, el método propuesto permite el seguimiento de cubiertas vegetales y de sus dinámicas a altas resoluciones espaciales, espectrales y temporales.

Por último, el capítulo 6 contiene las conclusiones principales de esta tesis y una serie de recomendaciones para futuras investigaciones derivadas de este trabajo. La conclusión principal es que la fusión basada en el "desmezclado espectral" es capaz de producir imágenes con una resolución similar a la ofrecida por Landsat con muy pocos compromisos en la calidad espectral de las imágenes resultantes. Esto permite cartografiar y estudiar paisajes heterogéneos y fragmentados a altas resoluciones (incluso si éstos están frecuentemente cubiertos por nubes). Así pues, los resultados presentados en esta tesis deberían fomentar nuevos estudios sobre la fusión de datos provenientes de múltiples sensores y/o capturados a diferentes resoluciones como un medio para subsanar los déficits espaciales, espectrales y temporales de las misiones actuales y futuras de observación de la Tierra.

Colour figures

- Chapter 2

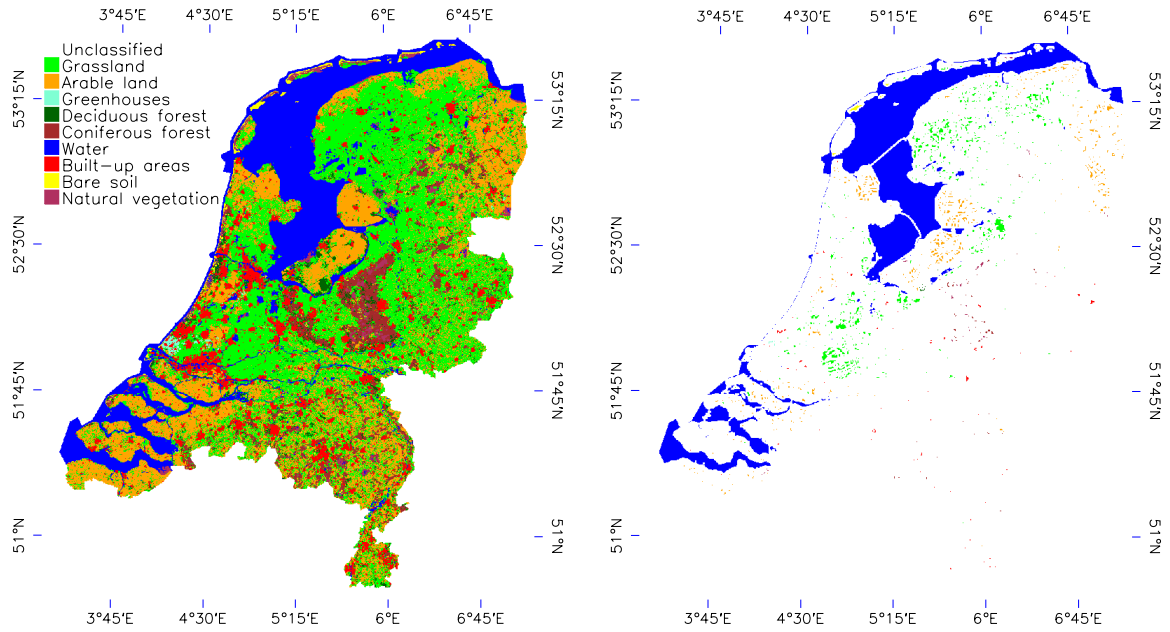

Figure 2.4. Left: The Dutch land use database LGN4 aggregated into 9 land use classes and resampled to 300 m pixel size. Right: 'Pure' pixel selection in The Netherlands using the Standard Purity Index (SPI) combined with the moving window filter.

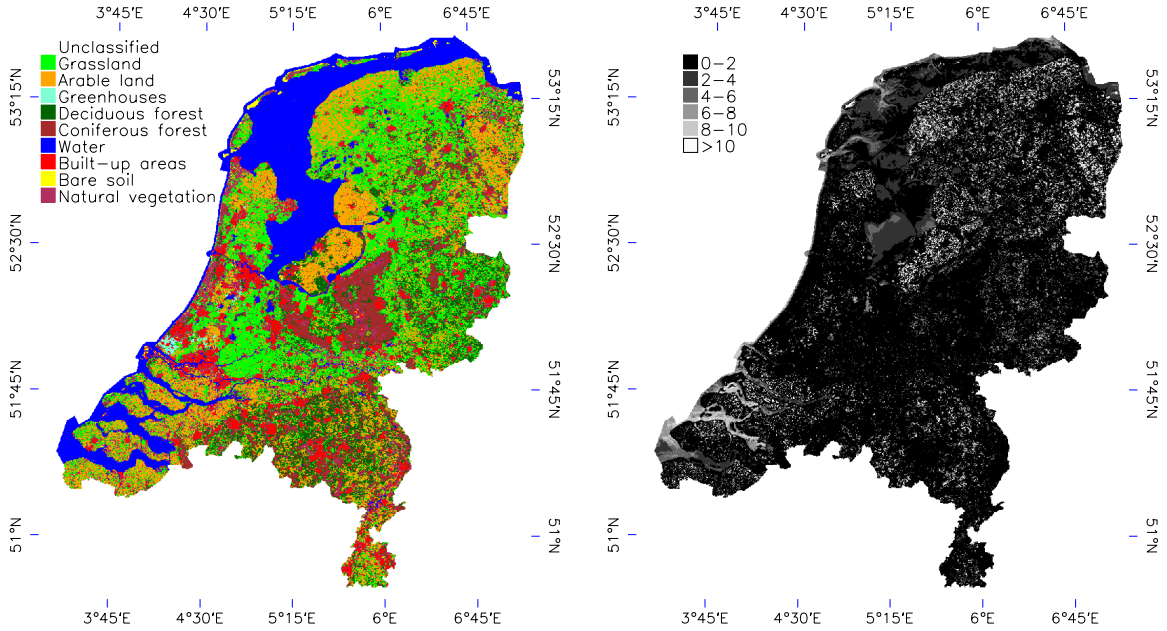

Figure 2.6. Left: classified image according to case 6 (Table 2-3); Right: corresponding RMSE image.

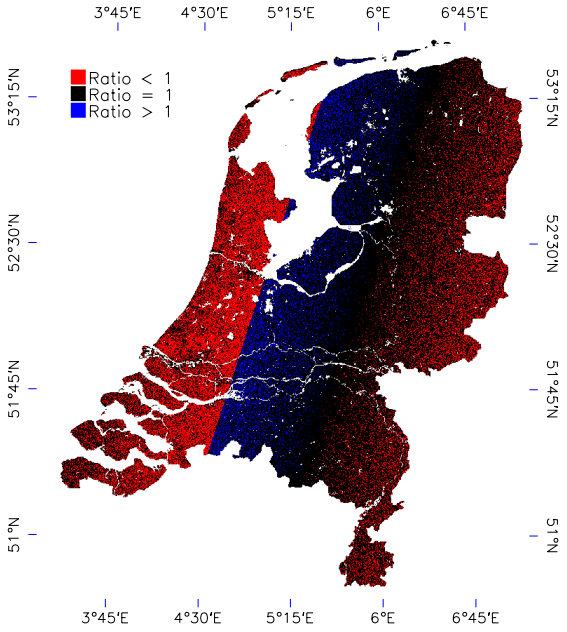

Figure 2.9. Ratio LSMILE-based/LRAW-based product (the colours red, black and blue indicate the areas where the ratio was smaller than one, equal to one or greater than one, respectively).

- Chapter 3

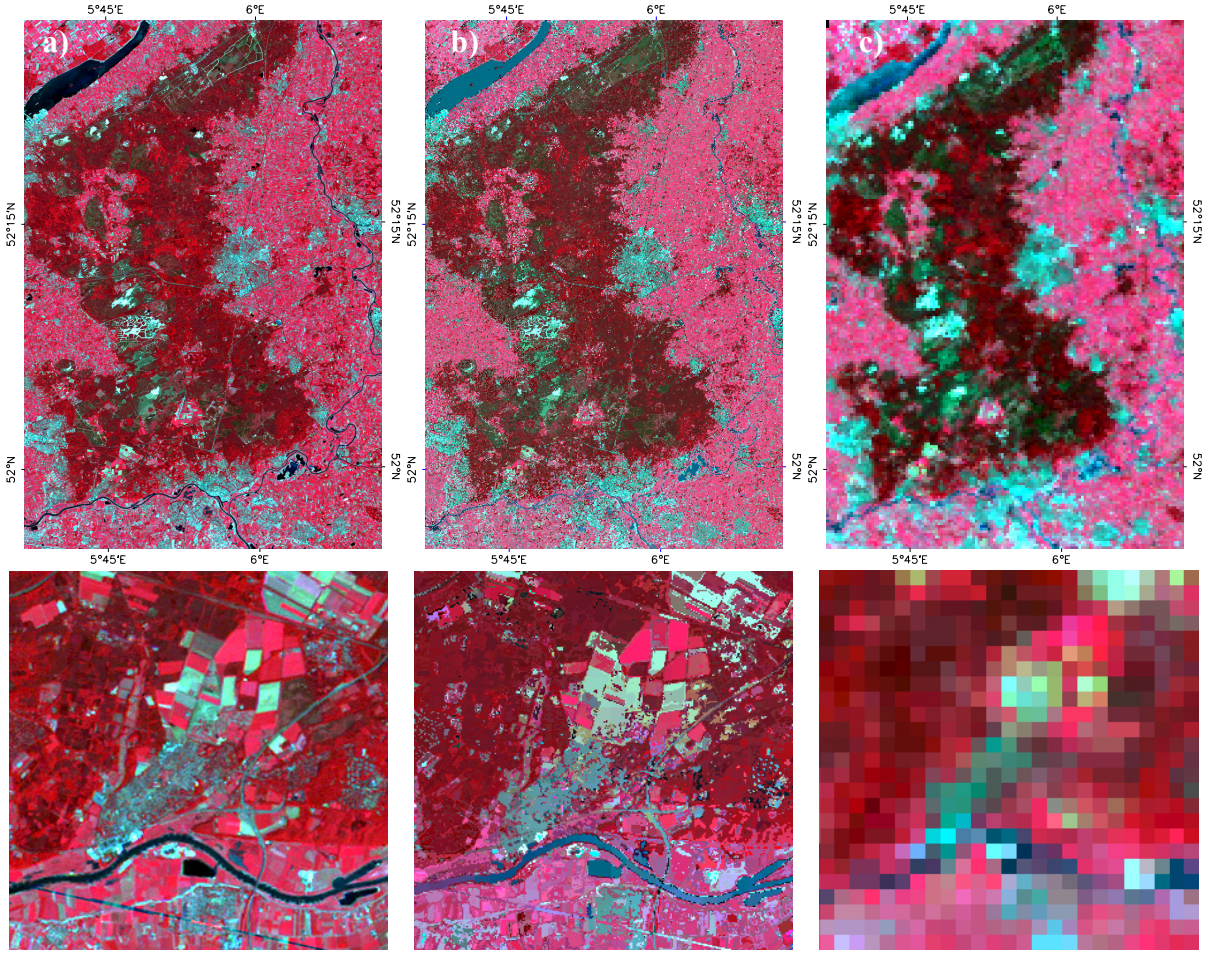

Figure 3.3. RGB color composite of bands 4, 3 and 2 of the TM image (a), bands 13, 7 and 5 of the fused image obtained for *nc* = 60 and *k* = 45 (b) and bands 13, 7 and 5 of the original MERIS FR image (c). Upper row shows the whole study area, whereas the lower row shows a subset of 25 by 25 MERIS FR pixels.

- Chapter 4

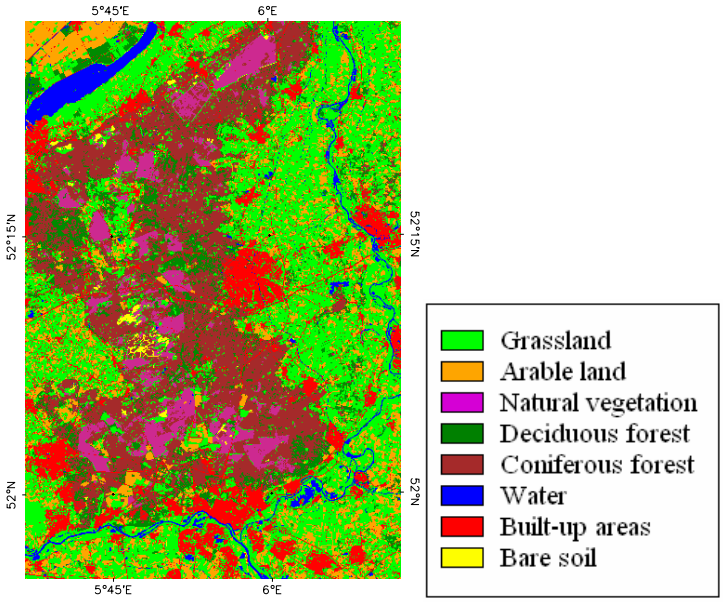

Figure 4.2. Thematically aggregated land cover map (LGN5) over the study area.

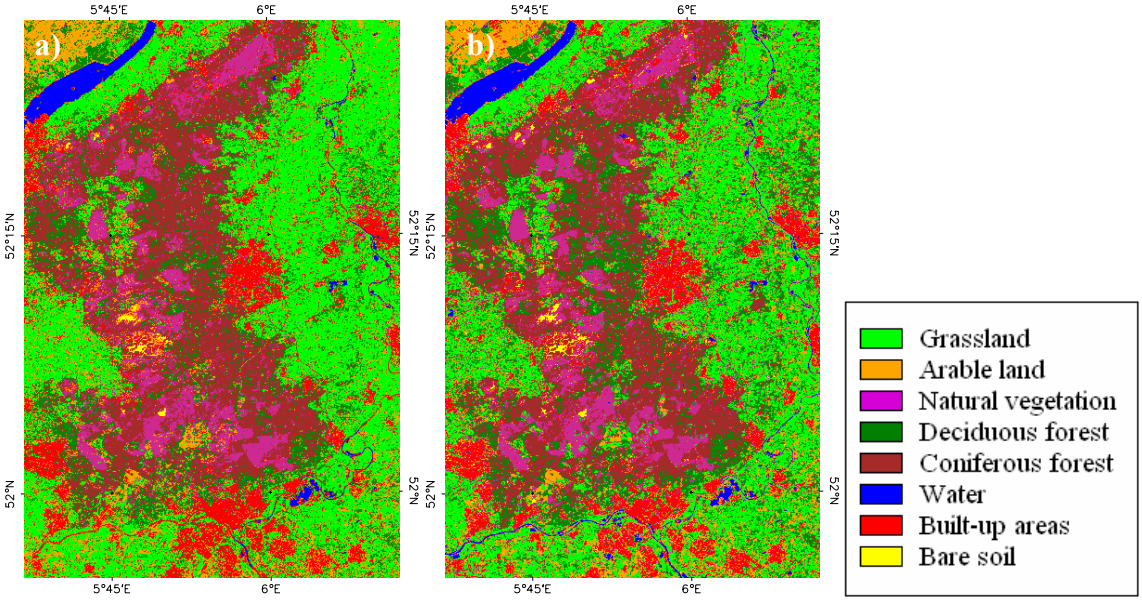

Figure 4.5. Classification results for the fused (a), and the Landsat TM (b) images.

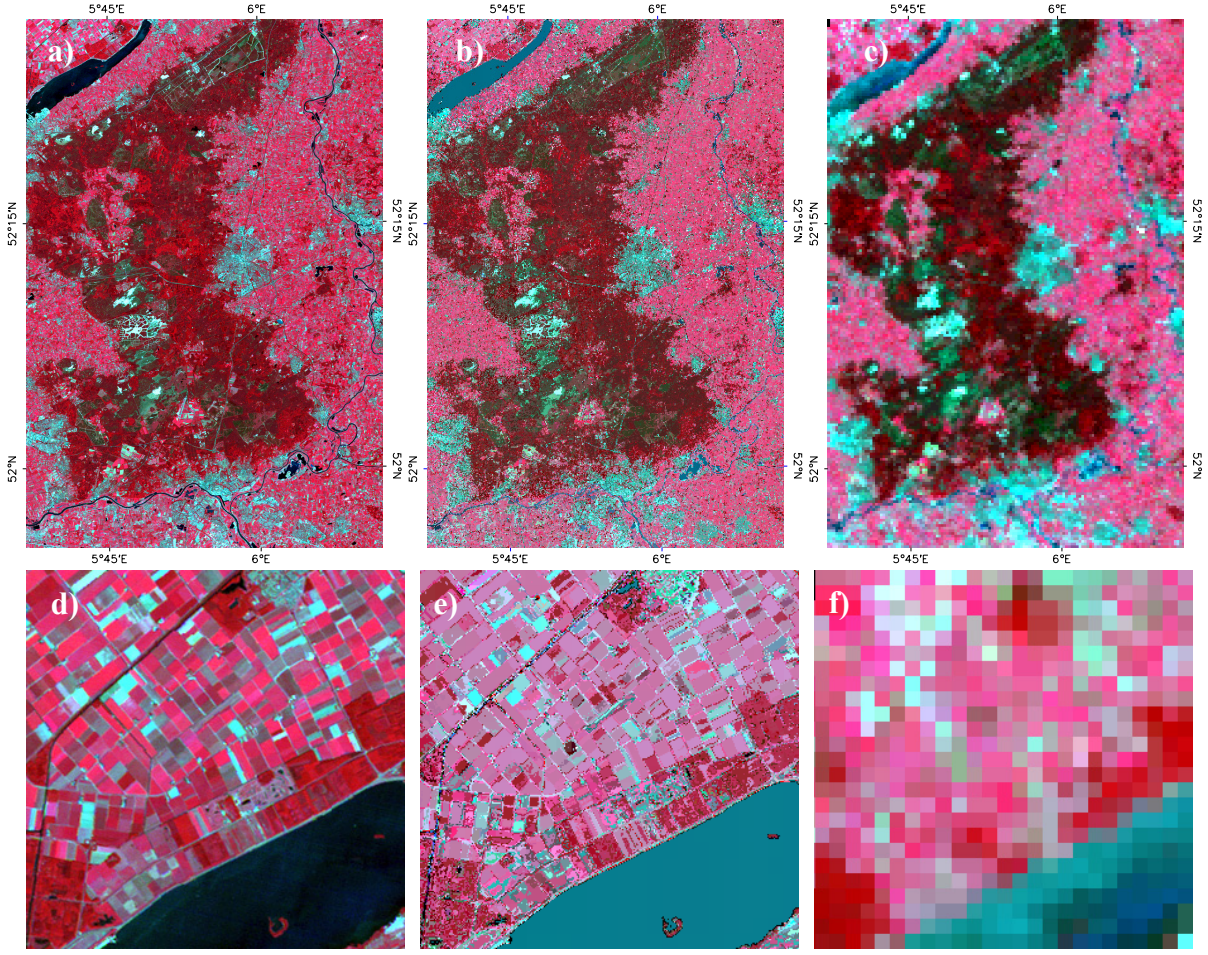

Figure 4.4. RGB color composite of bands 4, 3 and 2 of the TM image (a, d), bands 13, 7 and 5 of the fused image for *nc* = 60 and *k* = 45 (b, e) and bands 13, 7 and 5 of the original MERIS FR image (c, f). Upper row shows the whole study area, whereas the lower row shows a 25 by 25 pixel subset.

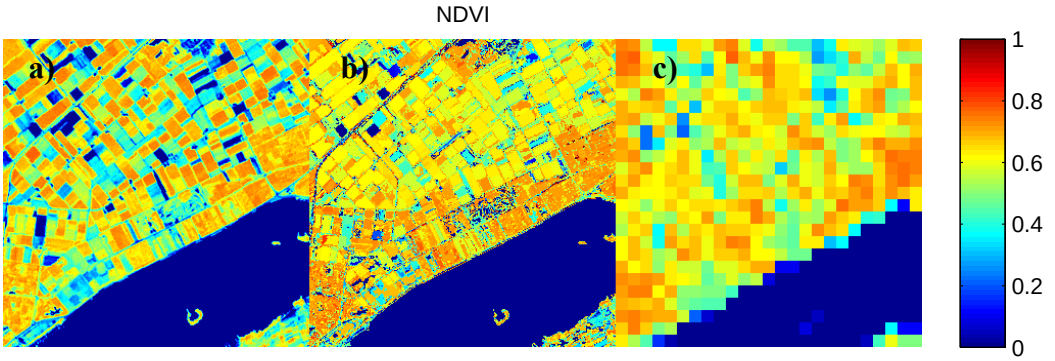

Figure 4.7. Example of the NDVI for the TM (a), the fused (b) and the MERIS FR image (c) for a 25 × 25 MERIS FR pixels subset of the study area.

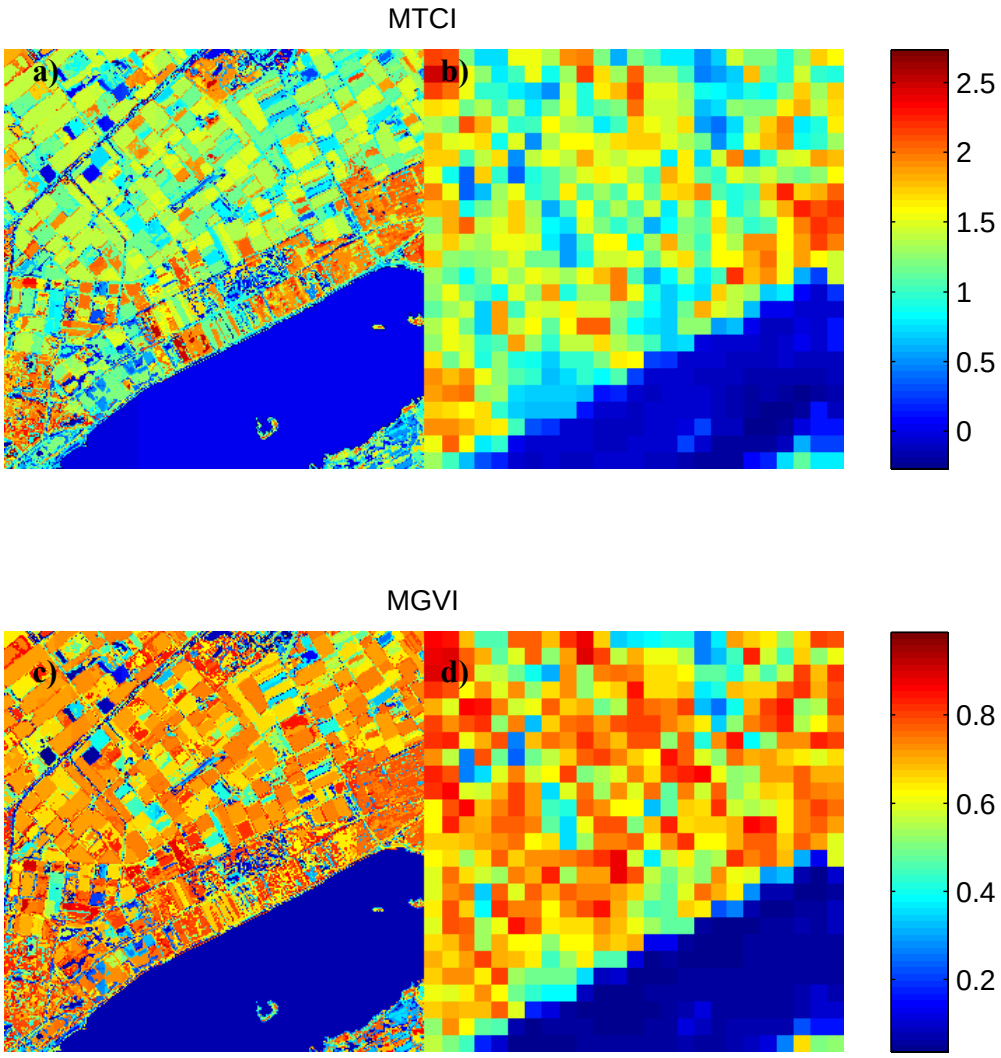

Figure 4.8. Example of the MTCI for the fused image (a) and the MERIS FR image (b) and of the MGVI for the fused image (c) and the MERIS FR image (d) for a 25 × 25 MERIS FR pixels subset of the study area.

- Chapter 5

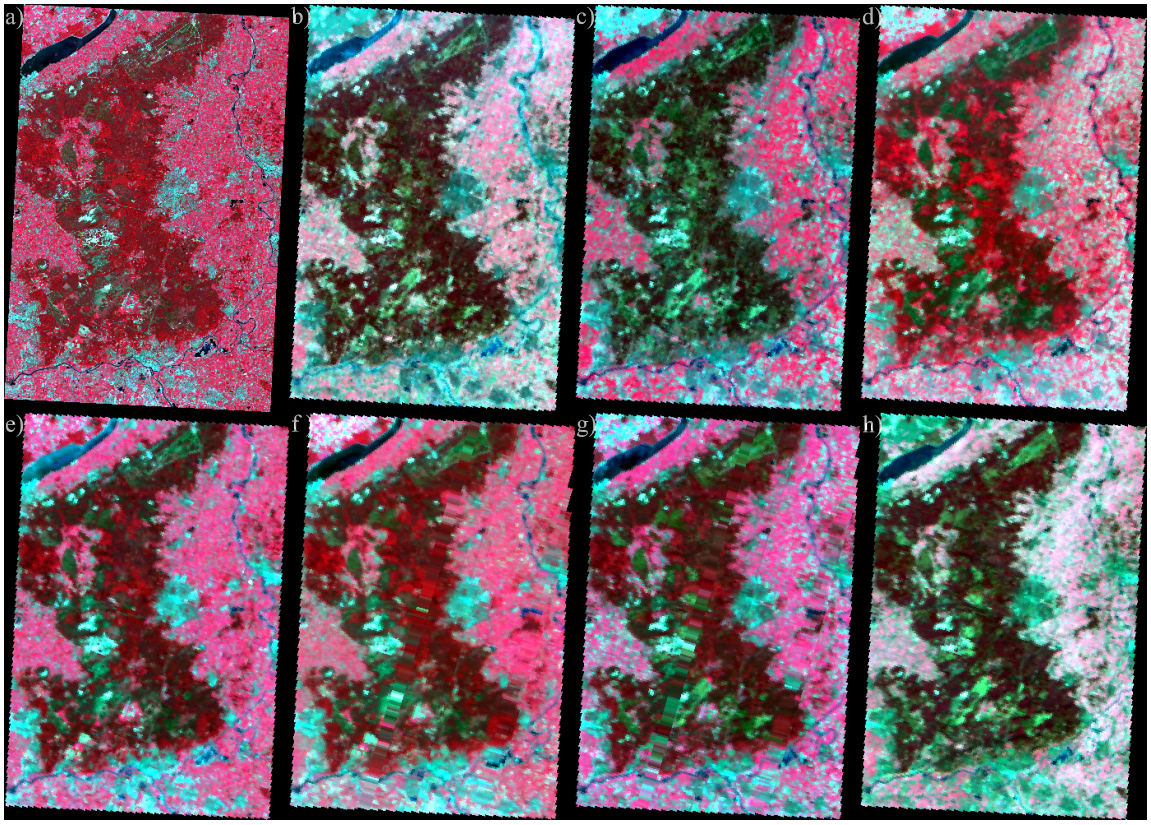

Figure 5.1. Study area as seen by Landsat TM on 10 July, 2003 (a) and by MERIS for the following dates of the same year: 18 February (b), 16 April (c), 31 May (d), 14 July (e), 6 August (f), 15 October (g) and 8 December (h).

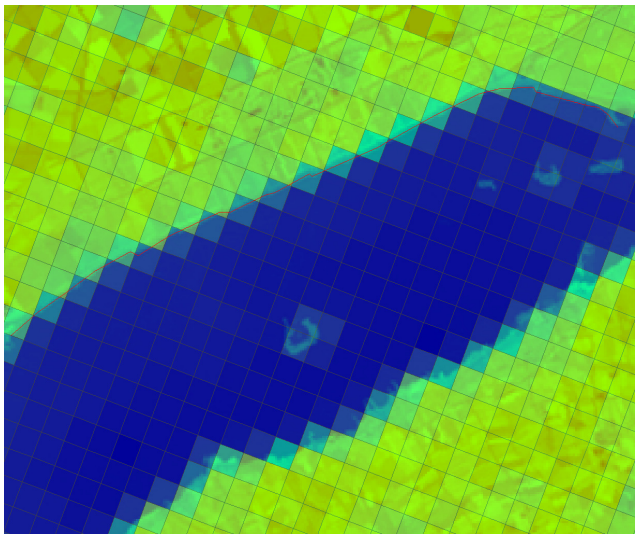

Figure 5.3. Co-registration of the MERIS and TM images of July: MERIS band 13 is depicted using a blue-green-red color table and TM is shown as semi-transparent background. The red line north of the water body shows the land-water-boundary as obtained from the TM image.

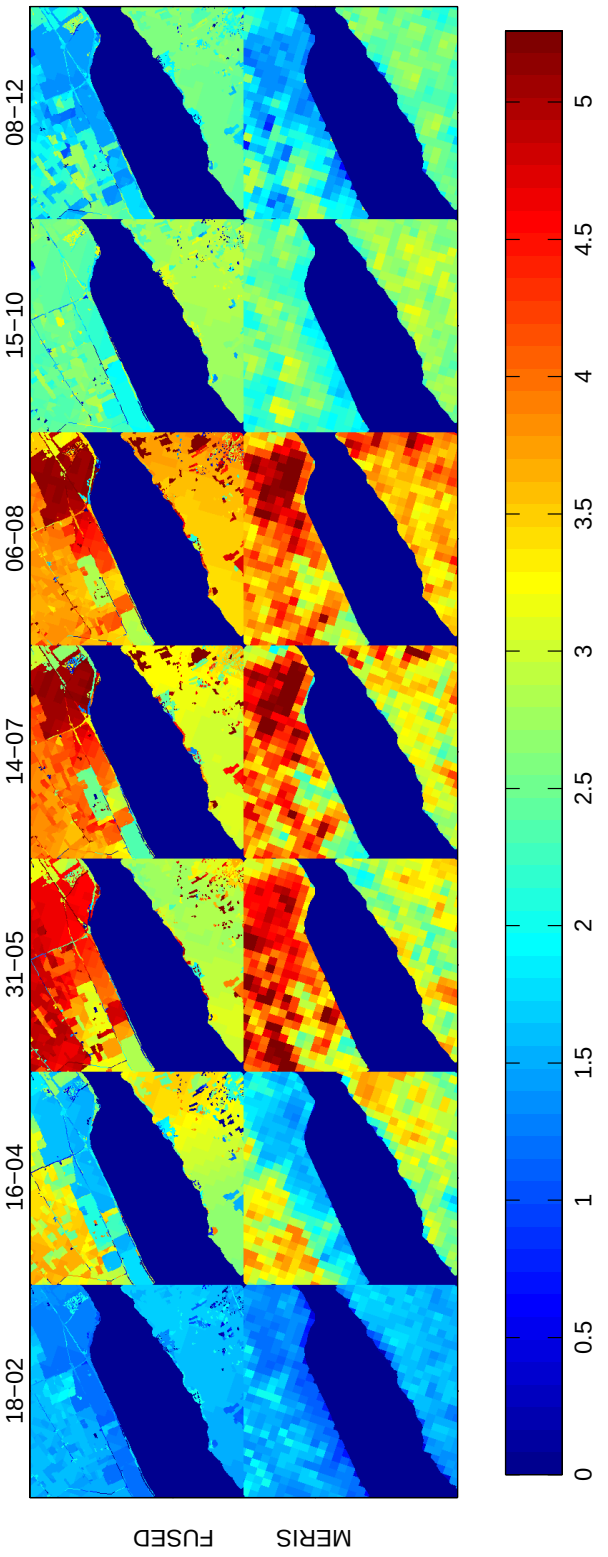

Figure 5.7. Temporal evolution of MTCI values for fused (top) and MERIS (bottom) data.

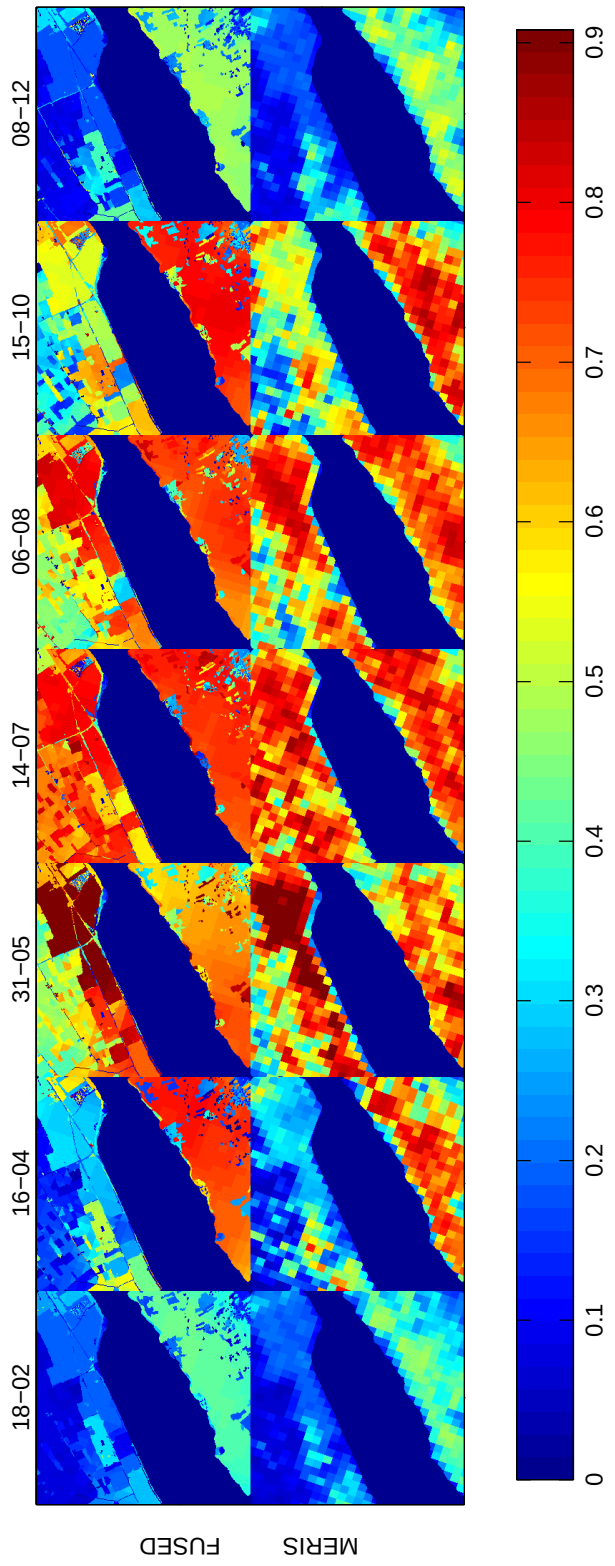

Figure 5.8. Temporal evolution of MGVI values for fused (top) and MERIS (bottom) data.

- Chapter 6

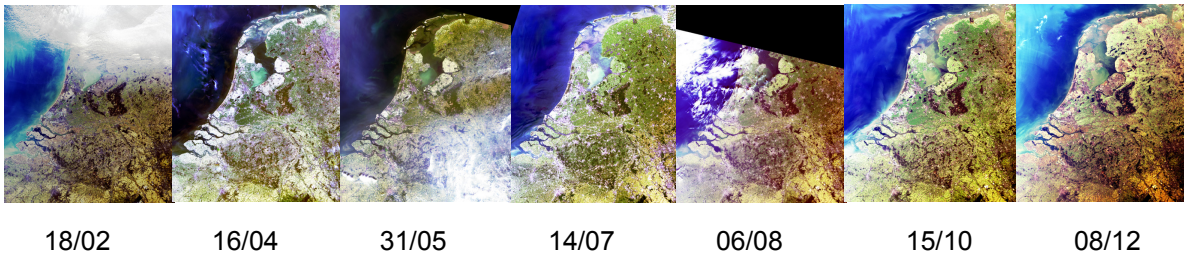

Figure 6.2. Time series of MERIS FR images for the year 2003.

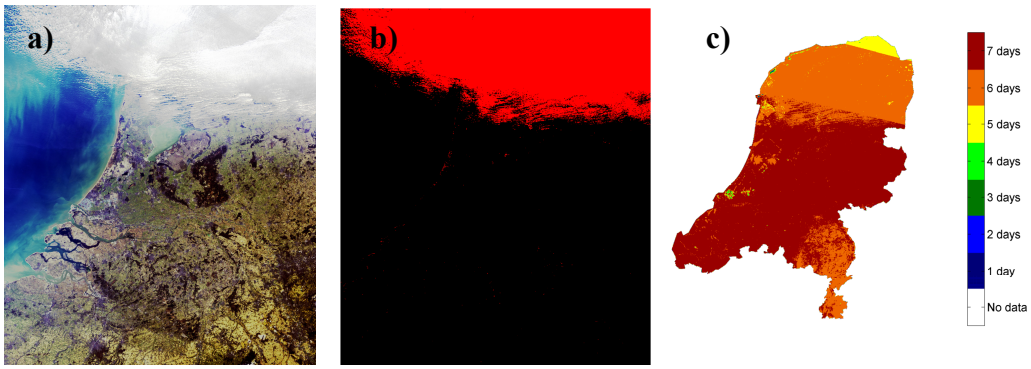

Figure 6.3. MERIS image of 18 February 2003 (a), corresponding cloud mask (b) and per-pixel number of cloud-free dates (c).

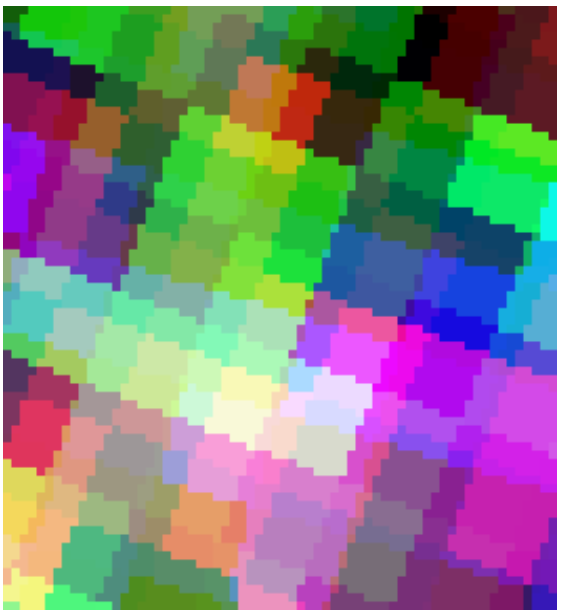

Figure 6.4. Detail of the ground instantaneous field of view for three MERIS MGVI images (16 April, 14 July and 15 October) displayed as an RGB color composite.

Acknowledgements

Wageningen, July 2008

Dear reader,

If you have gone through my thesis, you are now aware that MERIS images acquired over complex landscapes contain many mixed pixels. In my opinion, it is important to spend some time understanding what is "behind" each of these mixed pixels before deriving any product from the data.

Following this principle, here I would like to spend a few lines explaining you what is "behind" this PhD thesis. I shall term this process "PhD thesis unmixing" since the signal emitted during the last four years can be seen as a (complex) function of what I like to call my "personal endmembers", which (as you can imagine) are the people that in one way or another have contributed to this PhD thesis.

A convenient way to present endmembers is to group them in a so-called spectral library. So…, here you have my (spectral) library of acknowledgements[1]:

Supervisors: Michael Schaepman and Jan Clevers. Thank you very much!!

Co-authors: Wouter Dorigo, Allard de Wit, Jason Brazile and Ranvir Singh (literature review), Luis Gómez-Chova, Gustavo Camps-Valls, Luis Guanter, Javier Calpe and José Moreno (MERIS clouds), Georg Kaiser and Werner Schneider (temporal fusion), Mathias Kneubuehler (vicarious calibration) and Antonio Plaza (mathematical morphology). Thank you!! It was a pleasure to work with all of you!

PhD students, post-docs and other scientific staff: El-Sayed Omran, Yuan Zeng, Jacob van Etten and Lucía Yañez (office mates); Harm Bartholomeus, Sander Mücher, Li Jia, Fausto Acerbi, Lucie Homolova, Jochem Verrelst ,Valerie Laurent and Silvia Huber (the club of remote sensors). Maaike Bader, Pepijn van Oort, Lukasz Grus, Gerd Weitkamp, Watse Castelein and Nikée Groot (the SDI/GIS people). Thanks for helping me and for sharing your thoughts and (scientific) problems with me !!

MSc students[2]: Thank you for keeping me busy and, mostly, for asking the right questions!!

Colleagues from the Centre for Geo-Information: I sincerely thank you for facilitating and promoting scientific discussions during the thematic groups meetings and for taking care of every detail (so that everything at the department could run smoothly).

---

[1] Notice that : a) my "personal endmembers" are not "pure" – i.e they have played different roles, or they have played their role with different intensity, during the last four years – and b) although they could have been grouped in many ways, here (just for clarity) they are presented according to their main position/function.

[2] See some of the names on pages 140 and 141.

On the personal side:

Supporters from “far-away”: Elena Hsieh (US), José Luis Serrano, Sergio Castro and Luis Pérez (ES), Maaria Loivamaki (FI+DE) and Patricia Leblanc + Anouck (FR). Thanks for your *e*-support and for bringing news from other “worlds”. The truth is out there and we will find it together!

Familia: Gracias a mis padres, a mis tres hermanitas, a mis tíos y tías, a mis primos y primas y, por supuesto, a mi abuelas. Gracias por enseñarme a montar en bici cuando era un enano (al final, ha resultado ser bastante práctico…). Gracias por traer aires del sur a Wageningen, por escuchar mis “historias holandesas” y, sobretodo, por enseñarme a apreciar cosas que son invisibles a los ojos.

Familie: Bedankt voor alle gezellige momenten… en voor het lenen van de auto’s, en voor de bitterkoekjespuddingen en de appeltaarten, en voor de fietsreparaties, en voor het leren uitzwaaien en veel andere “Hollandse” dingetjes.

Paranymphs: Zbyněk Malenovský (V nouzi poznáš přítele) and Anne van Gijsel (the perfect travel companion to the infinite and beyond!!). Thanks for everything…

Finally, I would like to thank the anonymous reviewers of the manuscripts that form the basis of this thesis and the people that I might have unintentionally forgotten to include in this library of acknowledgements (sorry “shadow endmembers”!).

In appreciation of all what you have done for me, I would like to give you an advice that I first heard from Steve Jobs (Apple’s CEO; not that I ever met him but, you know…, part of the modern duties of any PhD student is to surf the web … and, from time to time, you find this kind of “inspiring nuggets”). The advice, valid whether you have, plan to have, or do not plan to have a PhD degree, says: “stay foolish, stay hungry!!!!”.

Kind regards,

Raul Zurita-Milla

Curriculum Vitae

First name	Raúl
Family name	Zurita-Milla
Date of birth	April 9, 1978
Place of birth	Córdoba, Spain
Contact	zurita.milla@gmail.com

Education

1995 – 1996	High School "Luis de Góngora", Córdoba, Spain. Pre-university year. Specialization in science and technology: mathematics, physics, chemistry and technical drawing. Graduated with honorary scholarship for academic excellence.
1996 – 2003	University of Córdoba, Spain. Agricultural Engineer. Specialization in rural engineering: construction, irrigation and hydrology, agricultural machinery, technical drawing and cartography.
2001 – 2003	Wageningen University, The Netherlands. MSc. in Geo-Information Science. Graduated with Distinction. MSc thesis "Retrieving biophysical variables from optical remote sensing data in the frame of precision farming". Supervision: Dr. S. Moulin and Dr. Ir. J.G.P.W. Clevers.
2004 – 2008	Wageningen University, The Netherlands. PhD thesis "Mapping and monitoring heterogeneous landscapes: spatial, spectral and temporal unmixing of MERIS data". Supervision: Prof. Dr. sc. nat. M.E. Schaepman and Dr. Ir. J.G.P.W. Clevers.

Training

2002 – 2003	National Institute of Agronomic Research (INRA), Avignon, France.
2003	Centre for Spatial Studies of the Biosphere (CESBIO), Toulouse, France.

List of publications

Peer reviewed journals:

Clevers, J.G.P.W., Schaepman, M.E., Mücher, C.A., de Wit, A.J.W., **Zurita-Milla, R.** and Bartholomeus, H.M. (2007). Using MERIS on Envisat for land cover mapping in The Netherlands. *International Journal of Remote Sensing*, 28, 637-652.

Dorigo, W.A., **Zurita-Milla, R.**, de Wit, A.J.W., Brazile, J., Singh, R. and Schaepman, M.E. (2007). A review on reflective remote sensing and data assimilation techniques for enhanced agroecosystem modeling. *International Journal of Applied Earth Observation and Geoinformation*, 9,165-193.

Gomez-Chova, L., **Zurita-Milla, R.**, Camps-Valls, G., Guanter, L., Clevers, J.G.P.W., Calpe, J. Schaepman, M.E. and Moreno, J. (2008). Cloud screening and multitemporal unmixing of MERIS FR data, in preparation.

Malenovsky, Z., Homolova, L., **Zurita-Milla, R.** , Kaplan, V., Martin, E., Gastellu-Etchegory, J.P., Schaepman, M.E., Pokorny, R., Clevers, J.G.P.W. and Cudlin, P. (2008). Mapping leaf chlorophyll content of Norway spruce crowns using imaging spectroscopy data of sub-meter spatial resolution, in preparation.

Malenovsky, Z., Martin, E., Homolova, L., Gastellu-Etchegorry, J.P., **Zurita-Milla, R.**, Schaepman, M.E., Pokorny, R., Clevers, J.G.P.W. and Cudlin, P. (2008). Influence of woody elements of a Norway spruce canopy on nadir reflectance simulated by the DART model at very high spatial resolution. *Remote Sensing of Environment*, 112, 1-18.

Malenovsky, Z., Albrechtova, J., Lhotakova, Z., **Zurita-Milla, R.**, Clevers, J.G.P.W., Schaepman, M.E. and Cudlin, P. (2006). Applicability of the PROSPECT model for Norway spruce needles. *International Journal of Remote Sensing*, 27, 5315-5340.

Zurita-Milla, R., Clevers, J.G.P.W., van Gijsel, J.A.E. and Schaepman, M.E. (2008). Using MERIS fused images for land cover mapping and vegetation status assessment in heterogeneous landscapes *International Journal of Remote Sensing*, in review.

Zurita-Millla, R., Kaiser, G., Clevers, J.P.G.W., Schneider, W. and Schaepman, M.E. (2008). Monitoring vegetation seasonal dynamics using Landsat TM and MERIS FR fused images. *Remote Sensing of Environment*, in review.

Zurita-Milla, R. and van Gijsel, J.A.E. (2008). An SVD-based band ranking method and its application for hyperspectral feature selection, in preparation.

Zurita-Milla, R., Clevers, J.G.P.W. and Schaepman, M.E. (2008). Unmixing-based Landsat TM and MERIS FR data fusion. *IEEE Geoscience and Remote Sensing Letter*s, 5, 453-457.

Zurita-Milla, R., Clevers, J.G.P.W., Schaepman, M.E. and Plaza, A.J. (2007). Retrieving subpixel land cover composition through an effective integration of the spatial, spectral and temporal dimensions of MERIS imagery. *Journal of Remote Sensing*, 11, 659-668.

Zurita-Milla, R., Clevers, J.G.P.W., Schaepman, M.E. and Kneubuehler, M. (2007). Effects of MERIS L1b radiometric calibration on regional land cover mapping and land products. *International Journal of Remote Sensing*, 28, 653-673.

Book chapter:

Clevers, J.G.P.W. and **Zurita-Milla, R.** (2008). Multisensor and multiresolution image fusion using the linear mixing model. In: T. Stathaki (Ed.), *Image Fusion: Algorithms and Applications*, (pp. 67-84). London, UK: Academic Press.

Other scientific contributions:

Acerbi-Junior, F.W., **Zurita-Milla, R.**, Clevers, J.G.P.W., and Schaepman, M.E. (2005). MODIS and Landsat TM image fusion using the SIFuLAP method for mapping the Brazilian savannas (Cerrado). In: *Proceedings of the 25th EARSeL Symposium "Global Developments in Environmental Earth Observation from Space"*, (pp. 71-79). Porto, Portugal: Millpress.

Clevers, J.G.P.W., **Zurita-Milla, R.**, Schaepman, M.E., and Bartholomeus, H. (2004). Using MERIS on ENVISAT for Land Cover Mapping. In: *Proceedings of the Envisat Symposium*.CD-ROM. Salzburg, Austria: ESA.

Gomez-Chova, L., **Zurita-Milla, R.**, Camps-Valls, G., Guanter, L., Clevers, J., Calpe, J., Schaepman, M.E., and Moreno, J. (2007). Cloud screening and multitemporal unmixing of MERIS FR data. In: *Proceedings of the Envisat Symposium*. CD-ROM. Montreux, Switzerland: ESA.

Gomez-Chova, L., **Zurita-Milla, R.**, Camps-Valls, G., Guanter, L., Clevers, J.G.P.W., Calpe, J., Schaepman, M., and Moreno, J. (2006). Multitemporal validation of an unmixing-based MERIS cloud screening algorithm. In: J. Sobrino (Ed.) *Proceedings of the 2nd International Symposium on Recent Advances in Quantitative Remote Sensing: RAQRS'II*, (pp. 119-124). Valencia, Spain

Kooistra, L., Clevers, J.G.P.W., Schaepman, M., van Dobben, H., Sykora, K., Holtland, J., Batelaan, O., Debruyn, W., Bogaert, J., Schmidt, A., Clement, J., Bloemmen, M., Mucher, C.A., van den Hoof, C., de Bruin, S., Stuiver, J., **Zurita-Milla, R.**, Malenovsky, Z., Wenting, P., Mengesha, T., van Oort, P.A.J., Liras Laita, E., Wamelink, W., Schaepman-Strub, G., Hung, L.Q., Verbeiren, B., Bertels, L., and Sterckx, S. (2005). Linking Biochemical and Biophysical Variables Derived from Imaging Spectrometers to Ecological Models - The HyEco'04 Group Shoot. In: M.S.W.P. B. Zagajewski (Ed.) *Proceedings of the 4th Workshop on Imaging Spectroscopy*, (p. 61). Warsaw, Poland: EARSeL.

Malenovsky, Z., **Zurita-Milla, R.**, Homolová, L., Martin, E., Schaepman, M.E., Gastellu-Etchegory, J.P., Clevers, J.G.P.W., and Cudlín, P. (2007a). Physically-based retrievals of Norway spruce canopy variables from very high spatial resolution hyperspectral data. In: *Proceedings of the IEEE International Geoscience and Remote Sensing Symposium (IGARSS), Sensing and Understanding our Planet*, (pp. 4057-4060). Barcelona, Spain

Malenovsky, Z., **Zurita-Milla, R.**, Homolova, L., Martin, E., Schaepman, M.E., Gastellu-Etchegory, J.P., Pokorny, R., and Clevers, J.G.P.W. (2007b). Retrieval of coniferous canopy chlorophyll content from high spatial resolution hyperspectral data In: *Proceedings of the 10th International Symposium on Physical Measurements and Spectral Signatures in Remote Sensing (ISPMSRS'07)*, (pp. 108-113). Davos, Switzerland: ISPRS.

Malenovsky, Z., Homolova, L., **Zurita Milla, R.**, Martin, E., Gastellu-Etchegory, J.P., Schaepman, M.E., Clevers, J.G.P.W., Pokorny, R., and Cudlin, P. (2006). Chlorophyll concentration of leaves and canopies estimated from spectroscopic measurements using the radiative transfer models. In: *Proceedings of the Airborne Imaging Spectroscopy Workshop*, (p. 2). Bruges, Belgium: Belspo.

Malenovsky, Z., Martin, E., Homolova, L., Pokorny, R., Schaepman, M.E., Gastellu-Etchegory, J.P., **Zurita Milla, R.**, Clevers, J.G.P.W., and Cudlin, P. (2005). Influence of forest canopy structure simulated using the discrete anisotropic radiative transfer (DART) model on the retrieval of spruce stands LAI. In: S. Liang, J. Liu, X. Li, R. Liu and M. Schaepman (Eds.), *Proceedings of the 9th International Symposium on Physical Measurements and Signatures in Remote Sensing (ISPMSRS)*, (p. 3). Beijing, China

Mengesha, T., Schaepman, M., de Bruin, S., **Zurita-Milla, R.**, and Kooistra, L. (2005a). Ground Validation of Biophysical Products Using Imaging Spectroscopy in Softwood Forests. In: F. Baret and M. Weiss (Eds.), *Proceedings of the VALERI Workshop*. CD-ROM. Avignon, France: INRA.

Mengesha, T., Kooistra, L., **Zurita-Milla, R.**, de Bruin, S., and Schaepman, M. (2005b). Methodology Comparison of Quantiative LAI Retrieval using Imaging Spectroscopy and Geo-Spatial Interpolation in a Softwood Forest. In: B. Zagajewski, M. Sobczak and W. Prochnicki (Eds.), *Proceedings of the 4th Workshop on Imaging Spectroscopy* (p. 141). Warsaw, Poland: EARSel.

Molina, R., Mateos, J., Katsaggelos, A.K., and **Zurita-Milla, R.** (2005). A new super resolution Bayesian method for pansharpening Landsat ETM+ imagery. In: S. Liang, J. Liu, X. Li, R. Liu and M. Schaepman (Eds.), *Proceedings of the 9th International Symposium on Physical Measurements and Signatures in Remote Sensing (ISPMSRS)*, (pp. 280-283). Beijing, China

Moulin, S., **Zurita-Milla, R.**, Guérif, M., and Baret, F. (2003a). Characterizing the spatial and temporal variability of biophysical variables of a wheat crop using hyper-spectral measurements. In: *Proceedings of the Proceedings Geoscience and Remote Sensing Symposium (IGARSS)*, (pp. 2206- 2208). Toulouse, France

Moulin, S., **Zurita-Milla, R.**, Guérif, M., Houlès, V., and Baret, F. (2003b). Comparison of 3 remote sensing sensors and 2 methods performances in the retrieval of biophysical variables on a wheat field. In: A. Werner and A. Jarfe (Eds.), *Proceedings of the 4th European Conference on Precision Agriculture (ECPA)*, (pp. 509-510). Berlin, Germany: Wageningen Academic Publishers.

Piquer-Rodriguez, M., **Zurita-Milla, R.**, Cabello-Pinar, J., Alcaraz-Segura, J., Crompvoets, J.W.H.C., and Bunce, R.G.H. (2007). Land-use change detection in arid environments in South-East Spain In: *Proceedings of the 7th IALE World Congress*, (p. 873). Wageningen, The Netherlands

Schaepman, M., **Zurita-Milla, R.**, Kneubühler, M., Clevers, J.G.P.W., and Delwart, S. (2004). Assessment of long-term vicarious calibration efforts of MERIS on land product quality. In. In: R. Meynart, S.P. Neeck and H. Shimoda (Eds.), *Proceedings of the SPIE - Sensors, Systems, and Next-Generation Satellites VIII*, (pp. 363-371.). Maspalomas, Spain: SPIE.

Verrelst, J., **Zurita-Milla, R.**, Koetz, B., Clevers, J.G.P.W., and Schaepman, M.E. (2007). Angular unmixing of photosynthetic and non-photosynethetic vegetation within a coniferous forest using CHRIS-PROBA. In: *Proceedings of the 10th International Symposium on Physical Measurements and Spectral Signatures in Remote Sensing (ISPMSRS)*, (pp. 355-360). Davos, Switzerland: ISPRS.

Zurita-Milla, R., Kaiser, G., Clevers, J.G.P.W., Schneider, W., and Schaepman, M.E. (2008). Monitoring vegetation dynamics using MERIS fused images. In: *Proceedings of the 2nd MERIS (A)ATSR workshop*, CD-ROM.Frascati, Italy: ESA.

Zurita-Milla, R., Gomez-Chova, L., Clevers, J.G.P.W., Schaepman, M.E., and Camps-Valls, G. (2007a). Multitemporal unmixing of MERIS FR data In: *Proceedings of the 10th International Symposium on Physical Measurements and Spectral Signatures in Remote Sensing (ISPMSRS)*, (pp. 238 - 243). Davos, Switzerland: ISPRS.

Zurita-Milla, R., Kaiser, G., Clevers, J.P.G.W., Schneider, W., and Schaepman, M.E. (2007b). Spatial unmixing of MERIS data for monitoring vegetation dynamics. In: *Proceedings of the Envisat Symposium*. Montreux, Switzerland: CD-ROM. ESA.

Zurita-Milla, R., Clevers, J.G.P.W., and Schaepman, M.E. (2006a). Landsat TM and MERIS FR image fusion for land cover mapping over The Netherlands. In: M. Braun (Ed.) *Proceedings of the 2nd EARSeL SIG Workshop on Land Use and Land Cover*, (pp. 34-40). Bonn, Germany: EARSeL.

Zurita-Milla, R., Malenovsky, Z., Homolová, L., Schaepman, M., Martin, E., Gastellu-Etchegorry, J.P., Clevers, J.G.P.W., and Cudlín, P. (2006b). A neural network inversion of the DART model to retrieve Norway spruce LAI at a very high spatial resolution. In: J. Sobrino (Ed.) *Proceedings of the 2nd International Symposium on Recent Advances in Quantitative Remote Sensing: RAQRS'II*, (pp. 84-89). Valencia, Spain

Zurita-Milla, R., Guillen-Climent, M.L., Schaepman, M., and Clevers, J.G.P.W. (2006c). Unmixing-based Landsat TM and MERIS image fusion for land cover mapping over The Netherlands. In: J.v. Genderen (Ed.) *Proceedings of the ISPRS Mid-term Symposium 2006 "Remote Sensing: From Pixels to Processes"*, (p. 6). Enschede, The Netherlands

Zurita-Milla, R., Clevers, J.G.P.W., and Schaepman, M.E. (2005a). Effects of MERIS L1b radiometric calibration on regional land cover mapping and land products. In: A.J.W. de Wit (Ed.) *GIN workshop*. Wageningen, The Netherlands

Zurita-Milla, R., Schaepman, M.E., and Clevers, J.G.P.W. (2005b). Possibilities of MERIS for sub-pixel regional land cover mapping. In: M. Owe and G. d'Urso (Eds.), *Proceedings of the SPIE - Remote Sensing for Agriculture, Ecosystems, and Hydrology VII* (pp. 264-273). Bruges, Belgium: SPIE.

Zurita-Milla, R., Clevers, J.G.P.W., Schaepman, M.E., and Plaza, A.J. (2005c). Retrieving sub-pixel land cover composition through an effective integration of the spatial, spectral and temporal dimensions of MERIS imagery. In: S. Liang, J. Liu, X. Li, R. Liu and M. Schaepman (Eds.), *Proceedings of the 9th International Symposium on Physical Measurements and Signatures in Remote Sensing (ISPMSRS)*, (pp. 426-428). Beijing, China

Zurita-Milla, R., Clevers, J.G.P.W., and Schaepman, M.E. (2005d). Sub-pixel regional land cover mapping with MERIS imagery. In: *Proceedings of the MERIS -(A)ATSR workshop*, CD-ROM. Frascati, Italy: ESA.

Zurita-Milla, R., Schaepman, M., and Clevers, J.G.P.W. (2005e). Using MERIS and MODIS for Land Cover Mapping in The Netherlands. In: M. Rast (Ed.) *Proceedings of the CEOS-IVOS Workshop on Inter-Comparison of Large Scale Optical and Infrared Sensors*, CD-ROM. Noordwijk, The Netherlands: ESA.

Zurita-Milla, R., Schaepman, M., Clevers, J.G.P.W., Kneubühler, M., and Delwart, S. (2004). Long-Term MERIS Land Product Accuracy Assessment based on Vicarious Calibration and Regional Validation. In: *Proceedings of the ENVISAT/ERS Symposium*, CD-ROM. Salzburg, Austria: ESA.

Zurita-Milla, R., Moulin, S., Zago, M., M., G., and V., H. (2003). Retrieving winter wheat LAI and Cab from Xybion airborne data. In: A. Werner and A. Jarfe (Eds.), *Proceedings of the 4th European Conference on Precision Agriculture (ECPA)*, (pp. 607-608). Berlin, Germany: Wageningen Academic Publishers.

Zurita, R., De Luna, E., and Navarro, C. (2004). The role of vegetative bands in sloping olive orchards - erosion rates and runoff (preliminary results). In: J. Benites, M. Pisante and F. Stagnari (Eds.), FAO *Land and Water Bulletin 10. Integrated soil and water management for orchard development*, (pp. 137-139). Mosciano S. Angelo, Italy:FAO.

Zurita, R., Castro, S., and Estévez, R. (2000). A Biometric Study of the Olive Tree: Physical Parameters and Mass Approach [in Spanish]. In: R. Muñoz (Ed.) *Proceedings of the III Jornadas ECOLIVA'2000*, (p. 9). Puente de Génave, Jaén, Spain

PE&RC PhD Education Certificate

With the educational activities listed below the PhD candidate has complied with the educational requirements set by the C.T. de Wit Graduate School for Production Ecology and Resource Conservation (PE&RC) which comprises of a minimum total of 32 ECTS (= 22 weeks of activities)

Review of Literature (7.0 ECTS)

- Remote sensing and data assimilation methods for agroecosystem modelling (2005 – 2006)

Laboratory Training and Working Visits (2.0 ECTS)

- MERIS pre-processing and cloud screening; University of Valencia, Spain (2006)

Post-Graduate Courses (6.3 ECTS)

- The art of modelling; PE&RC-SENSE (2004)
- Advanced statistics; PE&RC (2006)
- Spatio-temporal data analysis: R + SAGA + Google Earth; University of Amsterdam (2008)

Competence Strengthening / Skills Courses (7.8 ECTS)

- Scientific writing; PE&RC (2004)
- Techniques for writing and presenting a scientific paper; Wageningen Graduate Schools (2005)
- IDL-ENVI Application development for remote sensing; CREASO (2006)
- Teaching and supervising thesis students; OWU (2006)
- IDL programming; Fanning Consulting (2008)
- Career perspectives; Wageningen Graduate Schools (2008)

Discussion Groups / Local Seminars and Other Meetings (16.8 ECTS)

- Statistics, maths and modelling; PE&RC (2004-2008)
- Remote sensing thematic group; CGI-WUR (2004-2008)
- Spatial methods; PE&RC (2006-2008)
- Ecosystems and landscape thematic group; CGI-WUR (2006-2008)

PE&RC Annual Meetings, Seminars and the PE&RC Weekend (1.5 ECTS)

- PE&RC day "The Scientific Agenda. Who pulls the strings?" (2006)
- PE&RC weekend (2006)
- PE&RC day "Scaling from molecules to ecosystems" (2008)

International Symposia, Workshops and Conferences (23 ECTS)

- ENVISAT/ERS Symposium; Salzburg, Austria (2004)
- SPIE-Europe Remote Sensing; Bruges, Belgium (2005)
- MERIS-(A)ATSR Workshop; Frascati, Italy (2005)
- 9th International Symposium on Physical Measurements and Signatures in Remote Sensing (ISPMSRS); Beijing, China (2005)
- 2nd International Symposium on Recent Advances in Quantitative Remote Sensing; Valencia, Spain (2006)
- ISPRS Mid-term Symposium "Remote Sensing: From Pixels to Processes"; Enschede, The Netherlands (2006)
- 10th International Symposium on Physical Measurements and Signatures in Remote Sensing (ISPMSRS); Davos, Switzerland (2007)
- ENVISAT Symposium; Montreux, Switzerland (2007)

Courses in which the PhD Candidate Has Worked as a Teacher

- Remote Sensing (2005-2008); GRS-WUR

Supervision of MSc Students

- Supervisor of the following MSc theses at Wageningen University:
    - Crop area estimates from temporal unmixing: a case study using MERIS with artificial neural networks by Ernesto Bastidas Obando.
    - Possibilities and limitations of artificial neural networks for sub-pixel land cover mapping by Alemu Demeke Nigussie.
    - Modelling landuse changes in southeastern Spain using a Markovian approach by María Piquer Rodríguez.
    - Unmixing-based image fusion for land cover mapping over The Netherlands by María Luz Guillén Climent.
    - Comparison of MODIS and MERIS data for land cover mapping in The Netherlands by Hailu Shiferaw Desta.
    - Multitemporal land cover classification in The Netherlands with MERIS by Teshome Eshete Beediu.

- Advisor of the following MSc theses at Wageningen University:
    - Development of an imaging spectroscopy based method for mapping and monitoring plant functional types in river floodplains by Lucía Sánchez Prieto.
    - Estimating the agricultural area in Senegal from medium resolution images, using an up-scaling method based on artificial neural networks by Josefien Delrue.
    - Retrieving chlorophyll content from CASI data for the identification of iron chlorosis in olive orchards by Anne van Gijsel.
    - Estimation of leaf area index using optical field instruments and imaging spectroscopy by Alemu Gonsamo Gosa.
    - Imaging spectroscopy for ecological monitoring at the test site the Millingerwaard: species mapping using spectral libraries and soil-vegetation-atmosphere-transfer models by Elisa Liras Laita.